University of Alberta

Thermodynamic Investigation of Bio-Macromolecular Interactions

by

Maryam Kabiri

A thesis submitted to the Faculty of Graduate Studies and Research
in partial fulfillment of the requirements for the degree of

Doctor of Philosophy

in

Chemical Engineering

Chemical and Materials Engineering

© Maryam Kabiri
Spring 2014
Edmonton, Alberta

Permission is hereby granted to the University of Alberta Libraries to reproduce single copies of this thesis and to lend or sell such copies for private, scholarly or scientific research purposes only. Where the thesis is converted to, or otherwise made available in digital form, the University of Alberta will advise potential users of the thesis of these terms.

The author reserves all other publication and other rights in association with the copyright in the thesis and, except as herein before provided, neither the thesis nor any substantial portion thereof may be printed or otherwise reproduced in any material form whatsoever without the author's prior written permission.

To my parents and my husband.

Abstract

The spontaneous assembly of polypeptides through non-covalent interactions at physiological conditions is the main focus of the presented work and will be discussed from two different perspectives: (i) the interaction of peptide chains with themselves leading to formation of higher order structures (self-assembling peptides); (ii) the interaction of polypeptides with nano-sized surfaces (protein-nanoparticle interactions).

Although self-assembling peptides are an important growing class of biomaterials, most of the works in this field have focused upon their various biomedical applications without highlighting the molecular mechanisms which result in their self-assembly into supra-molecular structures inside the body. Herein, through an in-depth thermodynamic analysis utilizing Isothermal Titration Calorimtry technique, the driving forces for self-assembly of ionic self-complementary peptide $RADA_4$ and its variants were identified implying great contribution of molecular hydration and charge to the self-assembly process. Furthermore, the interfacial molecules involved in self-assembly of these molecules was experimentally quantified. It was found that appending five serine residues to C-terminus of $RADA_4$ can overshadow the hydrophobic contribution of RADA segment leading to hydrogen bonding being the main driving force for self-assembly; while presence of 5 lysine residues inhibited $RADA_4$ self-assembly.

Secondly, the interaction of proteins with zwitterionic-modified nanoparticles (NPs) was investigated. Although widely studied, the underlying mechanism for the protein-repellent behavior of zwitterionic polymers is

largely unknown. A set of thermodynamic investigations was performed to study the interaction of two model proteins (with distinctly different adsorption behaviour) with the surface of zwitterionic-modified silica nanoparticles. The nature of the interaction between proteins and polymer-modified nanoparticle was identified along with highlighting the main driving forces leading to their adsorption onto the nanoparticle's surface. Moreover, the impact of zwitterion's spacer length and end-group chemistry on thermodynamics of protein adsorption was analyzed. Overall, our results indicated that the main advantage of zwitterionic polymer modification of surfaces are: i) an increase in water molecules at the interface, ii) lack of counter-ion release from surfaces and iii) lower structural reorganization of the system upon protein-surface interaction.

The findings presented in this work will fundamentally impact our understanding of nano-bio interfaces leading to development of more optimum nano-biomaterials in future.

Acknowledgments

I sincerely thank my supervisor Dr. Larry D. Unsworth for his insightful guidance and patience during my Ph.D. study.

I also thank my colleagues Markian Bahniuk and Kyle Koss for turning the lab into a beautiful and fun working environment.

I am also grateful to my supervisory committee members Dr. Afsaneh Lavasanifar and Dr. Hasan Uludag for their valuable advice through-out my research.

This thesis was financially supported by operating grants from Natural Sciences and Engineering Research Council of Canada (NSERC), National Research Council-National Institute for Naotechnology (NRC-NINT), and Department of Chemical and Materials Engineering at University of Alberta.

Table of Contents

List of Tables

List of Figures

List of Abbreviations

AFM	Atomic Force Microscopy
Alpha-la	α-lactalbumin
CB	Carboxybetaine
CD	Circular Dichroism
DLVO	Derjaguin and Landau, Verwey and Overbeek
HLB	Hydrophilic/Lipophilic Balance
HSA	Human Serum Albumin
ITC	Isothermal Titration Calorimetry
NP	Nanoparticle
OEG	Oligo Ethylene Glycol
PB	Phosphobetaine
PCBMA	Poly(Carboxy Betaine Methacrilamaide)
PEG	Poly(Ethylene Glycol)
Phospho	Phosphonate
PI	Preferential Interaction
SAM	Self-Assembling Monolayer
SB	Sulfobetaine
SNP	Silica Nanoparticle
SSIS	Single Set of Independent Binding Sites
TEMPO	2,2,6,6-tetramethylpiperidine-N-oxyl
UCST	Upper Critical Solubility Temperature

Chapter 1

Introduction and Research Proposal[1]

[1]A portion of this chapter was published in: Binazadeh, M.; Kabiri, M.; Unsworth, L. D.," Poly (ethylene glycol) and Poly (carboxy betaine) Based Nonfouling Architectures: Review and Current Efforts", Proteins at Interfaces III: State of the Art, ACS Symposium Series **2012**, Volume: 1120, Pages: 621-643.

In this chapter, a detailed discussion on Isothermal Titration Calorimetry will highlight the advantages as well as the perceived shortcomings of this technique. The controversies associated with enthalpy-entropy compensation effect, in combination with an examination of this system of experiments in the context of both self-assembling peptides and protein adsorption will be discussed in the next sections. Furthermore, a thorough review of the literature in these two areas will be presented that highlights the general driving forces thought to underlie both self-assembly and protein adsorption, as well as the theoretical models describing thermodynamics of these phenomena. Finally, the research proposal will be presented in the last section of this chapter.

1.1. Isothermal Titration Calorimetry

It is known that almost any type of molecular interaction is accompanied by some level of heat exchange between the interacting system and its surrounding medium. This is the fundamental concept that has led to development of Isothermal Titration Calorimetry (ITC) technique [1]. Through utilizing ITC the amount of heat released or absorbed upon molecular interactions, at constant temperature and pressure, can be evaluated. This technique has shown great potential for analyzing molecular interactions in a wide range of biological systems, such as protein-protein interactions [2], drug development [3,4], and enzymatic kinetic studies [5]. This is mostly due to the fact that ITC is the only analytical tool that can be used to provide a complete thermodynamic profile (i.e. binding constant (K), enthalpy change (ΔH), entropy change (ΔS), Gibbs free

energy change (ΔG)) for the interaction upon a single experiment. Moreover, since the heat exchange upon molecular interactions is a natural process, there is no requirement for modification of the molecules such as labeling, or immobilization of the interacting molecules when studied by ITC.

Although there are other techniques which are commonly utilized to study biomolceular interactions, each of them has certain advantages and drawbacks (See Table 1-1). In terms of calculating the binding constant of interactions, Surface Plasmon Resonance (SPR) is one of the most popular analytical tools. It does not require labeling however; the sample needs to be immobilized onto the surface of a cell chamber in order for the solution (containing the other molecule of interest) to flow upon it. Nuclear Magnetic Resonance (NMR) spectroscopy also provides high-resolution information regarding the structure of the formed complex, conformational changes of the molecules upon interaction as well as the kinetic parameters (such as binding constant). Nevertheless, the main disadvantages of this technique are the complexity of the instrument as well as the large amount of sample required to obtain a good signal. In the same way, the advantages and disadvantages of other methods are summarized in Table 1-1.

Table 1-1. Summary of common techniques used to study macromolecular interactions.

Technique	Measurement Range	Advantages	Disadvantages
Surface Plasmon Resonance (SPR)	K (10^3-10^{13} M^{-1})	High sensitivity, Small sample volume (μL range)	Expensive, Denaturation of immobilized probe, Undesired adsorption of molecules to instrumental components (needles and tubes), Effect of M_w on signal resolution [6]
Nuclear Magnetic Resonance (NMR)	K (10^3-10^6 M^{-1})	High resolution, Information on structural nature of complex and conformational changes	Expensive, M_w of the sample is limited to less than 40 kDa, Large amount of sample required (mL range) [6,7]
Analytical Ultracentrifugation (AUC)	K (10^3-10^8 M^{-1})	Small sample volume (μL range), Applicable to homomeric interactions	Expensive, Lengthy run-time per sample, May not detect non-specific interactions [7]
Quartz Crystal Microbalance (QCM)	K (10^5-10^{10} M^{-1})	Easy to use, Affordable	Low sensitivity, Requires immobilization, Effect of interfacial parameters (hydration, conformational changes) on measurements [6]
UV-Vis Spectroscopy	K (10^4-10^{11} M^{-1})	Easy to use, Affordable	Low resolution, Requires labeling [8]
Isothermal Titration Calorimetry (ITC)	K (10^3-10^9 M^{-1})	Easy to use, High sensitivity, Applicable to study of homomeric as well as non-specific interactions, Can lead to a complete thermodynamic profile	Inaccuracy of the data due to errors associated with concentration determination, The prerequisite for the energy profile of the interaction to have an enthalpic component [6,9]

A typical ITC instrument consists of two cells (sample cell and reference cell) placed inside an adiabatic jacket (Figure 1-1). The instrument constantly monitors the temperature of the cells, while maintaining a null temperature difference between the cells. As the two cells are kept at thermal equilibrium, the incremental injection of the solution inside the syringe into the sample cell and the subsequent interaction between molecules will result in temperature difference between ITC cells. That necessitates energy for maintaining the null temperature difference between two cells (the energy which is then translated into heat change).

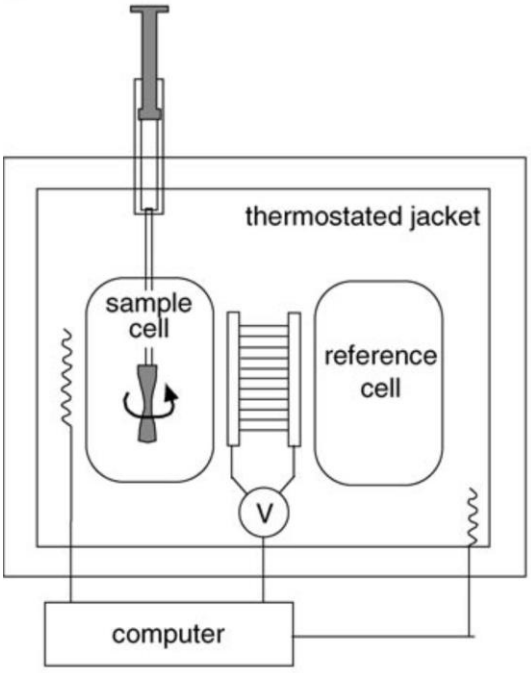

Figure 1-1. Simplified scheme of an Isothermal Titration Calorimeter (Copyright 2004 by John Wiley & Sons Inc.) [10]

While the temperature of the cells is regulated by a feed-back control system, the reference cell serves as a temperature reference through-out the

measurements. Upon each injection, the interaction inside the sample cell will cause the cell's temperature to fluctuate. The amount of heat absorbed or released (as the feed-back signal) will be detected by ITC within a short time (less than 10 seconds). ITC measurements are based on the first law of thermodynamic, *viz*., changes in internal energy of a system (ΔU) is equal to the difference between the amount of heat exchanged with its surroundings (Q) and the amount of work (W) done by the system (i.e. $\Delta U = Q - W$). For the systems being analyzed using ITC (i.e. at constant pressure and volume), W is equal to zero. Hence, it can be concluded that $\Delta U = Q \propto \Delta H$. This is basically the reason that interactions merely driven by entropy cannot be studied *via* ITC [11]. However, the fact that enthalpic contribution to the energy domain of an interaction is negligible might still be a valuable result that can only be obtained through running an ITC experiment.

The enthalpy change of an interaction can be calculated from raw ITC signal. However, in order to calculate the equilibrium binding constant and binding stoichiometry, the raw heat signal needs to be fitted using an appropriate model for the interaction. In general, the most common model used for describing non-specific interactions studied using ITC is the "single set of independent binding sites" model, derived from the Langmuir model. Hence, there are prerequisites associated with using this model: one of the most important requirements being that the system should reach a dynamic equilibrium state and for this condition to hold, the interaction of interest must be reversible. The

concepts of equilibrium and reversibility (as related to the interactions studied herein) will be discussed later in this chapter.

Another factor which needs to be taken into account while analyzing ITC data is that in some cases, even if the data can be fitted with the model, the model might not necessarily represent the most precise description of the interaction under study. For instance, there might be two identical binding sites (with equal K and ΔH) which are not independent but the data associated with them can be very well fitted to the model for "single set of independent binding sites". This might happen when the binding of the first site affects only the binding constant (K) of the second site but not the ΔH parameter, resulting in an ITC thermogram which is very similar to the case when the binding sites are independent of each other [12]. Such confusions can be avoided by taking advantage of the available information on structure and chemistry of the molecules under study. Nevertheless, when studying biological systems, it has been said that "all models are wrong, but some are useful" [13].

The interactions can only take place if the Gibbs free energy associated with them is negative ($\Delta G < 0$). The Gibbs free energy is defined by two components, *viz.*, enthalpy and entropy ($\Delta G = \Delta H - T\Delta S$). Almost any type of non-covalent interaction that occurs at molecular interfaces is accompanied by a specific set of thermodynamic parameters which makes it distinguishable from other types of phenomena. This is referred to as "thermodynamic signatures" which is very useful in interpreting the results obtained *via* ITC and speculating

about the driving forces of interactions. Such conclusions can be mostly drawn based on both "sign" and "magnitude" of these parameters such as enthalpy and entropy. For example, it is known that the magnitude of enthalpy change is closely related to the length and angle of the bonds formed among interacting molecules (such as hydrogen bonds) [11]. On the other hand, the sign of enthalpy and entropy indicates their contribution to a negative Gibbs free energy change, such that negative ΔH and positive ΔS are considered favorable to the interactions. While formation of non-covalent bonds among interacting molecules usually results in negative ΔH, the desolvation of interacting surfaces is a very common cause for observed positive ΔS. In case of a negative (favorable) ΔH, ΔS can be either positive (favorable) or negative (unfavorable). The unfavorable ΔS, however, should have a magnitude which allows for a negative ΔG; otherwise the interaction won't take place. On the other hand, it is also possible that the interaction of molecules inside the system gives rise to an observed positive (unfavorable) ΔH. In this case, $T\Delta S$ has to be positive (favorable) and have a larger magnitude than ΔH (so that $\Delta G < 0$). Such a condition is usually indicative of "hydrophobic forces" driving the molecular interactions.

In addition to the contribution of enthalpy and entropy to the Gibbs free energy changes, the relationship between enthalpy and entropy (i.e. enthalpy-entropy compensation) is another factor which needs to be considered. This will be discussed in details, in the following section.

1.2. Enthalpy-Entropy Compensation in Macromolecular Interactions

During the 1950's, an interesting observation in organic chemistry was reported [12]; it was found that the equilibrium constant/free energy change of an interaction remains nearly constant upon introducing some changes in internal or external parameters of a non-covalent macromolecular interacting system. Whereas, the enthalpy and entropy change of that interaction exhibit a drastic variation instead. This has given rise to the empirically-originated concept of enthalpy-entropy compensation. It was found that the free energy change can remain constant mainly due to a compensatory relationship between enthalpy and entropy changes which (in most cases) were found to be linearly correlated [13]:

$$T\Delta\Delta S = \alpha\Delta\Delta H \qquad \text{Equation (1-1)}$$

$$T\Delta S = \alpha\Delta H + T\Delta S_o \qquad \text{Equation (1-2)}$$

$$\Delta G = (1-\alpha)\Delta\Delta H \qquad \text{Equation (1-3)}$$

The slope of the plot for ΔH *vs.* TΔS, denoted as $\boldsymbol{\alpha}$ in equation (1-2), represents the ratio of the enthalpy change compensated by entropy. Also, as shown in equation (1-3), the parameter (1-$\boldsymbol{\alpha}$) is a representative of the fraction of enthalpy change which contributes to free energy change of the system [13].

The enthalpy-entropy compensation (EEC) effect is particularly important in physiological media, as it is thought to result in the system being able to remain stable under constantly changing conditions of the surrounding environment (thermodynamic homeostasis). On the other hand, EEC has proved to be quite problematic in drug discovery studies; where improving the binding affinity of the

molecules (as well as subsequent variations in ΔG) is the main goal of the system's modifications [14]. The controversies associated with EEC concept have given rise to numerous attempts in explaining the origin and mechanism of this process. One of the simplest explanations utilized the relationship between favourable enthalpic outcome of a non-covalent bond formation and the entropic penalty associated with structural confinement caused by molecular binding (or interaction). Although this could qualitatively describe a pathway that leads to EEC, it was shown that this is not a universal model which can be applied to any system [15]. Another physical description of EEC involves the "solvent cage" theory [16]: If the first encounter of the two interacting molecules is not successful, the interacting species will be trapped inside a cage constructed of solvent molecules. The formation of solvent cage can cause the collisions to become more efficient (and result in interaction) through increasing the chance of new collisions between interacting molecules with more favourable orientation and energy. The EEC effect can take place as the increase in internal energy (i.e. enthalpy) gets counter-balanced with an increase in the vibrational movements of the interacting molecules (i.e. entropy) trapped in a solvent cage [16].

It was also proposed that EEC might stem from a process which restricts the free energy change of the system to a finite range (also called "free energy windows") [14]. This process could be a result of instrumental limitations (such as in Isothermal Titration Calorimetry, where only a specific range of binding constants can be detected) or an intrinsic property of the system. Unlike free

energy changes, no such boundaries were described for enthalpy and entropy; instead it was shown that they are able to exhibit a wide range of values [17] and this might be responsible for their compensatory behaviour.

In some cases, the EEC effect was attributed to the propagation of experimental error in analyzing thermodynamic data obtained *via* van't Hoff method or ITC [15]. The fact that van't Hoff enthalpy (ΔH_{vH}) is derived from temperature-dependence of K (equilibrium constant) (i.e. $d \ln K / dT^{-1} = -\Delta H_{vH}/R$) creates a correlation between enthalpy, entropy and free energy changes. Therefore, it was suggested that a linear relationship between enthalpy and entropy measured *via* van't Hoff equation should not be regarded as an EEC effect. In case of ITC, although the equilibrium constant and enthalpy change are measured independently, there were some concerns raised regarding underestimation of errors associated with ITC results [15]. It was proposed that the logarithmic relationship between equilibrium constant (K) and free energy change ($\Delta G = -RT \ln K$) may cause the errors associated with K to get substantially suppressed in reported numbers for ΔG. Subsequently, the error in ΔH would be much larger than the errors in ΔG. This might result in negligible ΔG values compared to ΔH; making the latter linearly correlated to TΔS (as in: $\Delta G - \Delta H = -T\Delta S$). A more recent investigation on this subject, however, proved that propagation of experimental error can result in a "fake" EEC effect only if the slope of the plot for ΔH *vs.* ΔS (i.e. isokinetic temperature, T_c) is equal or lower than the mean experimental temperature (T_m) [16]. It is noteworthy that this does

not necessarily imply that all data sets with $T_c \leq T_m$ do not account for a true EEC relationship. It is just that in such cases, error propagation should definitely be taken into account while explaining the results [16].

In a recent report by Whitesides group [18], through selection of a protein with a rigid structure which underwent an enthalpically-driven hydrophobic interaction with its ligand, the contribution of the protein's conformational changes to EEC was cancelled. This was done in order to be able to specifically probe the contribution of water networks (associated with the ligand) to EEC phenomenon. Utilizing ITC, not only a strong EEC relationship was demonstrated for this system, but also a significant contribution of structural and thermodynamic properties of the hydration shell to EEC was highlighted [18]. Perhaps, performing such fundamental investigations on the role of counter-ion movements in EEC would deliver equally interesting results.

1.3. Peptide Self-Assembly

Formation of cellular membranes and sub-cellular compartments through self-assembly of lipid bi-layers, polymerization of highly organized nucleic acid chains which eventually develop into DNA, and the remarkable role of proteins and peptides in cell signaling and trans-membrane exchanges are among examples of molecular self-assembly evolved by nature [19]. Constituted of inherently biocompatible amino acids, self-assembling peptides are an emerging class of biomaterials which have found wide-ranging applications in regenerative medicine, drug delivery, bio-sensing, etc. [20-23]. It is believed that a molecular-

level understanding of peptide self-assembly will provide grounds for development of rationally designed peptide structures with the most desirable function.

Perhaps one of the main reasons that self-assembling peptides are an active area of biomedical research is the possibility to fine-tune these molecules with respect to their final application. They can self-assemble into different types of nano-structures (fibers, micelles, tapes, cylinders, vesicles, etc.) through adopting different conformations (β-sheet, α-helix, β-hairpin, etc.) [22]. Identification of the factors and conditions that drive a peptide molecule to adopt a specific secondary conformation, which will then lead to formation of higher order structures, is of critical importance. Different combinations of 20 amino acids, provided by nature, allow for the development of a broad range of peptide molecules with different properties. Some of these residues can influence the peptide structure in certain ways. For instance, the proline (P) residue is known to be responsible for turns in β-hairpin structures as well as the beginning of α-helix strands [24,25], or cysteine (C) residues can promote cross-linking through disulfide bond formation [26]. It has been suggested that peptide length and its sequence are the major factors determining the final type of the supramolecular architectures [23]. But as Hecht *et. al.* pointed out, the secondary structure of the assemblies relies mostly on the periodicity of the sequence rather than its chemistry [27]. Hence in the following section, we shall introduce the different categories of self-assembling peptides based on their sequence arrangements. A

common characteristic of most self-assembling peptides is that their sequence mainly consists of hydrophobic residues, which drive the aggregation, along with a couple of polar or charged amino acids in their sequence which gives them the desired solubility characteristic [28]. However, it seems that it is the position of these charged residues along the peptide sequence that determines the ultimate secondary and tertiary structures of the assembled peptides.

1.3.1. Univalent Peptides

This class of self-assembling peptides are mainly hydrophobic amino acids doped with single-charge-type residues. One of the simplest structures in this category was proposed by Schweitzer-Stenner group, 12-mer or 16-mer alanine-based peptides consisted of AAKA repeats that form stable β-sheet structures at acidic pH and subsequently develop into stable hydrogel systems [28]. This was quite surprising, since the lysine (K) residue is known to become highly protonated at low pH and hamper the self-assembly through electrostatic repulsions [29]. The authors hypothesized that formation of a regular layer of β-sheet strands was hindered by charge-charge interaction of lysine residues. However, the hydrophobic interaction between alanine residues might be responsible for formation of β-hair pin structures with lysine residues sticking outward. The hair pin structures can stack on top of each other through hydrogen bonding between lysine residues and peptide carbonyls of other hair pins and give rise to the structural transition into β-sheets.

In order to look at the effect of hydrophobicity and/or aromaticity of residues on physicochemical properties of peptides, self-assembly of Ac-$(XKXK)_2$-NH_2 with X= Val, Ile, Phe, pentafluorophenylalanine (F_5-Phe), and cyclohexylalanine (Cha) was studied [29]. With the aim of inducing cross-β fibril formation in such peptides, solution ionic strength needed to be adjusted so as to overcome the electrostatic repulsion between lysine residues through charge screening effects. Interestingly, it was found that the required ionic strength for onset of peptide self-assembly was lower for peptides containing more hydrophobic residue at position X, independent of that residue's aromaticity. Instead, the effect of aromaticity was pronounced in the type of supramolecular structures formed; as peptides with aromatic residue at position X self-assembled into nano ribbons/nano tapes where non-aromatic sequences aggregated into fibrils with a diameter of 3-15 nm. Furthermore, the hydrogels formed by aromatic peptides demonstrated a more rigid behaviour than the ones containing non-aromatic residues [29].

Recently, Schneider *et.al*. determined the role of hydrophobic character of the sequence along with its length, in hydrogel properties [30]. In a quest for developing injectable peptide-based hydrogel systems which can undergo triggered self-assembly, they studied a small library of short single-charge-type peptides varying in sequence length and hydrophobic character. The optimized peptide LK13 demonstrated random coil structure in aqueous solutions; however addition of salts led to β-sheet formation by the peptide which eventually formed

a hydrogel network constituted of elongated fibrils [30]. Schneider group have also introduced a series of β-hair pin forming peptides containing lysine as the polar residue and valine as the hydrophobic amino acid [31]. The β-turn was induced in the structure by incorporating a central proline-based tetra-peptide which was flanked between two strands composed of alternating hydrophobic valine (V) and positive lysine (K) residues. The hairpin structures formed as a result of attractive interaction between hydrophobic residues and intermolecular hydrogen bonding between polar residues. These peptides maintain a random coil structure in solution, while pH and ionic strength have been used as factors to trigger their self-assembly into hairpin conformation. MAX1 peptide is an example of such structures [31].

Negatively charged groups of single-charge-type peptides were also developed. A series of proline-containing acidic peptides of the sequence Pro-Y-$(Z\text{-}Y)_5$-Pro where Y= Glu or Asp, and Z= Phe or Leu were studied [32]. These peptides formed gel at neutral pH which is a few units above their pK_a. It was hypothesized that peptide chains get attracted to each other through van der Waals interactions and form β-sheet structures with negatively charged groups sticking out of one side of the plane. These β-sheets acts as nucleation sites for the fibril elongation; a step in which cross-strand hydrogen bonds between acidic residues side-chains were thought to play a role in further stabilization of the self-assembled network [32].

1.3.2. Multivalent Peptides

This class of peptides contains oppositely charged residues either in separated segments or in an alternating fashion. Boden and coworkers have introduced P_{11}-I peptide which is a glutamine-based sequence with Arginie (R) and Glutamate (E) at positions 3 and 9, respectively [33]. This peptide was designed so as to self-assemble into anti-parallel β-sheet structure with hydrophilic characteristics on both sides of the peptide. It was also further modified into P_{11}-II with a sequence of Ac-QQRFQWQFEQQ-NH_2 [34]. This structure self-assembled not only due to attractive hydrophobic interaction between methylene side-groups of Glutamine residues but also due to π–π stacking between aromatic residues side-chains. The positioning of Arg3 and Glu9 still favored self-assembly into anti-parallel β-sheet structures. The amphiphilic nature of this peptide would result in self-assembled tapes with both hydrophobic and hydrophilic sides [34].

Other series of peptides with oppositely charged residues were developed by Zhang group [21,35]. These sequences are characterized by consisting of hydrophobic aminoacids on one side and alternating positively and negatively charged residues occupying the other side of the peptide chain. The alanine-based EAK8, EAK12, EAK16, RADA16-I, RADA16-II and the leucine-based KLD12 are among these peptides. These 8 to 16 residue peptides are capable of forming β–sheet structures in aqueous solutions [35]. The critical factor in rational design of self-assembling peptides is to engineer the structure in a way that uniform and reproducible aggregates form upon self-assembly. A β–sheet conformation alone

can develop into a variety of supramolecular structures including tapes, ribbons, fibrils and fibers. The major difference between these various structures is the number of β–sheets that interact with each other to form the final assembly [35]. A systematic study on the re-assembly process of ionic self-complementary peptides developed by Zhang group, proved dynamic re-assembly of RADA16–I peptide [36]. After disruption of self-assembled nanofibers by sonication, the structure was regained and they were able to reassemble into micron length nanofibers. Furthermore, the reassembled nanofibers were found to form a more rigid hydrogel structures compared to the one formed by the same peptide prior to sonication. A re-assembly model explaining the sliding diffusion of peptide segments with hydrophobic cohesive ends was proposed by the authors [36].

It is important to note that, not all peptides with oppositely charged groups form β–sheets. In fact since alanine residue has a high propensity of α–helix formation, there have been reports where 16-residue multivalent alanine-based peptides formed α–helix in water [37]. The 50 residue peptide Ac-$Y(AEAAKA)_8F$-NH_2 also forms stable α–helices in aqueous solutions [38].

As explained in previous section, MAX1 peptide is a single-charge-type peptide which forms β–hairpin structures upon external stimuli. By substitution of lysine15 in this sequence with aspartic acid, the overall charge of the peptide was reduced by one unit and MAX8 peptide was developed [39]. This single-residue alteration resulted in β–hairpin forming peptides with faster self-assembly kinetics and a more rigid hydrogel structure [39].

1.3.3. Peptides with a Hydrophobic Stretch Attached to a Hydrophilic Domain

This class of self-assembling peptides is quite similar to lipids found in cellular membranes. With distinctly hydrophilic heads and hydrophobic tails they can self-assemble to a variety of nano-structures depending on their length and chemical composition. These peptides can be categorized based on the character of the hydrophobic stretch in their structure; which can be either a peptidic domain or an alkyl chain.

The first category of these peptides which contain an apolar stretch of amino acids can be dibolock, triblock or even pentablock poly-peptides. It was found that the hydrogels formed by triblock poly-peptides were more rigid and demonstrated better resistance to ionic strength variations, compared to the ones prepared *via* diblocks at similar concentrations [40]. Deming group have put a lot of effort on developing such architectures including K_xL_y (with X and Y ranging from 20 to 80 and 10 to 30, respectively), K_xV_y, E_xL_y, $K_mL_nK_o$, and $K_mL_nK_oL_nK_m$ [40-46]. The presence of poly(L-leucine) as the hydrophobic domain promoted self-assembly into α–helix structures; whereas sequences containing poly(L-valine) gave rise to crystalline β–sheet formation [47]. Furthermore, it was found that the hydrophilic-lipophilic balance (HLB) inside the peptide sequence plays a critical role in self-assembly of such molecules; as the sequences with short hydrophobic segments did not show any gelation [41].

Interestingly, such amphiphilic peptide constructs do not necessarily have to be large poly-peptide molecules; as the short oligo-peptide introduced by Zhao *et.al.* was shown to be able to self-assemble into β–turns and β–sheets depending on its concentration [48]. Comprising of polar residues (lysine and glutamate) on one end and hydrophobic residues (phenylalanine and cysteine) on the other end, this 9-mer peptide hierarchically self-assembles to form extremely connected globular aggregates resembling "beads-on-a-thread" type of nanofiber network at high concentrations [48].

Peptides with a hydrophilic domain attached to alkyl chain represent the second category of amphiphilic peptides. Such N-terminally alkylated peptides self-assemble into micelles or bilayer structures in a concentration-dependant manner; such that tube or fiber structures are usually observed at high concentrations of these peptides [22]. Stupp *et.al.* have published a large body of work focused on such amphiphilic peptides with wide-ranging applications in regenerative medicine and drug delivery [49,50]. One of their innovative designs was a peptide amphiphile with 5 different domains: (1) a hydrophobic alkyl chain which induced amphiphilic characteristic to the peptide, (2) a cysteine stretch which created cross-links in self-assembled structure through di-sulfide bond formation, (3) a flexible linker containing 3 glycine residues, (4) one phosphorylated serine residue which could interact with Ca^{+} ions and induce biomineralizetion, and (5) an RGD motif to promote cell adhesion. The cryo-TEM

imaging of this peptide demonstrated its ability to form nanofibers with a diameter of 7.6 nm in water [51].

Bolaamphiphiles are another class of *de novo* designed peptides with amphiphilic characteristics which are comprised of one alkyl chain flanked by two hydrophilic peptide segments. They can form different self-assembled structures including micelles, vesicles, and fibers depending on the length of the linker sequence [52,53]. Overall, the final assembled nano-structures formed by amphiphilic peptides are known to be controlled by their concentration, HLB ratio, steric constraints of different residues, and solution pH/ ionic strength.

1.3.4. Driving Forces Responsible for Peptide Self-Assembly

Herein, we focus on three types of intermolecular forces which are more commonly present among building blocks of self-assembling peptides *i.e.* amino acids. It is thought that peptide self-assembly is the result of a balance between hydrophobic interactions, electrostatic forces, and hydrogen bonding.

1.3.4.1. Hydrophobic Interactions

Taking into account the chemical structure for different categories of self-assembling peptides, explained above, it can be concluded that hydrophobic residues are a common building block among all categories. This is in agreement with the fact that hydrophobic interactions are known as one of the driving forces responsible for supramolecular structure formation by almost all self-assembling peptides [54]. The long-range nature of hydrophobic attractive forces (~13 nm)

compared to that of repulsive hydration forces (~ 3 nm) might also be responsible for a more dominant role of these forces in self-assembly process [55]. It is important to note that for peptides with aromatic side chains (such as peptides containing phenylalanine or tryptophan) π–π stacking would also be involved in interactions as a sub-category for hydrophobic forces.

Hydrophobic forces, perhaps, serve as the main rational in the design of peptide amphiphils (containing either alkyl chain or apolar amino acid stretch) as it is basically the disruption of organized hydration shell around apolar segments and the subsequent release of water molecules which usually results in formation of supramolecular structures by these peptides. This type of driving force, however, is comprised of different factors determining whether it is favorable for an interaction to be driven hydrophobically or not. As Tirrel *et.al.* pointed out [54], the overall free energy of a hydrophobic interaction (ΔG) can be a combination of the following terms:

$$\Delta G = \Delta G_{Hydrophobic} + \Delta G_{Contact} + \Delta G_{Hydrophobic\ packing} + \Delta G_{Headgroup}$$

Equation (1-4)

where $\Delta G_{Hydrophobic}$ is the energy associated with repellence of hydrophobic tail of the peptide amphiphile from water into assembled structure (which should be negative). As these hydrophobic segments come to each other, the solvent on their surface is displaced; this "contact" free energy is expected to be positive. Further interaction of hydrophobic segments would result in reduction of molecular degrees of freedom of interacting species which will eventually reduce

the entropy of the system creating a positive $\Delta G_{Hydrophobic\ packing}$. The final term refers to the interaction between headgroups of the peptide chain which can be attractive (e.g. hydrogen bonding) or repulsive (e.g. electrostatic interaction or steric hydration) [54].

The role of hydrophobic driving forces is more particularly pronounced in salt-triggered self-assembly processes, where the charge-screening effects make the hydrophobic interactions (among apolar residues) more dominant and drive the peptide chains to form hierarchical aggregates in solution. Such mechanisms are of critical importance, specifically in biomedical applications of self-assembling peptides.

1.3.4.2. Electrostatic Forces

While hydrophobic forces are thought to be the major driving force, especially in initiating the self-assembly process, electrostatic interactions are usually employed to manipulate the geometrical characteristics of assemblies and induce structural specificity through uniquely matched oppositely charged building blocks. Ionic strength of the solution, type of salt ions, and pH are thought to be the factors capable of modulating electrostatic interactions. The Debye-Hückle theory provides insight into the double-layer formation on the surface of charged particles in ionic solutions. According to this theory, the repulsive double-layer potential (Ψ_x) decays exponentially with the distance (x) as follows:

$$\Psi_x \simeq \Psi_0 e^{-kx}$$ Equation (1-5)

where, 1/k is called the Debye length and is the characteristic decay length of the double-layer potential. Both ion valence and salt concentration affect the Debye length; as higher salt concentrations and/or larger ion valence of the salt used would result in more complete charge-screening [56].

As explained earlier, self-assembly is a mechanism that can be governed by several different forces. In colloid science, the DLVO theory (proposed by Derjaguin and Landau, Verwey and Overbeek) describes the interplay between repulsive double-layer potential and attractive van der Waals forces, where double-layer potential dominates at larger distances and as the distance decreases the attractive van der Waals interactions becomes more important [57]. However, this theory assumes a uniform distribution of charges on the surface of molecule rather than isolated charged segments and this might limit the application of this theory in describing peptide self-assembly process.

1.3.4.3. Hydrogen bonding

It was previously assumed that hydrogen bonding involves sharing of one hydrogen atom between two electronegative atoms; a hypothesis which made this type of bonding a subcategory of covalent interactions. It was not until the 1960's that the electrostatic nature of hydrogen bonds became accepted along with the understanding that the hydrogen atom is not shared and basically remains covalently bound to its neighbor electronegative atom [57]. The strength of the

hydrogen bond is known to be ~5-10 kT (where k is the Boltzmann constant and T is the temperature) which is in a medium range compared to stronger ionic and covalent bonds and weaker van der Waals interactions. Despite the electrostatic nature of hydrogen bonding, it does not exhibit a purely charge-charge or dipole-dipole interaction characteristics; instead it falls in-between and mostly demonstrates charge-dipole type of interactions [57]. Due to such complexities, quantification of hydrogen bonding did not prove to be straightforward. In fact, to the best of our knowledge, there has been no relationship proposed for calculation of the interaction potential for this type of molecular bonding. However, it was suggested that the equations describing the charge-dipole interactions can be applied to hydrogen bonding as well.

Hydrogen bonding has been shown to be important in peptide self-assembly. Polar residues such as serine and tyrosine with hydroxyl groups on their side chains are usually incorporated in the peptide sequences in order to induce hydrogen bonding. In a recent work, the phenylalanine residue in an amyloid-like fiber forming tripeptide with the sequence FFK was substituted by tyrosine [58]. This resulted in formation of thinner fibrils with an increased propensity for lateral association due to the hydrogen bonding. Interestingly, when both phenylalanine residues were substituted with tyrosine, the induced hydrogen bonding resulted in formation of spherical assemblies [58]. There have also been other self-assembling peptides designed specifically for the self-assembly to be driven by hydrogen bonding; an example of which are the cyclic D,L-peptides [59-61].

1.3.5. Thermodynamics of Peptide Self-Assembly

It is thought that thermodynamics of self-assembly provides insight toward predicting the type of supramolecular structure which will eventually form through aggregation of molecules [57]. This can fundamentally contribute to the rational design of self-assembling peptides leading to development of structures with specific and desired functions.

Chemical potential (μ) of molecules has been utilized by Israelachvili *et.al.* [57] as well as other groups [54] to describe the driving force for self-assembly of amphiphilic molecules. The concept was originally introduced for micelle formation [62], but was later extended to explain the self-assembly of molecules into different structures such as bilayers, vesicles, etc. It was shown that μ_N, the mean chemical potential of a molecule in self-assembled state with an aggregation number of N, relates to X_N, the concentration of self-assembled molecules with an aggregation number of N, *via* the following equation:

$$\mu_N = \mu_N^o + \frac{kT}{N}\log\left(\frac{X_N}{N}\right) \qquad \text{Equation (1-6)}$$

where μ_N^o is the mean interaction free energy (standard part of chemical potential) for each single molecule with an aggregation number of N, such that the free energy per each self-assembled unit would be $N\mu_N^o$ and k is the Boltzmann constant.

Utilizing the "law of mass action", the rates of association $(k_1 X_1^N)$and dissociation $\left(k_N(X_N/N)\right)$ for self-assembly of N particles can be determined. The

equilibrium constant (K) of interaction can also be derived using the free energies of the system, as the following:

$$K = exp[-N(\mu_N^o - \mu_1^o)/kT] \qquad \text{Equation (1-7)}$$

Considering that at equilibrium conditions the rate of association is equal to the rate of dissociation, we shall have:

$$K = \frac{k_1}{k_N} = \frac{X_N}{NX_1^N} = exp[-N(\mu_N^o - \mu_1^o)/kT] \qquad \text{Equation (1-8)}$$

Therefore, equation (1-6) can be re-written as the following:

$$X_N = N\left[X_1 exp\left(\frac{\mu_1^o - \mu_N^o}{kT}\right)\right]^N \qquad \text{Equation (1-9)}$$

It should be noted that in equation (1-9), ideal mixing along with dilute solution conditions are assumed [57]; the latter implies no interaction between assembled aggregates. Self-assembly is a spontaneous and thermodynamically-driven process, however, the pre-requisite for it to happen is that $\mu_N^o < \mu_1^o$. This means that μ_N^o should reach a minimum as N increases. Hence, the interaction free energy of the molecules that can self-assemble into basic structures such as rods, sheets and spheres was defined as the following [57]:

$$\mu_N^o = \mu_\infty^o + \frac{\alpha kT}{N^p} \qquad \text{Equation (1-10)}$$

where $\boldsymbol{\alpha}$ is a positive constant that depends on the strength of intermolecular interaction (in this regard, $\boldsymbol{\alpha}$kT is usually defined as the energy of monomer-monomer bonds in self-assembled state *vs.* the un-assembled

monomers) and p depends on the geometry of the self-assembled unit (as it equals to 1 for rods and cylinders, 1/2 for discs and sheets, and 1/3 for spheres).

Although equations (1-9) and (1-10) fundamentally describe the thermodynamics of self-assembly, application of these formula to the experimental data is not possible due to the difficulties associated with measurement of parameters such as μ_N^0 and X_N. Therefore, there have been attempts made toward relating these equations to the measurable experimental data. Through integrating equations (1-9) and (1-10), a critical concentration was determined (equation 1-11); at which increasing the solute concentration does not result in a drastic change in solution's monomer concentration implying the onset of self-assembly process. Classically called the critical micelle concentration (CMC); this concentration is a parameter which can be measured not only for micelle-forming molecules but for any other self-assembling system:

$$CMC = exp\left(-\frac{\mu_1^o - \mu_N^o}{kT}\right) \qquad \text{Equation (1-11)}$$

The pioneering work of Emerson and Holtzer linked the CMC parameter to free energy changes [63,64], such that:

$$\Delta G_N = RT \ln(CMC) \qquad \text{Equation (1-12)}$$

In the quest to determine other thermodynamic parameters, temperature dependence of CMC has been widely employed as a tool to measure the enthalpy of self-assembly (*via* van't Hoff equation). However, there have been limitations

associated with this method. As Holtzer *et.al.* pointed out the partial molal Gibbs free energy is defined as the following [64]:

$$dG_N = V_N dP - S_N dT + \left(\frac{\partial G_N}{\partial N}\right)_{T,P} dN \qquad \text{Equation (1-13)}$$

The last term in equation (1-13) corresponds to the potential change in number of monomers due to temperature variations. Knowing the partial molal free energy, the partial molal free energy change can be calculated:

$$d(\Delta G_N) = \Delta V_N\, dP - \Delta S_N\, dT + \left[\frac{\partial (G_{N+1} - G_N)}{\partial N}\right]_{T,P} dN \qquad \text{Equation (1-14)}$$

Using equation (1-14) the temperature coefficient of ΔG_N can be determined as the following:

$$\frac{\partial \Delta G_N}{\partial T} = -\Delta S_N + \left[\frac{\partial (G_{N+1} - G_N)}{\partial N}\right]_{T,P} \left(\frac{\partial N}{\partial T}\right)_P \qquad \text{Equation (1-15)}$$

By substituting the standard thermodynamic relationship ($\Delta G_N = \Delta H_N - T\Delta S_N$) as well as equation (1-12) into equation (1-15), we shall have:

$$RT^2 \left[\frac{\partial \ln(CMC)}{\partial T}\right]_P = -\Delta H_N + T \left[\frac{\partial (G_{N+1} - G_N)}{\partial N}\right]_{T,P} \left(\frac{\partial N}{\partial T}\right)_P \qquad \text{Equation (1-16)}$$

The left side of equation (1-16) corresponds to van't Hoff relationship. However, the last term of this equation clearly demonstrates that van't Hoff equation can be employed in calculating enthalpy of assembly only if $\left(\frac{\partial N}{\partial T}\right)_P$ is zero. This condition holds when the temperature variation does not affect the aggregation number [64]. Therefore, calorimetry has been suggested as a more

reliable technique compared to van't Hoff for measurement of the enthalpy of self-assembly.

Table 1-2. Highlights of the works discovering mechanisms of molecular self-assembly

Molecule	Technique	Information	Citation
$C_{16}A_4G_3S(P)KGE$-COOH	Oscillatory Rheology	Counter-ion screening triggers the self-assembly	[56]
Eggshell Matrix Protein (Pelovaterin)	ITC	Nanosphere self-assembly is entropically-driven	[68]
Enamel Matrix Protein (Amelogenin)	ITC	Self-assembly is entropically-driven with hydrophobic interactions being the main driving force	[69]
Poly-amidoamine dendrimer and azo-dye	ITC, Dynamic Light Scattering	The size of self-assembled structure is correlated to the free energy of association	[70]
L- and D- $(FKFE)_2$	ITC	Self-assembly into "rippled b-sheet" format is more enthalpically favourable than self-assembly into fibrils composed of all-L or all-D peptides	[71]
$(RADA)_4$ $(RADA)_4$-S_5 $(RADA)_4$-K_5	ITC, AFM	Self-assembly is entropically-driven, Hydrophobic interactions are driving $(RADA)_4$ self-assembly and hydrogen bonding is the main driving force for $(RADA)_4$-S_5 self-assembly, Counter-ions do not play a critical role in self-assembly	[72]

At the end, it is important to note that the information presented above highlights the great potential of fundamental studies on peptide self-assembly.

Despite the importance of understanding the underlying mechanisms of peptide self-assembly, there have been only a limited number of works reported that mechanistically discuss this phenomenon. Most of which, however, have utilized simulation techniques [65-67]. The works that have investigated molecular self-assembly utilizing evidence-based experimental approaches are summarized in Table 1-2.

1.4. Non-Specific Protein Adsorption

1.4.1. Strategies to Inhibit Non-Specific Protein Adsorption

In order to be able to develop strategies for impeding non-specific protein adsorption to surfaces, it is necessary to obtain a mechanistic understanding of the molecular basis of this process. Since the 1960's [73], when the first paper on non-specific protein adsorption was published, there have been different lines of thoughts introduced, each of which deals with fouling-resistance from a different perspective. The earliest theories were focused upon the role of steric repulsion forces in repelling a protein from the surface (physical viewpoint). However, years later, the water structure at the interface and hydrogen bonding was proposed to play a critical role in fouling-resistance of surfaces (chemical viewpoint) [53]. Furthermore, the conformation of the molecules at the interface had to be brought into play due to the angle-dependency of hydrogen bonding [74].

Although widely studied, the use of poly ethylene glycol (PEG) as a non-fouling coating has some major disadvantages, namely, loss of function due to

oxidation *in vivo* [76,77] and possible toxicity of its degradation by-products [78]. It has also been shown that the anti-fouling properties of PEG is reduced upon exposure to complex media (blood serum or plasma) as compared to model media (single protein) [79]. Recently, surfaces grafted with zwitterionic polymers have been shown to be a very promising alternative non-fouling architecture that exhibits a higher *in vivo* stability than PEG [80]. A sub-category of these materials include polybetaines, which are distinguished by carrying a positive and a negative charge on the same monomer segment of the polymer chain. The family of polybetaines includes phosphobetaines (PB), sulfobetaines (SB), and carboxybetaines (CB) [81]. There have been a number of studies examining how the physicochemical properties of polybetaines affect their non-fouling characteristics (Table 1-3). In general, it has been seen that grafting density was one of the most widely discussed factors, where increasing the grafting density of zwitterionic polymer was shown to increase the hydrophilicity of the surface as well as its resistance to protein adsorption [82-84]. Conversely, increasing the thickness of the polymer film on the surface did not follow the same trend as the grafting density [85]. In fact, studies have shown that there is an optimum thickness for the grafted film (measured by either ellipsometry or atomic force microscopy), at which the protein adsorption onto surfaces grafted with polybetaines was undetectable using surface plasmon resonance techniques [85-88].

Table 1-3. Important papers on polybetaines and studies published on the role of physicochemical properties in their anti-fouling behaviour.

Author, year	System	Major Conclusion
Kadoma et.al., 1978 [89]	PB	First report on synthesis and blood compatibility
Lowe et.al. 2000 [90]	SB	First report on anti-fouling behaviour
West et.al., 2004 [91]	SB and PB	Superior anti-fouling properties of PB compared to SB, the major drawback of PB: very complex synthetic methods
Chen et.al., 2005 [92]	PB	Two important factors for anti-fouling properties: Charge balance and minimized dipole
Zhang et.al., 2006 [93]	CB	First report on synthesis, grafting and super-low fouling behaviour
Zhang et.al., 2006 [94]	SB	Optimum film thickness (5-12 nm): highly resistant to fibrinogen adsorption
Zhang et.al., 2008 [95]	CB	Longer spacer groups: more protein adsorption onto surface
Yang et.al., 2009 [85]	CB	Optimum film thickness (21 nm): ultra-low protein adsorption (i.e. <5 ng/cm^2)
Shih et.al., 2010 [96]	SB	Optimum M_w for ultra-low fouling properties: 135 kDa at physiologic temperature
Chang et.al., 2011 [97]	SB	Plasma treatment time of 90 seconds: the surface with highly balanced charge and lowest protein adsorption
Chang et.al., 2012 [83]	SB	Higher grafting density: lower protein adsorption and better capacity in stem cell preservation
Brault et.al., 2012 [82]	CB	Minimum of ~1.5 for refractive index: ultra-low protein adsorption

It is thought that optimal architectures for inhibiting protein adsorption should meet the following criteria: i) hydrophilicity, ii) surface charge neutrality, and iii) being an H-bond acceptor (not a donor) [98]. Surface hydration has a long history for being considered as a major factor in dictating the non-fouling

behaviour of materials [99,100]. Along with this, it was proposed that the superior anti-fouling properties of polybetaines may be due to a very stable hydration shell created by strong electrostatic interactions with water [101]. This is opposed to neutral and hydrohphilic PEG where the hydration layer formed on its surface occurs through hydrogen bonding, which is much weaker than the electrostatic force driving the interaction of zwitterion with water molecules [86,92,96]. Attesting to the differences in strength of interaction of water is the free energy changes for hydration of grafted zwitterionic polymer chains (-404 kJ/mol and -519 kJ/mol for carboxybetaine and sulfobetaine, respectively) that are significantly lower than that for grafted oligo(ethylene glycol) (-182 kJ/mol) [102]. Although the total surface energies of different polybetaines was shown to be in the same range (~ 66 mJ/m^2) [103], considering the Hofmeister series for different salts [104] it can be concluded that the interaction of all different types of polybetaines (bearing phosphonate, sulfonate, or carboxylate moieties) with water would not necessarily be the same. Simulation studies performed on carboxybetaine and sulfobetaine proved that the positively charged group on the zwitterionic segment (i.e. quaternary amine group present on both of these polymers) is more hydrated than their negatively charged group [103]. On the other hand, comparison between the negatively charged groups of these polymers led to the conclusion that a larger number of water molecules with higher mobility were bound to the chaotropic sulfonate moiety rather than kosmotropic carboxylate moiety. It was speculated that this is the main reason for lower friction on the surface of sulfobetaine compared to carboxybetaine [105,106].

These are important indications which might be helpful in designing novel zwitterionic molecules in future.

Previously, nonfouling characteristics of high molecular weight PEG were attributed to ‘steric repulsion’ mechanisms [107-110]. However, work surrounding the use of self-assembled monolayers (SAM) of oligo(ethylene glycol) (OEG) exhibited excellent resistance to protein adsorption [111,112]. Considering monodispersity and the confined boundaries of OEG-SAM, the idea of ‘steric repulsion’ being the only major mechanism for inhibiting surface protein interactions was in serious question [113]. Instead, polymer hydration (both internal and on the layers surface) began to be recognized as an important factor for imbuing antifouling behaviour to PEG-coated surfaces [114-116]. The impact of hydration on protein-repellent properties of zwitterionic-based materials was firstly discussed by Ishihara *et.al.* [117]. Results of their study suggested the significant role of free water surrounding 2-methacryloyloxyethyl phosphorylcholine (MPC) polymer in its resistance to protein adsorption. He *et.al.* [118] also utilized molecular simulation to study phosphorylcholine-SAMs as a model system. It was shown that the residence time of water molecules near the zwitterionic surface was much longer compared to those in the vicinity of OEG surface. It was also speculated that this hydration layer above the zwitterionic surface may greatly impact the propensity for proteins to adsorb [118]. The results of Nuclear Magnetic Resonance (NMR) studies on poly (sulfobetaine methacrylate) revealed that there are almost eight water molecules more tightly bound to sulfobetaine segments vs. only one water molecule bound to EG

segment in PEG. Furthermore, the water molecules within the zwitterion-bound hydration layer showed higher mobility compared to those associated with PEG [119]. Hence it was proposed that dynamic profile, quantity and state of the water molecules within the hydration layer are crucial factors that dictate the protein surface interaction.

Although different in structure, ion pairing between the protein and the surface (instead of surface hydration) was introduced as an influential factor that may also govern the non-fouling properties of these materials. More specifically, Estephan *et.al.* [120] attributed the anti-fouling behaviour of PEG and zwitterionic materials largly to the neutrality of their surface charge, which results in lack of counter-ion release from the surface of these materials upon exposure to protein solutions. However, current proposed mechanisms are largely lacking a detailed understanding of the interactions at the molecular level.

1.4.2. Driving Forces Responsible for Non-Specific Protein Adsorption

According to van Oss *et.al.* [121] the primary interfacial forces that contribute to the adsorption of a protein to a surface include van der Waals forces (F_{vdw}), electrostatic forces (F_{el}), and electron-donor/electron-acceptor (Lewis acid-base) interactions (F_{ab}):

$$F = F_{vdw} + F_{el} + F_{ab} \qquad \text{Equation (1-17)}$$

In the following, we shall discuss these three types of primary forces involved in non-specific protein adsorption.

1.4.2.1. van der Waals forces

This type of force has apolar characteristics and includes three categories: dipole-dipole interactions (van der Waals-Keesom), dipole-induced dipole interactions (van der Waals-Debye), and fluctuating dipole-induced dipole interactions (van der Waals-London) [121]. Utilizing the surface thermodynamic method, Israelachvili *et.al.* calculated the van der Waals interaction free energy (ΔG_{vdw}) as the following [57]:

$$\Delta G_{vdw} = -\frac{A}{12\pi \ell_o^2} \qquad \text{Equation (1-18)}$$

where ℓ_o is the distance between two van der Waals interacting surfaces which is usually measured to be 1.57± 0.09 Å, and A is the Hamaker constant. It is important to note that the Hamaker constant is proportional to the apolar factor of surface tension, which can be obtained *via* contact angle measurements [121]. The solution properties (such as pH, ionic strength, etc.) do not contribute to van der Waals interactions, and this type of force is normally dependant on the chemical characteristics of the interacting surfaces [57].

1.4.2.2. Electrostatic Interactions

The polar nature of the biological environment makes it necessary to consider the importance of electrostatic interactions in protein adsorption studies. The DLVO theory links electrostatic interactions to van der Waals forces in order to explain the stability of colloidal systems. Although DLVO theory is based on a balance between attractive van der Waals and repulsive electrostatic interactions,

the latter can be either attractive or repulsive in aqueous media depending on the sign and value of the surface potential of interacting surfaces. It is important to note that unlike van der Waals forces, the electrostatic interactions depend strongly on solution properties such as pH and ionic strength [57].

Utilizing the surface potential of the molecules (Ψ_o), the free energy of electrostatic interaction (ΔG_{el}) between a sphere with radius R and a flat surface at a distance ℓ was calculated [121]:

$$\Delta G_{el} = R\Psi_o^2 \varepsilon \, ln[1 + exp(-\kappa \ell)] \qquad \text{Equation (1-19)}$$

where ε is the dielectric constant of the solvent, and 1/κ is the Debye length which is the thickness of the electronic double layer. This parameter is proportional to the inverse of ion concentration in solution as well as the inverse of valence of those ions. Therefore, increasing the salt concentration in solution (ionic strength) or utilizing salts with a higher valence would result in a thinner double layer (smaller Debye length) and thereby lower ΔG_{el}. This explains why high ionic strength can impede the electrostatic interactions in solutions (also known as charge-screening effects). Direct proportionality of Ψ_o to ζ-potential, would make the latter another determining factor in ΔG_{el} calculations. Knowing that ζ-potential, itself, is directly proportional to the viscosity and the inverse of dielectric constant (ε) would definitely have an impact on further investigation of interfacial forces in protein adsorption.

1.4.2.3. Electron Donor-Electron Acceptor Interactions (Lewis Acid-Base Interactions)

This type of interaction is normally categorized as polar interactions; however their origin is different from electrostatic or electrodynamic (van der Waals) forces. The two most important subsets of electron donor-electron acceptor interactions (ab interactions) are "hydrophobic force" and "hydration pressure" [121]. While hydrophobic forces mainly are categorized as attractive, the hydration pressure is known to have a repulsive character. Interestingly, despite the polar nature of ab interactions, solution ionic strength does not seem to contribute to the strength of this type of forces. The decay length of these forces in water is expected to be ~ 1 nm while the energy associated with them can be much larger than that of electrostatic or van der Waals interactions in aqueous media [121]. This is why the traditional DLVO theory, which only considers the interplay of van der Waals and electrostatic interactions, often fails to describe the total energy balance in water. Therefore an extended version of DLVO theory (XDLVO) was proposed which takes into account the ab forces between interacting molecules in aqueous solvents [121].

Hydrophobic attractions between apolar segments in aqueous media are basically driven by free energy of cohesion of water molecules which are strictly bound together *via* hydrogen bonding. In other words, it is the strong attachment of water molecules to each other which allows for the two hydrophobic segments to interact. This explains why van der Waals contribution to hydrophobic

interactions between apolar groups in water was found to be negligible [57]. It was also shown that hydrophobic attractions are mostly temperature-dependant: an effect usually observed for entropically-driven phenomena [57].

The repulsive hydration forces are usually observed at short distances between two extremely hydrophilic surfaces immersed in water. However, they can also manifest themselves as long-range repulsive forces between domains of extremely organized water shells surrounding hydrophilic entities [121].

Other than the primary forces involved in non-specific protein adsorption explained above, there are also other secondary types of forces that are not as common as the forces already mentioned; however they can play a critical role in protein adsorption process and should be taken into account depending on the characteristics of the systems under study. Among them are Brownian motions (which usually cause the osmotic pressure interactions), steric interactions, and depletion forces.

1.4.3. Understanding the Concept of Equilibrium in Protein Adsorption

The equilibrium condition for protein adsorption to a porous material with a constant mass (m^s) immersed in an aqueous solution containing n_0^f moles of protein with constant volume (V^f) and temperature (T) can be described in terms of chemical potential (μ) of the protein in free and adsorbed states as the following [122]:

$$\mu^a(n^a, m^s, T) = \mu^f\left(c = \frac{n^f}{V^f}, T\right) \qquad \text{Equation (1-20)}$$

where the sum of n^a (moles of the protein adsorbed) and n^f (moles of free protein in solution) should return the value for n_0^f (i.e. $n^a + n^f = n_0^f =$ constant). The concept of equilibrium in protein adsorption has been a source of controversy in this field, throughout the years. The classical paradigm for describing thermodynamics of protein adsorption is to utilize the Langmuir isotherm along with van't Hoff equation [123,124]. However, in order to be able to employ this method, it is necessary for the following conditions to hold [122]:

i) the adsorbed protein forms a monolayer on the surface;

ii) the binding sites are energetically-equivalent and independent;

iii) there is no protein-protein interaction inside the protein corona;

iv) the system is at an equilibrium state, requiring process reversibility.

As previously explained the results obtained by ITC for non-specific protein adsorption are usually analyzed using the model for "single set of independent binding sites" which is a derivation of the Langmuir model. A summary of the works investigating non-specific protein interactions with solid surfaces utilizing ITC is presented in Table 1-4.

Table 1-4. Summary of the works investigating protein-solid surface interactions *via* ITC.

Surface	Protein	Information	(Year) Citation
Acrylamide-based nanoparticles	HSA	Effect of hydrophobicity and curvature of nanoparticles on thermodynamic parameters was discussed	(2007) [125]
Amino acid-functionalized Au nanoparticles	Chymotrypsin, Histone, Cytochrom C	Distribution of charge and hydrophobic groups on NP surface affected enthalpy and entropy changes; EEC analysis confirmed biomimetic behaviour of nanoparticles	(2007) [126]
Zirconium Phosphate	Hemoglobin, Myoglobin, Lysozyme	Protein's surface charge influenced binding enthalpy; With polar groups playing a key-role, proton-coupled mechanisms was found to be the major protein binding process	(2009) [127]
ZnO nanoparticles	ToxRp	The interaction was enthalpically-driven with electrostatic and van der Waals forces playing a dominant role	(2010) [128]
PEG-functionalized iron oxide nanoparticles	BSA, IgG	Protonation of iron oxide core caused strong BSA adsorption	(2010) [129]
Spherical poly electrolyte brushes (with poly styrene core)	β-Lactaglobulin	Protein adsorption was driven by entropy caused by counter-ion release	(2010) [130]
Poly styrene-based nanoparticles	BSA	Effect of solution pH and overall charge of nanoparticles on protein adsorption was studied	(2011) [131]
Au nanoparticles/ Au nanorods	BSA	Higher binding constants and entropy changes was observed for nanorod structures; Exothermic binding to nanoparticles *Vs.* endothermic binding to nanorods was observed	(2011) [132]
Au nanoparticles	HSA	Electrostatic interactions and hydrogen bonding were driving the adsorption	(2012) [133]
Polymer-functionalized Zno nanoparticles	BSA	Electrostatic interactions were driving the adsorption	(2012) [134]
Acrylamide-base nanoparticles	Heparin	Interaction is enthalpically-driven with hydrogen bonding, ionic interactions, and desolvation of polar groups as the main driving force	(2012) [135]

On the other hand, a paradigm dealing with protein adsorption as being "not-irreversible" has been postulated. This was firstly shown through solution-depletion experiments confirming dissociation of adsorbed proteins from the surface in solution [138]. It should be noted that calling a process "not-irreversible" does not necessarily indicate "reversibility" of that process [139]. In other words, a process can be "not-irreversible" but not "reversible"; as the condition for reversibility of a process is that all variables (e.g. concentration, pressure, etc.) describing the system at any point along the reverse pathway of a process (i.e. desorption) represent the same value for that particular state in the direct order of that process (i.e. for this case adsorption). According to Vogler *et.al.* [139] thermodynamic equilibrium and reversibility are the two characteristics of ideal systems which are very hard to achieve through experimental methods used in the lab for protein adsorption studies. However, as they also have pointed out, lack of ideality in a system does not interfere with application of thermodynamics as a modeling tool.

The recently introduced concept of "hard" and "soft" protein corona formation on the surface of nanomaterials is another factor which should be considered while discussing the reversibility of protein adsorption. It was observed that, upon exposure of a surface to the complex physiological media, the proteins with a high affinity for the surface get strongly adsorbed and form a tightly-bound "hard" corona on the surface with very slow exchange rates. On the other hand, the proteins with a lower affinity for the surface create a "soft" corona consisting of loosely-bound proteins on the surface which can get rapidly

exchanged with the other proteins present in surrounding media [140-142]. A study on NIPAM/BAM copolymer nanoparticles proved that the soft corona dissociates from the surface during ~10 minutes; however, it can take ~8 hours before the desorption of hard corona even begins [143].

The equilibrium is known as the state of a system in which the net displacement of balance within that system is zero. Such condition in which the reaction (here: protein desorption) does not take place despite the affinity for it is not zero (thereby the system's balance is maintained) is called a false equilibrium or meta-stable state [144]. It was claimed that systems within a prolonged meta-stable state can be analyzed thermodynamically in the same way as the ones at equilibrium condition [144]. However, it should be noted that the parameters obtained in this way cannot be referred to as the parameters for equilibrium state and should be distinguished through using appropriate nomenclatures such as "apparent" parameter.

1.5. Research Proposal

1.5.1. Rationale

The complex nature of macromolecular interactions usually makes it very hard to identify the molecular-level mechanisms that ultimately dictate the result of these interactions. This is especially evident in the case of biological systems, where the complex interaction of molecules in various situations may be responsible for driving biomacromolecular interactions themselves, but also have a broader effect at the cell and/or tissue level. Clarifying the molecular-level

interactions of bio-macromolecules is not a trivial task and therefore several experimental techniques currently exist for studying various aspects of these interactions; including but not limited to: Surface Plasmon Resonance (SPR), Analytical Ultracentrifugation (AUC), and Isothermal Titration Calorimetry (ITC). All of these techniques have advantages and disadvantages in their application to the study of these systems (See Table 1-1). This thesis will endeavor to further the understanding of bio-macromolecular interactions using Isothermal Titration Calorimetry technique, coupled with a detailed thermodynamic analysis for two extremely important biomaterial systems, *viz.* peptide self-assembly and non-fouling polymer modified surfaces. These systems were chosen to be studied due to the fact that they are wide-spread in application, have some degree of freedom due to molecular complexity, whilst lending themselves to this style of experimentation. Furthermore, as reviewed above, the underlying mechanisms proposed as the driving force for peptide self-assembly and non-specific protein adsorption are extremely similar. With that in mind, herein we present a fundamental thermodynamic investigation of peptide self-assembly and protein adsorption to gain a molecular-level understanding of these processes; a knowledge which will definitely lead to design and engineering of advanced bio-compatible/bio-mimetic materials in future.

1.5.2. Objectives

This thesis will be an endeavor to answer the following questions:

- What is the role of hydration and charge in peptide self-assembly?

- What is the contribution of hydrophilic/hydrophobic forces to self-assembly process? Can it be fine-tuned utilizing peptide chemistry?
- What is the role of interfacial molecules (waters and ions) in peptide self-assembly?
- Fouling resistance of zwitterionic polymers have been attributed to the balance of their surface charges; what happens at the interface of these polymers and an electrostatically-interactive protein? What happens in case of a hydrophobically-interactive protein?
- How does zwitteration of a surface impact the thermodynamics of its interaction with proteins?
- What is the nature of zwitterionic surface's interaction with proteins?
- It has been suggested that longer spacer group inside the zwitterion will lead to lower fouling resistance; does thermodynamics of adsorption approve this?
- What is the role of water molecules and counter-ions? How do they engage in the adsorption or repulsion of the protein from the surface?
- Can an enthalpy-entropy compensation profile be defined for these systems?

1.5.3. Scope of Dissertation

In the following chapter, self-assembly of RADA16 peptide will be thermodynamically investigated. In order to be able to identify the role of hydration and charge in peptide self-assembly, other variants of this peptide (with different chemistries) should be studied as well. Appending residues such as serine (which is neutral and promotes hydrogen bonding) or lysine (which is positively charged) to the peptide chain will be considered. With the aim of quantifying the hydrophilic/hydrophobic contributions to the assembly process, experiments should be performed at different temperatures to be able to calculate the heat capacity change (which is usually known as an indicator for changes in the solvent exposed surface area). Furthermore, variations in solvent composition (i.e. osmolyte or salt concentrations) and its effect on thermodynamic profile can be utilized to probe the number of water molecules and counter-ions involved in self-assembly (**Chapter 2**).

In order to investigate the thermodynamics of non-specific protein adsorption, silica nanoparticles (NPs) modified with zwitterionic carboxybetaine polymer will be used. Through utilizing polymers with different end-group chemistry and/or zwitterion's spacer length, the impact of polymer characteristics on thermodynamic properties of protein adsorption can be determined. Since both size and charge of the protein molecule can play a critical role in its adsorption to surfaces, the adsorption of two model proteins with different size and similar surface charge (i.e. α-Lactalbumin (**Chapter 3**) and Human Serum Albumin

(**Chapter 4**)) to polymer-functionalized NPs will be investigated using ITC. Another factor which should be taken into account is the temperature which can contribute to both adsorption process and energy profile of the system. To fulfill the aim of quantifying the interfacial parameters driving the protein adsorption, it is necessary to probe the interfacial molecules (counter-ions and water molecules). This can be performed through investigating the effect of solution's ionic strength on thermodynamic properties of the adsorption. Furthermore, analysis of enthalpy-entropy compensation effects for these systems can deliver valuable information regarding conformational changes as well as the extent of dehydration of the interface upon protein adsorption (**Chapters 3 & 4**).

1.6. References

[1] Ladbury, J. E.; Doyle, M. L. Biocalorimetry 2: Applications of calorimetry in the biological sciences. Chichester, West Sussex, England: John Wiley & Sons **2004**.

[2] Wu, J. G.; Li, J. Y.; Li, G. Y.; Long, D. G.; Weis, R. M. *Biochemistry* **1996**, 35 (15), 4984–4993.

[3] Garciafuentes, L.; Reche, P.; Lopezmayorga, O.; Santi, D. V.; Gonzalezpacanowska, D.; Baron, C. *Eur. J. Biochem.* **1995**, 232 (2), 641–645.

[4] Qu, X. G.; Ren, J. S.; Riccelli, P. V.; Benight, A. S.; Chaires, J. B. *Biochemistry* **2003**, 42 (41), 11960–11967.

[5] Livingstone, J. R. *Nature* **1996**, 384 (6608), 491–492.

[6] Cheng, C. I.; Chang, Y-P; Chu, Y-H *Chem. Soc. Rev.* **2012**, 41, 1947–1971.

[7] Rowe, A. J. *Methods* **2011,** 54, 157–166.

[7] Chiad, K.; Stelzig, S. H.; Gropeanu, R.; Weil, T.; Klapper, M.; Müllen, K. *Macromolecules* **2009**, 42, 7545–7552.

[8] Devred, F.; Barbier, P.; Lafitte, D.; Landrieu, I.; Lippens, G.; Peyrot, V. *Methods in Cell Biol*. **2010**, 95, 449–480.

[9] Velázquez-Campoy, A.; Ohtaka, H.; Nezami, A.; Muzammil, S.; Freire, E. *Current Protocols in Cell Biology* **2004**, 17, 1-24.

[10] Ladbury, J. E.; Chowdhry, B. Z. *Chem. Biol*. **1996**, 3, 791–801.

[12] Leffler, J. E. *J. Org. Chem.* **1955**, 20, 1202.

[13] Rekharsky, M. V.; Inoue, Y.; *Chem. Rev.* **1998,** *98,* 1875-1917.

[14] Cooper, A.; Johnson, C. M.; Lakey, J. H.; Nollmann, M. L. *Biophysical Chemistry* **2001**, 93, 215-230.

[15] Chodera, J. D.; Mobley, D. L. *Annu. Rev. Biophys.* **2013**, 42, 121–42.

[16] Perez-Benito, J. F. *Monatsh Chem* **2013**, 144, 49–58.

[17] Sharp, K. *Protein Sci.* **2001**, 10, 661-667.

[18] Breiten, B.; Lockett, M.R.; Sherman, W.; Fujita, S.; Al-Sayah, M. H.; Lange, H.; Bowers, C.M.; Heroux, A.; Krilov, G.; Whitesides, G. M. *J. Am. Chem. Soc.* **2013**, 135, 15579−15584.

[19] Ulijn, R. V.; Smith, A. M. *Chem. Soc. Rev.* **2008**, 37, 664–675.

[20] Maude, S.; Ingham, E.; Aggeli, A. *Nanomedicine* **2013**, 8, 823–847.

[21] Hausera, C. A. E.; Zhang, S. *Chem. Soc. Rev.* **2010**, 39, 2780–2790.

[22] Dasgupta, A.; Mondal, J. H.; Das, D. *RSC Adv.* **2013**, 3, 9117–9149.

[23] Zhao, X.; Pan, F.; Xu, H.; Yaseen, M.; Shan, H.; Hausera, C. A. E.; Zhang, S.; Luab, J. R. *Chem. Soc. Rev.* **2010**, 39, 3480–3498.

[24] Mart, R. J.; Osborne, R. D.; Stevens, M. M.; Ulijn, R. V. *Soft Matter* **2006**, 2, 822.

[25] Schneider, J. P.; Pochan, D.; Ozbas, J.; Rajagopal, B. K.; Pakstis, L.; Kretsinger, J. *J. Am. Chem. Soc.* **2002**, 124, 15030.

[26] Hartgerink, J. D.; Beniash, E.; Stupp, S. I. *Science* **2001**, 294, 1684.

[27] Xiong, H.; Buckwalter, B. L.; Shieh, H-M; Hecht, M. H. *Proc. Natl Acad. Sci. USA* **1995**, 92, 6349–6353.

[28] Measey, T. J.; Schweitzer-Stenner, R. *J. AM. CHEM. SOC.* **2006**, 128, 13324-13325.

[29] Bowerman, C. J.; Liyanage, W.; Federation, A. J.; Nilsson, B. L. *Biomacromolecules* **2011**, 12, 2735–2745

[30] Geisler, I. M.; Schneider, J. P. *Adv. Funct. Mater.* **2012**, 22, 529–537.

[31] Pochan, D. J.; Schneider, J. P.; Kretsinger, J.; Ozbas, B.; Rajagopal, K.; Haines, L. *J. Am. Chem. Soc.* **2003**, 125, 11802–11803.

[32] Rapaport, H.; Grisaru, H.; Silberstein, T. *Adv. Funct. Mater.* **2008**, 18, 2889–2896.

[33] Aggeli, A.; Bell, M.; Boden, N.; Keen, J. N.; McLeish, T. C. B.; Nyrkova, I.; Radford, S. E.; Semenov, A. *J. Mater. Chem.* **1997**, 7, 1135–1145.

[34] Aggeli, A.; Nyrkova, I. A.; Bell, M.; Harding, R.; Carrick, L.; McLeish, T. C. B.; Semenov, A. N.; Boden, N. *Proc. Natl. Acad. Sci. U. S. A.* **2001**, 98, 11857–11862.

[35] Yang, Y.; Khoe, Y.; Wang, X.; Horii, A.; Yokoi, H.; Zhang, S. *Nano Today* **2009**, 4, 193-210.

[36] Yokoi, H.; Kinoshita, T.; Zhang, S. *Proc. Natl. Acad. Sci. U. S. A.* **2005**, 102, 8414-8419.

[37] Marqusee, S.; Robbins, V. H.; Baldwin, R. L. *Proc. Natl. Acad. Sci. U. S. A.* **1989,** 86, 5286-5290.

[38] Scholtz, J.M; Marqusee, S.; Baldwin, R. L.; York, E. J.; Stewart, J. M.; Santoro, M; Bolden, D. W. *Proc. Natl. Acad. Sci. U. S. A.* **1991**, 88, 2854-2858.

[39] Branco, M.; Nettesheim, F.; Pochan, D. J.; Schneider, J. P.; Wagner, N. J. *Biomacromolecules* **2009**, 10, 1374–1380.

[40] Nowak, A. P.; Sato, J.; Breedveld, V.; Deming, T. J.; *Supramol. Chem.* **2006**, 18, 423–427.

[41] Nowak, A. P.; Breedveld, V.; Pakstis, L.; Ozbas, B.; Pine, D. J.; Pochan, D.; Deming, T. J. *Nature* **2002**, 417, 424–428.

[42] Nowak, A. P.; Breedveld, V.; Pine, D. J.; Deming, T. J. *J. Am. Chem. Soc.* **2003**, 125, 15666–15670.

[43] Pochan, D. J.; Pakstis, L.; Ozbas, B.; Nowak, A. P.; Deming, T. J. *Macromolecules* **2002**, 35, 5358–5360.

[44] Holowka, E. P.; Pochan, D. J.; Deming, T. J. *J. Am. Chem. Soc.* **2005**, 127, 12423–12428.

[45] Li, Z.; Deming, T. J. *Soft Matter* **2010**, 6, 2546–2551.

[46] Breedveld, V. A.; Nowak, P.; Sato, J.; Deming, T. J.; Pine, D. J.; *Macromolecules* **2004**, 37, 3943–3953.

[47] Katchalski, E.; Sela, M. *Adv. Protein Chem.* **1958**, 13, 243–492.

[48] Ruana, L.; Zhanga, H.; Luoa, H.; Liua, J.; Tanga, F.; Shib, Y. K.; Zhao, X. *Proc. Natl. Acad. Sci. U. S. A.* **2009**, 106, 5105–5110.

[49] Matson, J. B.; Zha, R. H.; Stupp, S. I. Current Opinion in Solid State and Materials Science 15 (2011) 225–235

[50] Aida, T.; Meijer, E. W.; Stupp, S. I. *Science* **2012**, 335, 813-817.

[51] Hatgerink, J. D.; Beniash, E.; Stupp, S. I. *Science* **2001**, 294, 1684–1688.

[52] Franceschi, S.; Viguerie, N.; Riviere, M.; Lattes, A. *New J. Chem.* **1999**, 23, 447–452.

[53] Claussen, R. C.; Rabatic, B. M.; Stupp, S. I. *J. Am. Chem. Soc.* **2003**, 125, 12680–12681.

[54] Tu, R. S.; Tirrell, M. *Adv. Drug Deliv. Rev.* **2004**, 56, 1537–1563.

[55] Butt, H. J. Biophys. J. o Biophysical Society Volume 60 December 1991 1438-1444.

[56] Stendahl, J. C.; Rao, M. S.; Guler, M. O.; Stupp, S. I. *Adv. Funct. Mater.* **2006**, *16*, 499–508.

[57] Israelachvili, J. *Intermolecular and Surface Forces*, Academic Press, San Diego, CA **1992.**

[58] Cao, M.; Cao, C.; Zhang, L.; Xia, D.; Xu, H. *J. Colloid Interface Sci.* **2013**, 407, 287–295.

[59] Urry, D.W. *Proc. Natl. Acad. Sci. U. S. A.* **1971**, 68, 672.

[60] Desantis, P.; Morosett, S.; Rizzo, R. *Macromolecules* **1974**, 7, 52– 58.

[61] J.D. Hartgerink, Granja, J. R.; Milligan, R. A.; Ghadiri, M. R. *J. Am. Chem. Soc.* **1996**, 118, 43– 50.

[62] Tanford, C. *The hydrophobic effect*. New York: John Wiley & Sons **1980**.

[63] Emerson, M. F.; Holtzer, A. *J. Phys. Chem.* **1965**, *69*, 3718.

[64] Holtzer, A.; Holtzer, M. F. *J. Phys. Chem.* **1974**, *78*, 1442.

[65] Fu, I. W.; Markegard, C. B., Chu, B. K.; Nguyen, H. D. *Adv. Healthcare Mater.* **2013**, 2, 1388–1400.

[66] Dagdas, Y. S.; Tombuloglu, A.; Tekinay, A. B.; Dana, A.; Guler, M. O. *Soft Matter* **2011**, 7, 3524.

[67] Cheng, L.; Englander, O.; Paravastu, A.; Oates, W. S. *J. Chem. Phys.* **2011**, 135, 055102.

[68] Lakshminarayanan, R.; Vivekanandan, S.; Samy, R. P.; Banerjee, Y.; Chi-Jin, E. O.; Teo, K. W.; Jois, S. D. S.; Kini, R. M.; Valiyaveettil, S. *J. Am. Chem. Soc.* **2008**, 130 (14), 4660-4668.

[69] Lakshminarayanan, R.; Yoon, I.; Hegde, B. G.; Fan, D.; Du, Ch.; Moradian-Oldak, J. *Proteins* **2009**; 76, 560-569.

[70] Willerich, I.; Gröhn, F. *J. Am. Chem. Soc.* **2011**, 133, 20341-20356.

[71] Swanekamp, R. J.; DiMaio, J. T. M.; Bowerman, C. J.; Nilsson, B. L. *J. Am. Chem. Soc.* **2012**, 134, 5556−5559.

[72] Kabiri, M.; Bushnak, I.; McDermot, M. T.; Unsworth, L. D. *Biomacromolecules* **2013,** 14, 3943-3950.

[73] van Oss, C. J.; Singer, J. M. *J. Reticuloendothelial Soc.* **1966,** 3, 29.

[74] Morra, M. *J. Biomater. Sci. Polym. Ed.* **2000**, 11, 547–569.

[76] Li, L. Y.; Chen, S. F.; Jiang, S. Y. *J. Biomater. Sci., Polym. Ed.* **2007**, *18*, 1415–1427.

[77] Shen, M. C.; Martinson, L.; Wagner, M. S.; Castner, D. G.; Ratner, B. D.; Horbett, T. A. *J. Biomater. Sci., Polym. Ed.* **2002**, *13*, 367–390.

[78] Knop, K.; Hoogenboom, R.; Fischer, D.; Schubert, U. S. *Angew. Chem., Int. Ed.* **2010**, *49*, 6288–6308.

[79] Hucknall, A.; Rangarajan, S.; Chilkoti, A. *Adv. Mater.* **2009**, *21*, 2441–2446.

[80] Jiang, S.; Cao, Z. *Adv. Mater.* **2010**, *22*, 920–932.

[81] Chen, S. F.; Li, L. Y.; Zhao, C.; Zheng, J. *Polymer* **2010**, *51*, 5283–5293.

[82] Brault, N. D.; Sundaram, H. S.; Li, Y. T.; Huang, C. J.; Yu, Q. M.; Jiang, S. Y. *Biomacromolecules* **2012**, *13*, 589–593.

[83] Chang, Y.; Higuchi, A.; Shih, Y. J.; Li, P. T.; Chen, W. Y.; Tsai, E. M.; Hsiue, G. H. *Langmuir* **2012**, *28*, 4309–4317.

[84] Zhao, J.; Shi, Q.; Luan, S.; Song, L.; Yang, H.; Shi, H.; Jin, J.; Li, X.; Yin, J.; Stagnaro, P. *J. Membr. Sci.* **2011**, *369*, 5–12.

[85] Yang, W.; Xue, H.; Li, W.; Zhang, J. L.; Jiang, S. Y. *Langmuir* **2009**, *25*, 11911–11916.

[86] He, Y.; Hower, J.; Chen, S. F.; Bernards, M. T.; Chang, Y.; Jiang, S. Y. *Langmuir* **2008**, *24*, 10358–10364.

[87] Huang, C. J.; Brault, N. D.; Li, Y. T.; Yu, Q. M.; Jiang, S. Y. *Adv. Mater.***2012**, *24*, 1834–1837.

[88] Yang, W.; Chen, S. F.; Cheng, G.; Vaisocherova, H.; Xue, H.; Li, W.; Zhang, J. L.; Jiang, S. Y. *Langmuir* **2008**, *24*, 9211–9214.

[89] Kadoma, Y.; Nakabayashi, N.; Masuhara, E.; Yamauchi, J. *Kobunshi Ronbunshu* **1978**, *35*, 423–427.

[90] Lowe, A. B.; Vamvakaki, M.; Wassall, M. A.; Wong, L.; Billingham, N. C.; Armes, S. P.; Lloyd, A. W. *J. Biomed. Mater. Res.* **2000**, *52*, 88–94.

[91] West, S. L.; Salvage, J. P.; Lobb, E. J.; Armes, S. P.; Billingham, N. C.; Lewis, A. L.; Hanlon, G. W.; Lloyd, A. W. *Biomaterials* **2004**, *25*, 1195–1204.

[92] Chen, S.; Zheng, J.; Li, L.; Jiang, S. *J. Am. Chem. Soc.* **2005**, *127*, 14473–14478.

[93] Zhang, Z.; Chao, T.; Chen, S. F.; Jiang, S. Y. *Langmuir* **2006**, *22*, 10072–10077.

[94] Zhang, Z.; Chen, S. F.; Chang, Y.; Jiang, S. Y. *J. Phys. Chem. B* **2006**, *110*, 10799–10804.

[95] Zhang, Z.; Vaisocherova, H.; Cheng, G.; Yang, W.; Xue, H.; Jiang, S. Y. *Biomacromolecules* **2008**, *9*, 2686–2692.

[96] Shih, Y. J.; Chang, Y. *Langmuir* **2010**, *26*, 17286–17294.

[97] Chang, Y.; Chang, W. J.; Shih, Y. J.; Wei, T. C.; Hsiue, G. H. *ACS Appl.Mater. Interfaces* **2011**, *3*, 1228–1237.

[98] Holmlin, R. E.; Chen, X. X.; Chapman, R. G.; Takayama, S.; Whitesides, G.M. *Langmuir* **2001**, *17*, 2841–2850.

[99] Noh, H.; Vogler, E. A. *Biomaterials* **2007**, *28*, 405–422.

[100] Parhi, P.; Golas, A.; Vogler, E. A. *J. Adhes. Sci. Technol.* **2010**, *24*, 853–888.

[101] Chen, N.; Maeda, N.; Tirrell, M.; Israelachvili, J. *Macromolecules* **2005**, *38*, 3491–3503.

[102] Shao, Q.; He, Y.; White, A. D.; Jiang, S. Y. *J. Phys. Chem. B* **2010**, *114*, 16625–16631.

[103] Wu, L.; Jasinski, J.; Krishnan, S. *J. Appl. Polym. Sci.* **2012**, *124*, 2154–2170.

[104] Cacace, M. G.; Landau, E. M.; Ramsden, J. J. *Q. Rev. Biophys.* **1997**, *30*, 241–277.

[105] He, Y.; Shao, Q.; Chen, S. F.; Jiang, S. Y. *J. Chem. Phys.* **2011**, *135*.

[106] Colak, S.; Tew, G. N. *Biomacromolecules* **2012**, *13*, 1233–1239.

[107] McPherson, T.; Kidane, A.; Szleifer, I.; Park, K. *Langmuir* **1998**, *14*, 176–186.

[108] Jeon, S. I.; Lee, J. H.; Andrade, J. D.; de Gennes, P. G. *J. Colloid Interface Sci.* **1991**, *142*, 149.

[109] Pertsin, A. J.; Grunze, M.; Garbuzova, I. A. *J. Phys. Chem. B* **1998**, *102*, 4918–4926.

[110] Tasaki, K. *J. Am. Chem. Soc.* **1996**, *118*, 8459–8469.

[111] Prime, K.; Whitesides, G. *Science* **1991**, *252*, 1164–1167.

[112] Palegrosdemange, C.; Simon, E. S.; Prime, K. L.; Whitesides, G. M. *J. Am.Chem. Soc.* **1991**, *113*, 12–20.

[113] Herrwerth, S.; Eck, W.; Reinhardt, S.; Grunze, M. *J. Am. Chem. Soc.* **2003**, *125*, 9359–9366.

[114] Zheng, J.; Li, L.; Tsao, H.-K.; Sheng, Y.-J.; Chen, S.; Jiang, S. *Biophys. J.***2005**, *89*, 158–166.

[115] He, Y.; Chang, Y.; Hower, J. C.; Zheng, J.; Chen, S.; Jiang, S. *Phys. Chem.Chem. Phys.* **2008**, *10*, 5539–5544.

[116] Hower, J. C.; He, Y.; Jiang, S. *J. Chem. Phys.* **2008**, *129*, 215101.

[117] Ishihara, K.; Nomura, H.; Mihara, T.; Kurita, K.; Iwasaki, Y.; Nakabayashi, N. *J. Biomed. Mater. Res.* **1998**, *39*, 323–330.

[118] He, Y.; Hower, J.; Chen, S.; Bernards, M. T.; Chang, Y.; Jiang, S. *Langmuir* **2008**, *24*, 10358–10364.

[119] Wu, J.; Lin, W.; Wang, Z.; Chen, S.; Chang, Y. *Langmuir* **2012**, *28*, 7436–7441.

[120] Estephan, Z. G.; Schlenoff, P. S.; Schlenoff, J. B. *Langmuir* **2011**, *27*, 6794–6800.

[121] van Oss, C. J. *Interfacial Forces in Aqueous Media*; Marcel Dekker: New York, **1994**.

[122] Keller, J. U. *J. Non-Equilib. Thermodyn*. **2009**, 34, 1-34.

[123] Fontan, R. C. I.; Minim, L. A.; Bonomo, R. C. F.; da Silva L. H. M.; Minim, V. P. R. *Fluid Phase Equilibria* **2013**, 348, 39-44.

[124] Zabka, M.; Rodrigues, A. E. *Separation science and technology* **2007**, 42 739-768.

[125] Lindman, S.; Lynch, I.; Thulin, E.; Nilsson, H.; Dawson, K. A.; Linse, S. *Nano Lett.* **2007**, 7, 914-920.

[126] De, M.; You, C.; Srivastava, S.; Rotello, V. M., *J. Am. Chem. Soc.* **2007**, 129, 10747-10753.

[127] Duff Jr., M. R.; Kumar, C. V. *Langmuir* **2009**, 25(21), 12635–1264.

[128] Chatterjee, T.; Chakraborti, S.; Joshi, P.; Singh, S.P.; Gupta, V.; Chakrabarti, P. *FEBS J.* **2010**, 277, 4184–4194.

[129] Liu, Sh.; Han, Y.; Qiao, R.; Zeng, J.; Jia, Q.; Wang, Y.; Gao, M. *J. Phys. Chem. C* **2010**, *114*, 21270–21276.

[130] Henzler, K.; Haupt, B.; Lauterbach,K.; Wittemann, A.; Borisov, O.; Ballauff, M. *J. Am. Chem. Soc.* **2010**, 132, 3159–3163.

[131] Baier, G.; Costa, C.; Zeller, A.; Baumann, D.; Sayer, C.; Araujo, P. H.; Mailänder, V.; Musyanovych, A.; Landfester, K. *Macromol. Biosci.* **2011**, 11, 628–638.

[132] Chakraborty, S.; Joshi, P.; Shanker, V.; Ansari, Z. A.; Singh, S. P.; Chakrabarti, P. *Langmuir* **2011**, 27, 7722–7731.

[133] Goy-López, S.; Juárez, J.; Alatorre-Meda, M.; Casals, E.; Puntes, V. F.; Taboada, P.; Mosquera, V. *Langmuir* **2012**, 28, 9113−9126.

[134] Chakraborti, S.; Joshi, P.; Chakravarty, D.; Shanker,V.; Ansari, Z. A.; Singh, S. P.; Chakrabarti, P. *Langmuir* **2012**, 28, 11142−11152.

[135] Zeng, Z.; Patel, J.; Lee, S-H.; McCallum, M.; Tyagi, A.; Yan, M.; Shea, K. J. J. *Am. Chem. Soc.* **2012**, 134, 2681−2690.

[136] Norde, W.; Haynes, C. A. *Proteins at Interfaces II. ACS Symp.Ser.* **1995**, 602, 26.

[137] Haynes, C. A.; Norde, W. *J. Colloid Interface Sci.* **1995**, 169, 313.

[138] Leibner, E. S.; Barnthip, N.; Chen, W.; Baumrucker, C. R.; Badding, J. V.; Pishko, M.; Vogler, E. A. *Acta Biomater* **2009**, 5, 1389-1398.

[139] Vogler, E. A. *Biomaterials* 33 (2012) 1201-1237.

[140] Walczyk, D.; Bombelli, F. B.; Monopoli, M. P.; Lynch, I.; Dawson, K. A. *J. Am. Chem. Soc.* **2010**, *132*, 5761–5768.

[141] Lynch, I.; Cedervall, T.; Lundqvist, M.; Cabaleiro-Lago, C.; Linse, S.; Dawson, K. A. *Ad*V. *Colloid Interface Sci.* **2007**, *167*, 134–135.

[142] Walkey, C. D.; Chan, W. C. W. *Chem. Soc. Rev.* **2012**, 41, 2780–279.

[143] Cedervall, T.; Lynch, I.; Lindman, S.; Berggard, T.; Thulin, E.; Nilsson, H.; Dawson, K. A.; Linse, S. *Proc. Natl. Acad. Sci. U. S. A.* **2007**, 104, 2050–2055.

[144] Jennissen, H.P. Protein Adsorption Hysteresis. In *Surface and Interfacial Aspects of Biomedical Polymers" Vol.2, Protein Adsorption*., pp. 295-320. Plenum Press, New York. **1985**.

Chapter 2

Toward a Mechanistic Understanding of Ionic-Self Complementary Peptide Self-Assembly: Role of Water Molecules and Ions[1]

[1]A version of this chapter was published in: Kabiri, M.; Bushnak, I.; McDermot, M. T.; Unsowrth, L. D., "Toward a Mechanistic Understanding of Ionic Self-Complementary Peptide Self-Assembly: Role of Water Molecules and Ions", *Biomacromolecules* **2013,** 14, 3943-3950.

Author Contribution: KM wrote the manuscript and performed the ITC experiments as well as the data analysis.

2.1. Introduction

In general, self-assembly results in the formation of higher order structures from molecular level building blocks through non-covalent interactions and solvation effects. Individually these interactions are relatively weak, but when present in large numbers their cumulative impact ultimately dominates the structural and conformational behavior of the assembly [1]. The main differences observed between self-assembling peptides and other self-assembling molecules (e.g. DNA, collagen, elastin, etc.) arises from the fact that peptides can have a broad range of both chemical composition and structure [2]. As early as 1993, the first work on self-assembling peptides was published, which detailed the formation of extended β–sheet like structures (hollow cylinders) from the self-assembly of small cyclic peptides [3]. Nanofiber forming peptide amphiphiles designed by Stupp *et. al.* also proved fundamental insight that facilitated wide-ranging applications, especially in regenerative medicine [4,5]. Since then major contributions have provided insight into the chemical and structural principles that generally dictate the self-assembly process, where peptides have been grouped according to structure and resulting assembly [1]: Type I, with supposed hydrophilic and hydrophobic sides form anti-parallel β–sheet structures in aqueous solution[4-7]; Type II, molecular structure is responsive to environmental changes and can act as molecular actuators[8-11]; Type III, self-assemble only on surfaces and can be used for surface engineering [12-14]; Type IV, self-assemble into nanotubes and nanovesicles and can be used for drug delivery[15-18]; and

Type V, self-assemble into scaffolds of negatively charged cavities that attract positively charged ions and therefore facilitate the biomineralization process [19,20]. $RADA_4$ based peptides are generally considered Type I ionic self-complementary oligopeptides; where one side of the molecule is thought to consist predominantly of nonpolar, hydrophobic alanine (A), and the other side of alternating oppositely charged amino acids (positively charged arginine (R) and negatively charged aspartic acid (D)) [21].

Hydrogels based on $RADA_4$ nanofibers have been used for culturing a variety of cell types [22-27] as well as encapsulation and delivery of different molecules *in vivo* [28-34]. However, a molecularly detailed understanding of $RADA_4$ self-assembly is necessary to be able to control the sequence-structure-property relationships of these systems and realize the potential of self-assembling peptide modalities. To date there have been a limited number of studies that have focused on elucidating mechanisms for $RADA_4$ self-assembly [35-37]. In general, it is thought that $RADA_4$ forms anti-parallel β-sheets with polar groups (of R and D residues) and hydrophobic groups (of A residues) segregated along the peptide axis. These β-sheets are thought to further self-assemble (through both ionic complementarity and hydrophobic forces) into nanofibers and that these nanofibers subsequently interact physically to form a hydrogel. The role of hydrophobic interactions as well as ion screening of charged groups along the peptide being thought to be pivotal to this [35-37]. However the fundamental mechanisms of this process are only postulated and remain largely unsubstantiated. In addition to this, previous efforts [1-3,21,22-34] have shown

that a variety of ‘ligands’ can be attached to this self-assembling backbone and it was assumed that their presence does not interfere with nanofiber formation. However, it stands to reason that there must be an effective upper limit to the length, charge or hydration of these ligands before nanofiber formation is retarded. In this study, the two amino acids lysine (K) and serine (S) were added to the C-terminus of $RADA_4$ so as to understand the effect of appended residue properties on peptide self-assembly. The chemical structure of $RADA_4$ as well as lysine and serine residues are presented in Figure 2-1. Lysine (K) is a polar amino acid with a positive charge at pH 7.4, while serine (S) is also polar but neutral at pH 7.4. The difference in pKa values for the side chain ionizable group of lysine (amino group) and serine (hydroxyl group) (i.e. 10.5 and 13, respectively) speaks to their different levels of polarity. Furthermore, nuclear magnetic resonance studies revealed a hydration number of 4.5 (moles of water per mole of amino acid) for lysine and 2 for serine [38]. On the other hand, their hydration potential at pH 7 was shown to be dramatically different (-9.52 kcal/mol for lysine and -5.06 kcal/mol for serine residue) [39].

We hypothesized that the different hydration properties of these two amino acids will result in drastic variation in self-assembly process of $RADA_4$. Moreover, prior to moving into more complex systems (i.e. peptides with enzymatic cleavable domains, angiogenic motifs, etc.) these simple systems will provide a basis for future experiments.

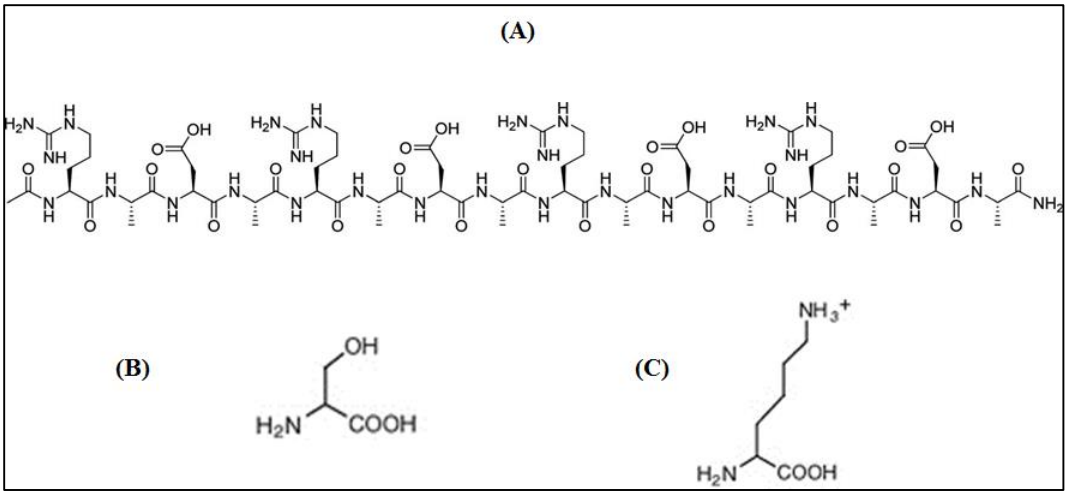

Figure 2-1. Chemical structure of (A) $RADA_4$, (B) Serine, and (C) Lysine molecules.

To this end, the Isothermal Titration Calorimetry (ITC) technique was used to study the dis-assembly of nanofibers so as to gain insight into their self-assembly mechanisms [40]. ITC has previously been utilized to probe the mechanisms involved in formation of higher order structures of different proteins and peptides through looking at the thermodynamics of their dis-assembly/dissociation [41-46]; where enthalpy determined using ITC directly related to the enthalpy of assembly [44]. Utilizing this method, the main driving force as well as the role of water molecules and ions in self-assembly of $RADA_4$ peptide systems is discussed and a systematic analysis of self-assembly process presented.

2.2. Materials and Methods

$RADA_4$, $RADA_4$-K_5, and $RADA_4$-S_5 (96+% purity) were purchased from RS Synthesis (Louisville, KY, USA), stored as a powder at -20°C, reconstituted

with appropriate buffer when needed, and used without further purification. The N- and C-termini were protected by acetyl and amide groups, respectively. Phosphate buffered saline (PBS) was prepared by dissolving sodium chloride, potassium chloride, disodium hydrogen phosphate, and potassium dihydrogen phosphate (J.T. Baker, analytical grade) in Milli-Q water (18Ω) . Phosphate buffer (PB) for Atomic Force Microscopy experiments was prepared using analytical grade disodium phosphate and potassium phosphate from Sigma-Aldrich. Sucrose and sodium chloride were used for varying osmolality and ionic strength of the buffer, respectively (purchased from Sigma-Aldrich).

2.2.1. Atomic Force Microscopy (AFM)

AFM images were collected using a NanoWizard II atomic force microscope (JPK Instruments AG) in air, in intermittent mode from all of the surfaces. Silicon cantilever probes with a length of 240 μm, resonance frequency of 50-90 KHz, spring constant of 0.7-3.8 N/m, and tip radius of ≤7 nm were used (Olympus AC240TS, Japan). All peptide solutions used in AFM studies were prepared in Phosphate Buffer (10mM, pH 7.4). Stock solutions of the peptide (1% w/v), were initially prepared in Mili-Q water and diluted with PB prior to experiments. The pH of all solutions was adjusted using 1 mM HCl and/or 1mM NaOH to get a final pH of ~7.4. $RADA_4$, $RADA_4$-S_5 and $RADA_4$-K_5 peptide solutions (PB; pH 7.4) were sonicated for 30 minutes and left at room temperature for 1 hour. Phosphate buffer was used so as to avoid the formation of salt crystals upon drying. The final concentration of samples were 60 μM for both $RADA_4$ and

$RADA_4$-S_5, and 4mM for $RADA_4$-K_5. Two drops (~5 µl) of each peptide solution were placed on freshly cleaved mica substrates (Muscovite MICA, V-1 quality, from emsdiasum, Hatfeild, PA, USA) for 1 minute before rinsing three times with MiliQ water. The surfaces were dried in a desiccator before imaging occurred.

2.2.2. Isothermal Titraton Claorimetry (ITC)

For all ITC experiments, phosphate buffer saline (PBS, 50 mM, pH 7.4) was used as solvent. ITC experiments were performed using Nano-ITC (950 µl, TA Instruments, New Castle, DE) with the reference cell filled with degassed distilled water for all the experiments. Prior to each experiment, all peptide solutions and working buffer were degassed under vacuum, at room temperature, for 10 minutes. Highly concentrated peptide solution (1-4 mM) in 50 mM PBS was pipetted into ITC cell containing buffer. It should be noted that for studies looking at the effect of peptide chemistry on self-assembly, concentration of samples used (4mM) was picked well above CAC in order to probe the effect of chemistry exclusive of concentration effects. In all experiments, a small amount of the sample (1 µl) was firstly injected into the cell and the heat signal ignored for the enthalpy calculation so as to compensate for the error generated by insertion of the needle, leakage of the solution inside the syringe, etc. After a 300 s interval, the experiment was followed by 20 more injections (12.5 µl injection volume and 300 s injection interval). The stirring speed inside the reaction cell was set at 270 rpm.

2.3. Results and discussion

A mechanistic understanding of peptide self-assembly remains elusive, primarily due to the fact that the various interactions responsible for initiating self-association are difficult to isolate and study systematically. And, in fact most studies in the literature only attempt to define nanofiber formation using AFM to show the presence of nanofibers or lack thereof; a situation that may be artifact-prone for the drying process itself can radically alter the solution concentration of peptides with time, as well as the fact that if mixtures of peptides are studied it is very difficult to prove homogeneous incorporation. As a model for discussing peptide self-assembly in general, $RADA_4$ was studied herein. The main intermolecular interactions of interest for self-assembly of peptides in aqueous solutions revolve around understanding hydrophobic/hydrophilic and electrostatic influences as a function of peptide chemistry. Uncovering the effects of hydrophobic or hydrophilic influences is possible through studying the energetics of peptide disassembly as a function of temperature [47,48]. Whereas, separate experiments can be conducted to determine the uptake or release of water molecules and counter-ions upon assembly: components thought also to be critical to self-assembly of these peptides.

2.3.1. Study of Nanofiber formation by AFM

The results from the AFM images (Figure 2-2 a and b) show the self-assembled nanofibers adsorbed from $RADA_4$ and $RADA_4$-S_5 solutions. Solutions of $RADA_4$-K_5 did not result in any observed nanofibers. As shown in Figure 2-2c, the deposits of $RADA_4$-K_5 are comprised mainly of small aggregates of

random shapes and sizes. While these aggregates were mostly circular in shape with diameters ranging from 40 nm to 1 μm; some irregular-shaped aggregates (with sizes ranging from nano to micron scale) was also observed. Examples of both circular and the irregular shapes are present in Figure 2-2c.

The lack of observed nanofibers in Figure 2-2c is likely not due to an inability of $RADA_4$-K_5 nanofibers to adsorb to the substrate. In fact, the positively charged K units should enhance adsorption to mica surfaces. Measurements from the AFM images revealed that the $RADA_4$ nanofibers are 1.3 ± 0.3 nm in height; which is consistent with previous literature [22,24,49,50]. The height of the $RADA_4$-S_5 nanofibers are 1.6 ± 0.4 nm and lastly, the $RADA_4$-K_5 aggregates ranged in size and shape from small 10 nm to larger 40 nm in height. The observed difference in fiber size for $RADA_4$ and $RADA_4$-S_5 was expected due to the different length of the peptide chain for these molecules (presence of S_5 motif on one end of $RADA_4$). Conclusively, the AFM images clearly demonstrate the presence of nanofibers in $RADA_4$ and $RADA_4$-S_5 solutions and the lack of nanofibers in $RADA_4$-K_5 solution.

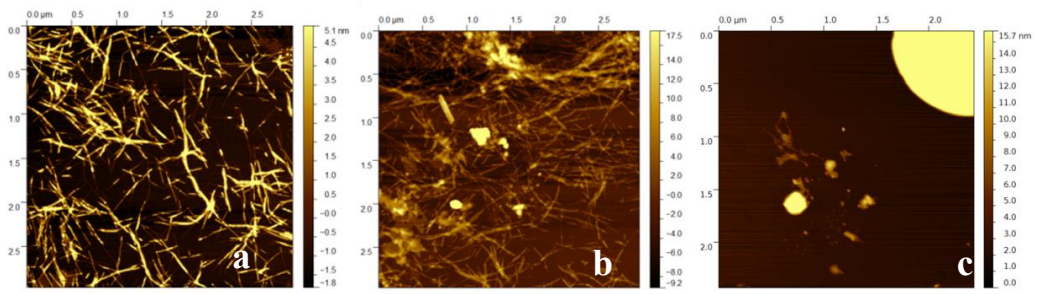

Figure 2-2. AFM images of (a) $RADA_4$ (b) $RADA_4$-S_5 and (c) $RADA_4$-K_5 peptides physisorbed on mica from pH 7.4 solutions. The images show the self-assembled nanofibers in, (a) and (b), but not in (c).

2.3.2. Analysis of Peptide Self-assembly by ITC

ITC was employed so as to provide a better understanding of the self-assembly process. Three different peptide systems were investigated to understand how polarity of the C-terminal peptide affects peptide self-assembly, *viz.* $RADA_4$, $RADA_4$-K_5, and $RADA_4$-S_5. Figure 2-3 shows an example of the thermograms obtained upon peptide dissociation. Injection of $RADA_4$-S_5 nanofiber solution into buffer generated endothermic heat signals due to nanofiber dis-assembly (Figure 2-3). When the peptide concentration in the ITC reaction cell is below the critical concentration peptide (critical assembly concentration, CAC) required for nanofiber assembly, this dilution results in dissociation of nanofibers; the energetics of which are represented by the heat evolved upon dilution (Figure 2-3, Top).

It should be noted that at CAC, an apparent equilibrium between nanofiber dissociation and assembly is achieved. As long as the final concentration of the peptide inside the cell, after each injection, remains below the CAC then the

dilution results predominately in dissociation of the self-assembled structure. As the peptide concentration within the sample volume incrementally increases with each injection, the dissociation process gradually comes into apparent equilibrium with association process. This was observed when the endothermic peaks become exothermic, being directly related to dilution of the peptide solution only. Minimal background heat effects (caused by mixing of solvent, perturbation due to stirring, etc.) were evaluated by injecting peptide solution into peptide solution (data not shown) and was subtracted from this raw data in order to isolate the heat produced only due to nanofiber disassembly. In order to calculate enthalpy change upon dissociation, the area under each injection peak in the raw data was divided by the injected mole number of peptide to obtain molar heat of disassembly and plotted against the concentration of peptide inside the cell (Figure 2-3, Middle). Moreover, from this data, CAC of the peptide was determined using the first derivative of the enthalpy curve with respect to the peptide concentration (Figure 2-3, Bottom) to identify the minimum, yielding the CAC value [42].

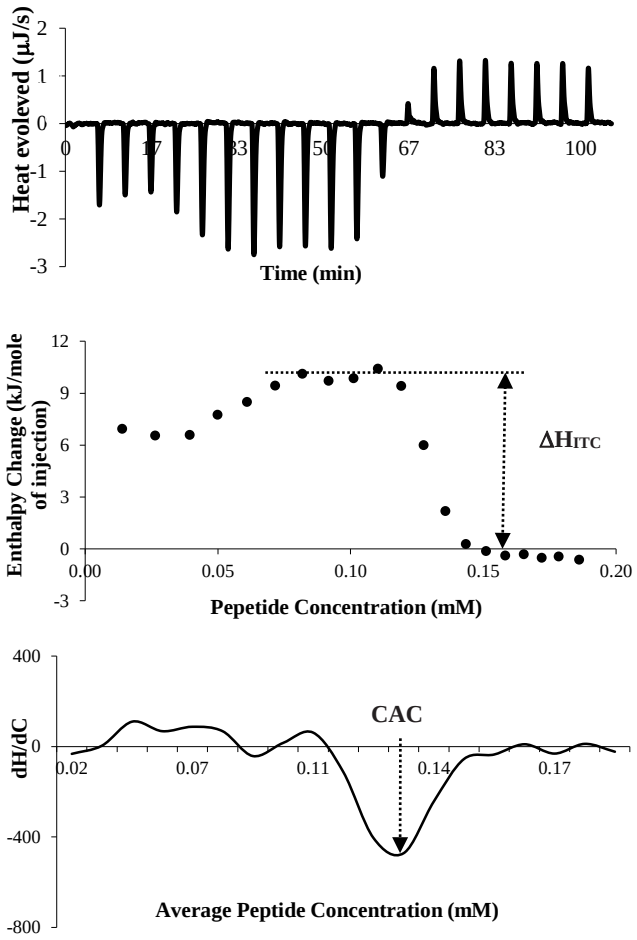

Figure 2-3. Representative ITC data showing raw results and critical analysis points. Top: Raw data for titration of $RADA_4$-S_5 peptide (1 mM) into buffer at 25°C. Each peak corresponds to an injection volume of 12.5 µL. Middle: Molar enthalpy change for dilution of peptide solution. Values obtained by integrating the area under each peak in the raw data after subtracting background, divided by the moles in each injected volume. Bottom: Determination of peptide critical assembly concentration (CAC). The plot shows the first derivative (dH/dC) calculated numerically using the enthalpy change values. The CAC is the minimum value from the derivative curve; CAC= 0.138±0.008 mM.

Dilution of the peptide solution caused dissociation of assembled structures for only $RADA_4$ and $RADA_4$-S_5 peptides, but no measureable heat change occurred upon dilution of $RADA_4$-K_5 solution (Figure 2-4). These findings supported AFM results (Figure 2-2) that showed no K_5 assembly occurred. Results presented in Figure 2-4 confirm that additional amino acids in $RADA_4$ sequence can dramatically affect nanofiber formation, and that the physicochemical nature of lysine (K) hindered $RADA_4$-K_5 self-assembly. We hypothesize that strong interaction of water molecules with the side chain of lysine is the main factor preventing self-assembly of the peptide chains. However, the positive charge present on each lysine molecule might also lead to electrostatic repulsion between peptide chains. There are also other works [51,52] that have shown peptides containing lysine residues either do not self-assemble or they self-assemble only upon neutralization of this residue *via* pH adjustments. It should be noted that, unlike those studies, the consequence of adding 5 lysine residues to only one end of a 16-residue anti-parallel β-sheet forming peptide is discussed herein.

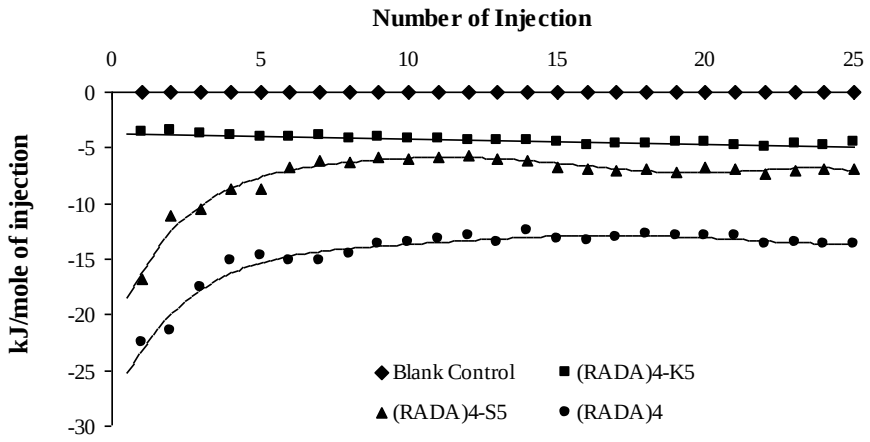

Figure 2-4. Effect of peptide chemistry on self-assembly. The plot shows the enthalpy curve upon injection of peptide (4mM) or buffer (in case of blank experiment) into buffer at 25°C, obtained *via* ITC. The black lines were produced to guide the eye.

Previous work has suggested that micellization can be adopted as a model for understanding more complicated macromolecular structure formations [53]. As $RADA_4$ self-assembly results in formation of regular structures, proceeds in a sequential manner, and may also follow a first-order growth kinetic [54]; it seems to be quite similar to micellization process. On the other hand, the fact that this theory has been employed in ITC study of rod-like micelle formation [55] provides further support for using this established ITC protocol to look at $RADA_4$ nanofiber formation. Hence, the Gibbs free energy change upon peptide assembly (ΔG_a) was calculated using the relationship for standard free energy of micellization in water [55]:

$$\Delta G_a = +RT\ln(cac') \qquad \text{Equation (2-1)}$$

Where, R is the gas constant; T is the temperature; and cac′ is the CAC expressed in mole fraction unit (i.e. cac′=CAC/molar concentration of water (~55.6 M)).

Based on this and other similar works [41-46], the ITC-measured enthalpy change is the enthalpy change upon nanofiber dissociation and is equal to enthalpy of association (ΔH_a) (such that $\Delta H_{ITC} = -\Delta H_a$). While entropy changes (ΔS) were obtained using the standard thermodynamic equation: $\Delta G = \Delta H - T\Delta S$. Self-assembly of the peptide systems at different temperatures are summarized in Table 2-1. Self-assembly of both peptides was shown to be exothermic (i.e. $\Delta H < 0$) while the enthalpy values were oppositely affected by increasing the temperature for the two systems (Table 2-1). A more detailed discussion regarding the effect of temperature on enthalpy changes will be presented in the next section.

Furthermore, as presented in Table 2-1, although both enthalpy and entropy are thermodynamically favorable, it may be concluded that the overall process of self-assembly is entropically driven since $|T\Delta S| > |\Delta H|$ [56]. On the other hand, for both $RADA_4$ and $RADA_4$-S_5, the temperature variations affected the entropy and enthalpy values in opposite ways, which may be a result of "enthalpy-entropy compensation" (an empirically-driven relationship) [57-59].

Table 2-1. Thermodynamic parameters for self-assembly of the peptides obtained *via* ITC experiments. The values denote the average ± SD, n=3.

Peptide	T[1] (°C)	ΔH_a (kJ/mol)	ΔG_a (kJ/mol)	$T\Delta S_a$ (kJ/mol)	CAC (mM)
$RADA_4$	25	-6.0±0.3	-31.9±0.1	25.9±0.3	0.144±0.003
	30	-7.6±0.3	-32.6±0.1	25.0±0.3	0.135±0.005
	37	-10.8±0.7	-33.1±0.1	22.3±0.8	0.145±0.005
	45	-14.9±0.3	-34.8±0.2	19.9±0.4	0.106±0.006
$RADA_4$-S_5	25	-9.9±0.4	-32.0±0.2	22.1±0.4	0.138±0.008
	30	-8.7±0.3	-32.4±0.1	23.7±0.3	0.145±0.005
	37	-7.9±0.2	-33.5±0.4	25.6±0.4	0.13±0.02
	45	-5.3±0.1	-35.0±0.1	29.7±0.5	0.098±0.002

[1]T: temperature, ΔH_a: enthalpy change (ΔH_a=-ΔH_{ITC}), ΔG_a: free energy change, ΔS_a: entropy change, CAC: critical assembly concentration. Subscript "a" represents "assembly".

Interestingly, the increase in temperature caused the self-assembly process to become slightly more thermodynamically favorable, as evidenced by the more negative ΔG_a values for higher temperatures in Table 2-1. For both peptides, a small negative slope was observed for changes in CAC as a function of temperature (Table 2-1). Bearing in mind that self-assembly of these molecules is entropically-driven, the increase in temperature would make the process more thermodynamically favorable and result in a lower CAC value. The temperature-dependence of CAC will be discussed utilizing van't Hoff equation later in this paper.

2.3.3. Investigation of Hydrophilic/Hydrophobic Interactions

A linear relationship between ITC-measured enthalpy (ΔH_{ITC}) and temperature for the two peptides under study was observed (Figure 2-5). The slope of which can be used to obtain heat capacity changes ($\Delta C_{p,dis} = \partial \Delta H_{ITC} / \partial T$), that have been shown to be related to the changes in solvent-accessible surface area upon any macromolecular transition (such as protein folding) [47,48]. In this regard, heat capacity change of a system may speak to the level of hydration/dehydration of polar or apolar surfaces involved in molecular interactions (e.g. protein adsorption) as well as formation of higher order structures (e.g. micelles, nanofibers, etc.) [60-70]. Hence, it has been used as a tool to determine the nature of the driving forces involved in different molecular interactions. Positive changes in heat capacity have been generally attributed to the (i) exposure of hydrophobic groups to a polar environment [71], and (ii) dis-assembly of ordered structures [72]. On the other hand, hydration of polar groups is known to result in a negative ΔC_P [71].

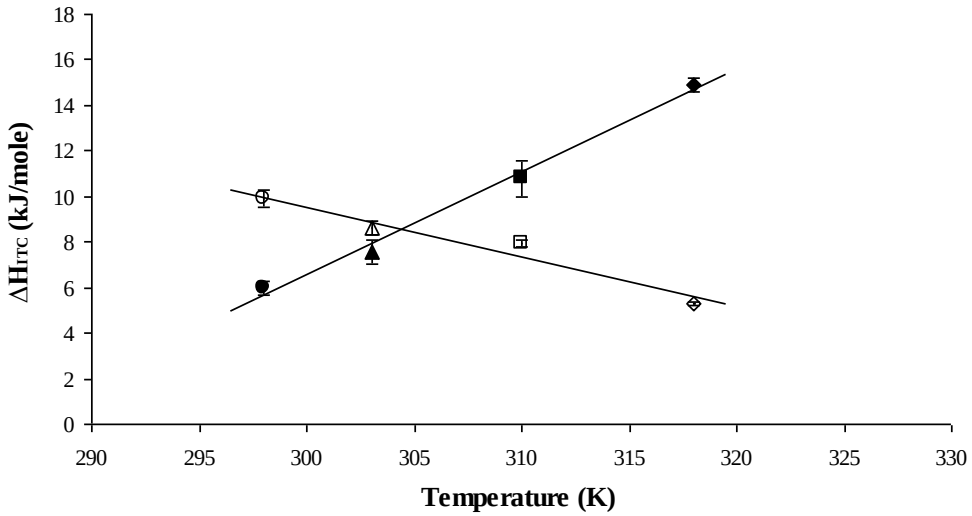

Figure 2-5. Enthalpy change as a function of temperature and fitting for $\Delta C_{p,dis}$, which is equal to 450±1 J/mol.K and −219±15 J/mol.K for $RADA_4$ (♦, ■, ▲, and ●) and $RADA_4$-S_5 (◊, □, Δ, and ○) peptides, respectively. Data represent average +/- 1 SD, n=3.

On the other hand, considering the negative sign for $\Delta C_{p,dis}$ of $RADA_4$-S_5, it is obvious that the effects associated with interaction of water with polar groups were far greater than the positive portion of heat capacity change due to disordering of the nanofiber structures or hydrophobic interaction of $RADA_4$ segment on $RADA_4$-S_5 peptide chain. Therefore, it can be suggested that polar interactions (including water incorporation) might play a major role in self-assembly of $RADA_4$-S_5. However, it is important to note that the sign for $\Delta C_{p,dis}$ might not truly reflect the type of such interactions and an in-depth study of inter-molecular events is required to be able to comment on the mechanisms at play. Therefore, we decided to probe water molecules and counter-ions in separate sets of experiments in order to identify the main driving force for self-assembly.

2.3.4. van't Hoff Analysis

Similar to heat capacity change, enthalpy change measured by ITC (ΔH_{ITC}) is also a global parameter and represents the sum of enthalpy changes that arise from a variety of events, including: i) disruption of non-covalent intermolecular bondings upon dissociation (ΔH_{dis}), ii) conformational rearrangements of dissociated structures (ΔH_c), and finally iii) reorganization of water molecules at the disrupted interface (ΔH_w) (i.e. $\Delta H_{ITC} = \Delta H_{dis} + \Delta H_c + \Delta H_w$). The disruption of self-assembled molecules is usually accompanied by uptake of energy. Therefore, ΔH_{dis} is expected to be positive. Also, transition from an ordered β-sheet conformation to un-ordered structures would cause an increase in the enthalpy (i.e. $\Delta H_c > 0$) [73]. The contribution of ΔH_w, however may be different for these two peptides due to different intermolecular forces involved in their self-assembly.

It should be noted that the only factor in enthalpy change which is directly related to nanofiber dissociation is ΔH_{dis}, and cannot be measured by ITC. Since ITC-measured enthalpy change involves all the factors mentioned above, it is not possible to isolate one from another. Another approach to determine the enthalpy change generated merely due to nanofiber dissociation is to calculate van't Hoff enthalpy (ΔH_{vH}). Many studies have shown that ΔH_{vH} is not necessarily equal to ΔH_{ITC} [74-77] and these discrepancies were attributed to the fact that in van't Hoff analysis the role of water molecules or counter-ions in the molecular interactions are not taken into account. van’t Hoff relationship is as follows:

$$\left(\frac{d\ln cac'}{dT^{-1}}\right)=\frac{\Delta H_{dis}}{R}$$ Equation (2-2)

The plot for ln (cac′) *vs.* T^{-1} is presented in Figure 2-6, and by calculating the slope of this curve at any given temperature, ΔH_{dis} was determined (Table 2-2). As it was already discussed, $\Delta H_{ITC} = -\Delta H_a$, therefore the enthalpy directly associated with dis-assembly shall be related to the pure enthalpy of assembly ($\Delta H_{assembly}$) as well.

The remaining portion of ΔH_{ITC} which was not considered in van't Hoff analysis and related to conformational changes or solvation events, shall be called residual enthalpy ($\Delta H_{res}=\Delta H_{ITC}-\Delta H_{dis}$). As can be seen in Table 2-2, for both peptide systems under study, the increase in temperature resulted in more thermodynamically favorable values for $\Delta H_{assembly}$. Although this is in agreement with the more negative ΔG_a at higher temperatures shown in Table 2-1, but contradicts the opposite behavior of ΔH_{ITC} for $RADA_4$ and $RADA_4$-S_5 with respect to temperature variations (presented in Figure 2-4). Therefore, we hypothesize that this discrepancy is due to contribution of ΔH_{res} term of enthalpy to ΔH_{ITC}.

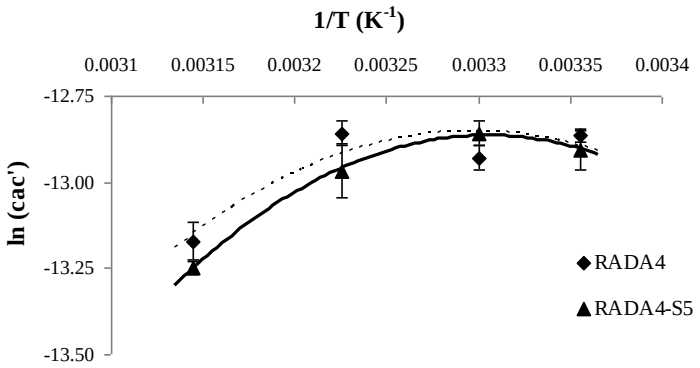

Figure 2-6. van't Hoff plot shows the temperature dependence of ln(cac′) for $RADA_4$ (♦) and $RADA_4$-S_5 (▲) peptides. The lines were produced by a second-order polynomial fit of the experimental data. Data represent the average +/- 1 SD, n=3.

As listed in Table 2-2, ΔH_{dis} calculated *via* van't Hoff equation is drastically different from values obtained using ITC (Table 2-1). Suggesting that water molecules/counter-ions might largely dictate nanofiber assembly processes. A set of ITC experiments at different osmolyte concentrations as well as different ionic strengths were performed so as to be able to isolate these effects.

Table 2-2. Thermodynamic parameters for peptide disassembly calculated *via* van't Hoff analysis.

Peptide	T (°C)	ΔH_{dis}(kJ/mol)= $-\Delta H_{assembly}$	ΔH_{res} (kJ/mol)
$RADA_4$	25	143	-137
	30	152	-145
	37	165	-154
	45	178	-163
$RADA_4$-S_5	25	264	-254
	30	273	-264
	37	285	-278
	45	299	-294

2.3.5. Role of Water Molecules in Peptide Self-Assembly

It is known that for reactions where hydration plays a significant role in; the addition of osmolytes to solution will change the equilibrium conditions due to their effect on the bulk water activity [75]. Hence, the difference in number of bound water molecules between self-assembled nanofiber and free peptide chain (ΔN_w) can be calculated utilizing the relationship between cac′ and the solution osmolality (osmolyte concentration, osmol) [78]:

$$\Delta N_w = -55.6 \frac{\partial \ln cac'}{\partial \ln [osmol]} \qquad \text{Equation (2-3)}$$

As illustrated in Figure 2-7, increasing the osmolality of the solution affected the disassembly of the two peptides in opposite ways; suggesting water activity plays an important but opposite role in the self-assembly of these structures.

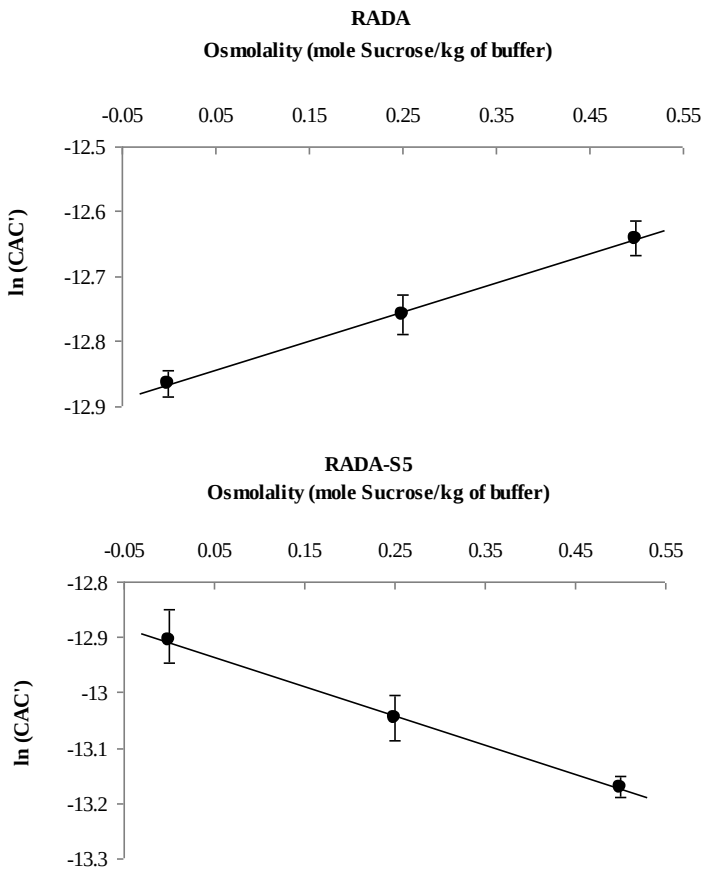

Figure 2-7. Role of hydration in peptide self-assembly. The plots show dependence of cac′ on osmolality of the solution adjusted using sucrose. The error bars represent SD (n=3).

Utilizing equation (2-3), the number of water molecules involved in self-assembly of $RADA_4$ and $RADA_4$-S_5 was calculated. Interestingly, it was found that upon self-assembly of $RADA_4$, water molecules were removed from the interface ($\Delta N_W = -25 \pm 1$), but the self-assembly of $RADA_4$-S_5 led to an incorporation of more water molecules (i.e. $\Delta N_W = +29 \pm 4$) into the formed complex. Considering if hydrophobic interactions do drive the self-assembly of $RADA_4$, removal of the waters from the interface was expected to be dominant

for both peptide systems. Furthermore, since polar interactions were shown to be important for $RADA_4$-S_5 self-assembly (as concluded from positive heat capacity changes), in conjunction with the increase in the number of water molecules associated with $RADA_4$-S_5 upon self-assembly, it can be concluded that hydrogen bonding (including water incorporation) is the main driving force for self-assembly of this peptide. The latter can be explained further knowing that due to the polar nature of serine residues, a portion of the free bulk water bound to this peptide chain may have been carried into the self-assembling interface. It is important to note that despite the removal of a portion of peptide-associated water molecules upon interaction of $RADA_4$ segment on $RADA_4$-S_5, a net positive value for ΔN_W (+29±4) was observed for this peptide. In fact, it is very likely that the S_5 segment alone has caused the incorporation of more than 29 water molecules to the self-assembled system.

2.3.6. Role of Ions in Peptide Self-Assembly

As previously proposed by other groups [22-24] the chemistry of $RADA_4$ peptides provide for a high potential for electrostatic interactions in self-assembly, necessitating an in-depth monitoring of ions participating in this process. The thermodynamic driving force for such interactions is thought to be the release of counter-ions from interacting surfaces [79]. Record *et.al.* have performed extensive analysis on the interaction of ions with nucleotides and proteins and its effect on equilibrium conditions of the reactions [79-81]. It is known that salt ions may influence the electrostatic interactions between charged macromolecules in

three different ways: direct participation in binding events, Debye-Hückel screening effects, or change of water activity [79].

The role of counter-ion exchange upon self-assembly was investigated by varying ionic strength of the solution (I). Using the following relationship, the number of counter-ions (ΔN_{CI}) involved in self-assembly process was calculated [80-81]:

$$\Delta N_{CI} = \frac{\partial \log cac'}{\partial \log I} \qquad \text{Equation (2-4)}$$

Figure 2-8 shows ion concentration dependence of CAC. The results of this analysis showed that at the neutral pH, the self-assembly of these two peptides was minimally affected by counter-ion exchange. A ΔN_{CI} of -0.27 ± 0.05 and -0.14 ± 0.05 were obtained for $RADA_4$ and $RADA_4$-S_5, respectively; suggesting that electrostatic interactions were not dramatically important in nanofiber formation for either of the peptides under study.

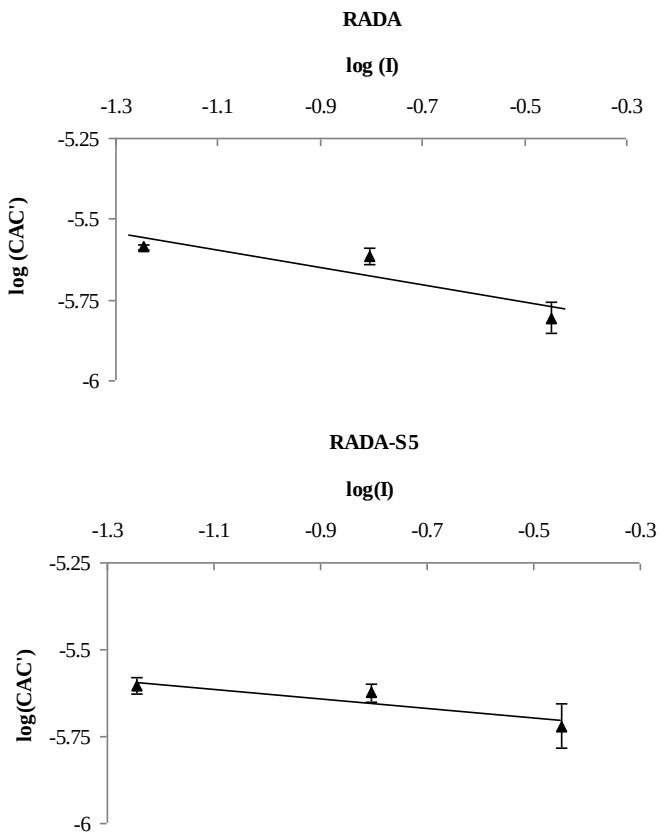

Figure 2-8. Role of counter-ions in peptide self-assembly. The plots show dependence of cac′ on ionic strength (I) of the solution adjusted using NaCl. The error bars represent SD.

2.4. Conclusion

In this study, ITC was employed to investigate self-assembly of $RADA_4$ based peptides at a molecular level. The different driving forces for self-assembly were identified experimentally and it was shown that appended residues to the peptide backbone can drastically influence this process. Moreover, ITC data indicated that self-assembly of both $RADA_4$ and $RADA_4$-S_5 peptides was entropically-driven. While we showed that increasing the temperature would

make self-assembly of these peptides more thermodynamically favorable, denaturation of peptide structure at higher temperatures should also be taken into account. Our results demonstrated that hydrophobic interactions (perhaps due to alanine residues) are the main driving force for self-assembly of $RADA_4$ peptide; clarifying previous reports suggesting that electrostatic interactions play a crucial role in nanofiber formation. This finding was further validated in this work by monitoring water molecules, as well as counter-ions upon self-assembly. As osmotic stress experiments proved the removal of water molecules from interface upon self-assembly of $RADA_4$, it was shown that $RADA_4$-S_5 self-assembly would lead to formation of a more hydrated interface; the events which might be responsible for the self-assembly process to be entropically-driven. The results presented in this study, may have fundamental implications in the design and engineering of future peptidic biomaterials with applications in drug delivery systems and tissue scaffolds.

2.5. References

[1] Zhang, S. *Biotechnol. Adv.* **2002**, *20*, 321–339.

[2] Colombo, G.; Soto, P.; Gazittrends, E. *Trends Biotechnol.* **2007**, *25*, 211-218.

[3] Ghadiri, M. R. *Nature* **1993**, *366*, 324–327.

[4] Stupp, S. I. *Biomaterials for regenerative medicine. MRS Bull.* **2005**, *30*, 546.

[5] Silva, G. A.; Czeisler, C.; Niece, K. L.; Beniash, E.; Harrington, D. A.; Kessler, J. A.; Stupp, S. I. *Science* **2004**, *303*, 1352.

[6] Zhang, S.; Holmes, T.; Lockshin, C.; Rich, A. *Proc. Natl. Acad. Sci. U. S. A.* **1993**, *90*, 3334–8.

[7] Zhang, S.; Holmes, T. C.; DiPersio, C. M.; Hynes, R. O.; Su, X.; Rich, A. *Biomaterials* **1995**, *16*, 1385–93.

[8] Mahato, M.; Arora, V.; Pathak, R.; Gautam, H. K.; Sharma, A. K. *Mol. BioSyst.* **2012**, *8*, 1742-1749.

[9] Ruana, L.; Zhanga, H.; Luoa, H.; Liua, J.; Tanga, F.; Shib, Y. K.; Zhao, X. *Proc. Natl. Acad. Sci. U. S. A.* **2009**, *106*, 5105-5110.

[10] Altman, M.; Lee, P.; Rich, A.; Zhang, S. *Protein Sci.* **2000**, *9*, 1095– 105.

[11] Tan, S.; Richmond, T. J. *Nature* **1998**, *391*, 660–6.

[12] Takahashi, Y.; Ueno, A.; Mihara, H. *Bioorg. Med. Chem.* **1999**, *7*, 177–85.

[13] Yoshiko, M.; Yoshiko, M.; Chieri, S.; Kazukiyo, K. *Trans. Mater. Res. Soc. Jpn.* **2006**, *31*, 549-552.

[14] Mrksich, M.; Whitesides, G. M. *Annu. Rev. Biophys. Biomol. Struct.* **1996**, *25*, 55 – 78.

[15] Biesalski, M.A.; Knaebel, A.; Tu, R.; Tirrell, M. *Biomaterials* **2006**, *27*, 1259–1269.

[16] Vaiser, V.; Struth, B.; Gellman, S.; Rapaport, H. *Chem.-- Eur. J.* **2011**, *17*, 14857 – 14866

[17] Vauthey, S.; Santoso, S.; Gong, H.; Watson, N.; Zhang, S. *Proc. Natl. Acad. Sci. U. S. A.* **2002**, *99*, 5355–60.

[18] Santoso, S.; Hwang, W.; Hartman, H.; Zhang, S. *Nano. Lett.* **2002**, *2*, 687–91.

[19] Duan, P.; Qin, L.; Zhu, X.; Liu, M. *Chem.--Eur. J.* **2011**, *17*, 6389 – 6395.

[20] Valery, C.; Artzner, F.; Paternostre, M. *Soft Matter* **2011**, *7*, 9583.

[21] Hartgerink, J. D.; Beniash, E.; Stupp, S. I. *Science* **2001**, *294*, 1684–8.

[22] Zhang, S.; Altman, M.; *React. Funct. Polym.* **1999**, *41*, 91–102.

[23] Ye, Z.; Zhang, H.; Luo, H.; Wang, S.; Zhou, Q.; Du, X.; Tang, C.; Chen, L.; Liu, J.; Shi, Y.K.; Zhang, E.; Ellis-Behnke, R.; Zhao, X. *J. Pept. Sci.* **2008**, *14*, 152–162.

[24] Hamada, K.; Hirose, M.; Yamashita, T.; Ohgushi, H. *J. Biomed. Mater. Res., Part A* **2008**, *84*, 128–36.

[25] Semino, C. E.; Kasahara, J.; Hayashi, Y.; Zhang, S. *Tissue Eng.* **2004**, *10*, 643–55.

[26] Sieminski, A. L.; Semino, C. E.; Gong, H.; Kamm, R. D. *J. Biomed. Mater. Res., Part A* **2008**, *82*, 494–504.

[27] Wang, S.; Nagrath, D.; Chen, P.C.; Berthiaume, F.; Yarmush, M. L. *Tissue Eng., Part A* **2008**, *14*, 227-36.

[28] Kisiday, J.; Jin, M.; Kurz, B.; Hung, H.; Semino, C.; Zhang, S. *Proc. Natl. Acad. Sci. U. S. A.* **2002**, *99*, 9996–10001.

[29] Davis, M. E.; Motion, J.; Narmoneva, D. A.; Takahashi, T.; Hakuno, D.; Kamm, R. D. *Circulation* **2005**, *111*, 442–50.

[30] Schneider, A.; Garlick, J. A.; Egles, C. *PLoS ONE* **2008**, *3*, 1410.

[31] Hsieh, P. C.; MacGillivray, C.; Gannon, J.; Cruz, F. U.; Lee, R. T. *Circulation* **2006**, *114*, 172.

[32] Hsieh, P., Davis, M. E.; Gannon, J.; MacGillivray, C.; Lee, R. T. *J. Clin. Invest.* **2006**, *116*, 237–48.

[33] Segers, V.; Tokunou, T.; Higgins, L. J.; MacGillivray, C.; Gannon, J.; Lee, R. T. *Circulation* **2007**, *116*, 1683–92.

[34] Davis, M. E; Hsieh, P.; Takahashi, T.; Song, Q.; Zhang, S.; Kamm, R. *Proc. Natl. Acad. Sci. U. S. A.* **2006**, *103*, 8155–60.

[35] Amosi, N.; Zarzhitsky, S.; Gilsohn, E.; Salnikov, O.; Monsonego-Ornan, E.; Shahar, R.; Rapaport, H. *Acta Biomater.* **2012**, *8*, 2466–2475.

[36] Chow, D.; Nunalee, M. L.; Lim, D. W.; Simnick, A. J.; Chilkoti, A. *Mater. Sci. Eng., R* **2008**, *62*, 125-155.

[37] Yokoi, H.; Kinoshita, T.; Zhang, S. *Proc. Natl. Acad. Sci. U. S. A.* **2005**, *102*, 8414-8419.

[38] Kuntz, D. I. *J. Am. Chem. Soc.* **1971**, *93*, 514-516.

[39] Wolfenden, R.; Andersson, L.; Cullis, P. M.; Southgate, C.C.B. *Biochemistry* **1981**, *20*, 849-855.

[40] Ababou, A.; Ladbury, J. E. *J. Mol. Recognit.* **2006**, *19*, 79-89.

[41] Bello, M.; Perez-Hernandez, G.; Fernandez-Velasco, D.A.; Arreguın-Espinosa, R.; Garcia-Hernandez, E. *Proteins* **2008**, *70*, 1475–1487.

[42] Beyer, K.; Leine, D.; Blume, A. *Colloids Surf., B* **2006**, *49*, 31–39.

[43] Barranco-Medina, S.; Kakorin, S.; Lazaro, J.J.; Dietz, K. J. *Biochemistry* **2008**, *47*, 7196–7204.

[44] Garidel, P.; Hildebrand, A. *J. Therm. Anal. Calorim.* **2005**, *82*, 483–489.

[45] Tsamaloukas, A. D.; Beck, A.; Heerklotz, H. *Langmuir* **2009**, *25*, 4393–4401.

[46] Desii, A.; Duce, C.; Ghezzi, L.; Monti, S.; Solaro, R.; Tine, M.R. *J. Therm. Anal. Calorim.* **2009**, *97*, 791–796.

[47] Livingstone, J. R.; Spolar, R. S.; Record, M. T. *Biochemistry* **1991**, *30*, 4237-4244.

[48] Spolar, R. S.; Livingstone, J. R.; Record, M. T. *Biochemistry* **1992**, *31*, 3947-3955.

[49] Zhang, H.; Luo, H.; Zhao, X. *J. Nanotechnol. Eng. Med.* **2010**, *1*, 011007-011013.

[50] Ho, D.; Fitzgerald, M.; Bartlett, C. A.; Zdyrko, B.; Luzinov, I. A.; Dunlop, S. A.; Iyer, K. S. *Nanoscale* **2011**, *3*, 907-910.

[51] Bowerman, C. J.; Liyanage, W.; Federation, A. J.; Nilsson, B. L. *Biomacromolecules* **2011**, *12*, 2735-2745.

[52] Guler, M. O.; Claussen, R. C.; Stupp, S. I. *J. Mater. Chem.* **2005**, *15*, 4507-4512.

[53] Kresheck, G. C.; Hargraves, W. A. *J. Colloid Interface Sci.* **1974**, *48*, 481-493.

[54] Cheng, L.; Englander, O.; Paravastu, A.; Oates, W.S. *J. Chem. Phys.* **2011**, *135*, 055102.

[55] Heerklotz, H.; Seelig, J. *Biochim. Biophys. Acta* **2000**, *1508*, 69-85.

[56] Bouchemal, K.; Couvreur, P.; Daoud-Mahammed, S.; Poupaert, J.; Gref, R. *J. Therm. Anal. Calorim.* **2009**, *98*, 57–64.

[57] Leffler; J. E. *J. Org. Chem*. **1955**, *20*, 1202-1231.

[58] Rekharsky, M. V.; Inoue, Y. *Chem. Rev.* **1998**, *98*, 1875-1917.

[59] Shi, Q-H; Shen, F-F; Sun, Sh. *Biotechnol. Prog.* **2010**, *26*, 134-41.

[60] Velazquez-Campoy, A.; Leavitt, S. A.; Freire, E. *Methods Mol. Boil. (N. Y., NY, U. S.)* **2004**, *261*, 35-54.

[61] Ladbury, J. E.; Wright, J. G.; Sturtevent, J. M.; Sigler, P. B. *J. Mol. Biol.* **1994**, *238*, 669–681.

[62] Guinto, E. R.; Di Cera, E. *Biochemistry* **1996**, *35*, 8800–8804.

[63] Morton, C. J.; Ladbury, J. E. *Protein Sci.* **1996**, *5*, 2115–2118.

[64] Holdgate, G. A.; Tunnicliffe, A.; Ward, W. H. J.; Weston, S. A.; Rosenbrock, G.; Barth, P. T.; Taylor, I. W. F.; Pauptit, R. A.; Timms, D. *Biochemistry* **1997**, *36*, 9663–9673.

[65] Clarke, C.; Woods, R. J.; Gluska, J.; Cooper, A.; Nutley, M. A.; Boons, G. J. *J. Am. Chem. Soc.* **2001**, *123*, 12238–12247.

[66] Bergqvist, S.; Williams, M. A.; O'Brien, R.; Ladbury, J. E. *J. Mol. Biol.* **2004**, *336*, 829–842.

[67] Geroult, S.; Virdee, S.; Waksman, G. *Chem. Biol. Drug Des.* **2006**, *67*, 38–45.

[68] Rau, D. *J. Mol. Biol.* **2006**, *361*, 352–361.

[69] Lopez, M. M.; Makhatadze, G. I. *Biophys. Chem.* **1998**, *74*, 117-125.

[70] Loladze, V. V.; Ermolenko, D. N.; Makhatadze, G. I. *Protein Sci.* **2001**, *10*, 1343–1352.

[71] Hildebrand, A.; Garidel, P.; Neubert, R.; Blume, A. *Langmuir* **2004**, *20*, 320-328.

[72] Cooper, A. *Biophys. Chem.* **2005**, *115*, 89–97.

[73] Lakshminarayanan, R.; Yoon, I.; Hegde, B. G.; Fan, D.; Du, Ch.; Moradian-Oldak, J. *Proteins: Struct., Funct., Bioinf.* **2009**, *76*, 560–569.

[74] Becker, A. L.; Welsch, N.; Schneider, C.; Ballauff, M. *Biomacromolecules* **2011**, *12*, 3936–3944.

[75] Suryawanshi, H.; Sabharwal, H.; Maiti, S.; *J. Phys. Chem. B* **2010**, *114*, 11155–11163.

[76] Gilli, P.; Ferretti, V.; Gilli, G. *J. Phys. Chem.* **1994**, *98*, 1515-1518.

[77] Naghibi, H.; Tamura, A.; Sturtevant, J. M. *Proc. Natl. Acad. Sci. U. S. A.*; **1995**, *92*, 5597-5599.

[78] Parsegian, V. A.; Rand, R. P.; Rau, D. C.; *Methods Enzymol.* **1995**, *259*, 43–94.

[79] Record, M. T.; Anderson, C. F.; Lohman, T. M. *Q. Rev. Biophys.* **1978**, *11*, 103-178.

[80] Ha, J-H; Capp, M. W.; Hohenwalter, M. D.; Baskerville, M.; Record, M. T. *J. Mol. Biol.* **1992**, *228*, 252-264.

[81] Record, M. T.; Zhang, W.; Anderson, C. F. *Adv. Protein Chem.* **1998**, *51*, 281–353.

Chapter 3

Protein adsorption onto PCBMA-modified silica nanoparticles: insight into classically held hydrophobically induced adsorption events

3.1. Introduction

Zwitterionic polymers proved to be very effective in inhibition of non-specific protein adsorption to surfaces [1,2]. Polybetaines are a sub-category of zwitterionic polymers and are characterized by a zwitterionic segment incorporated in each single monomer of their polymer chain. Three different types of polybetaines have been developed [3] including phosphobetaines (PB), sulfobetaines (SB), and carboxybetaines (CB). Although the effect of polybetaine's physicochemical properties (such as grafting density, film thickness, zwitterion's spacer length, molecular weight, refractive index, etc.) on their anti-fouling characteristics has been studied [4-9], the behaviour of these materials at the nano-bio interface has not yet been fully investigated. It is important to note that the interaction of materials with biological media is affected by their shape, where composition and organization of the protein corona on the surface can differ dramatically depending on whether it is a nanoparticle surface or a flat surface [10]. NP's large surface-to-volume ratio, and its comparable size to that of proteins, were suggested to be the main reasons behind different physiological responses to NPs compared to flat surfaces [10,11]. Hence, even though the protein adsorption on polybetaine-grafted flat surfaces has been an actively sought topic during the past few years, the need for characterizing anti-fouling properties of these materials when grafted to surface of NPs seems inevitable.

To best of our knowledge, scarce comprehensive studies on non-specific protein adsorption to polybetaine-grafted NPs have been carried out. For example, there has been a limited number of studies performed on the interaction of proteins with sulfobetaine modified NPs [12,13] as well as quantum dots [14]. Phosphorylcholine modified quantum dots [15] and poly (carboxybetaine acrylamide) (polyCBAA) grafted gold NPs [16] were also studied in terms of their interaction with human plasma. These works, however, mostly demonstrated low or zero protein adsorption to zwitterionic NPs under different solution conditions; without presenting an in-depth analysis of the underlying mechanisms responsible for such phenomenon.

As hydration is known to greatly influence the interaction of any surface with biological media [17,18], the electrostatically-bound water layer on the surface of zwitterionic coatings was proposed to be the main factor responsible for their excellent protein-repellent properties [2]. This idea was further supported by molecular simulation studies which confirmed a more stable hydration layer (i.e. more negative free energy change of hydration (ΔG_{hyd})) on the surface of grafted polybetaines compared to grafted oligo(ethylene glycol) chains (i.e. ΔG_{hyd} was -404 kJ/mol and -519 kJ/mol for carboxybetaine and sulfobetaine, respectively and -182 kJ/mol for oligo(ethylene glycol)) [19]. Recently, Estephan *et.al.* suggested that superior resistivity of zwitterionic sulfobetaine-modified silica surfaces (both planar and NP) is due to lack of counter-ion release upon their interaction with proteins; however they did not provide any experimental proof for their hypothesis [13]. It is known that non-specific protein adsorption to

surfaces is often entropically-driven. Three factors were proposed to be the source for this favorable entropy change upon protein adsorption [20-22]: i) removal of water molecules from interface (due to hydrophobic interactions); ii) removal of counter-ions from the interface (due to formation of ion pairs); and iii) conformational changes. While the conformational changes of the proteins interacting with poly(carboxybetaine)-modified NPs was studied in our previous work [24], the question regarding the role of water molecules and counter-ions in protein adsorption to the same surfaces is being addressed herein. In this regard, protein adsorption onto silica NPs modified with four different types of poly(carboxybetaine methacrylamide) (PCBMA) was investigated. The zwitterionic coatings were differing in length of spacer group inside the zwitterion (1 or 5 $-CH_2-$ group) and the chemistry of appended end-group (hydrophilic or hydrophobic groups). Human Serum Albumin (HSA), which is known as one of the major serum proteins always observed on the surface of various NPs -regardless of their compositional characteristics- [25] was used as a model protein in all experiments. Isothermal Titration Calorimetry (ITC) studies were carried out at different temperatures (25 and 37°C) as well as different solution ionic strengths to be able to gain a mechanistic understanding of the molecular events at play. The main objective of this study is to define what happens at the interface of protein and zwitterionic NPs in terms of reorganization of water molecules and exchange of counter-ions; the knowledge which will lead to design and engineer more successful protein-repellent architectures in future.

3.2. Materials and Methods

Silica NPs with an average diameter of 12 nm (Sigma-Aldrich) were functionalized with PCBMA according to the protocol already published [23, 25]. PCBMA chains were containing either one spacer group (C-1) or five of them (C-5), differing also in the chemistry of end-groups (either phosphonate (Phospho) or 2,2,6,6-tetramethylpiperidine-N-oxyl (TEMPO)). The procedures for synthesis, polymerization and characterization of all the NPs studied herein were previously reported [25]. Figure 3-1 represents the chemical structure of the polymer-modified nanoparticles. The focus of the present study is the interaction of these modified NPs systems with protein and its thermodynamic characterization.

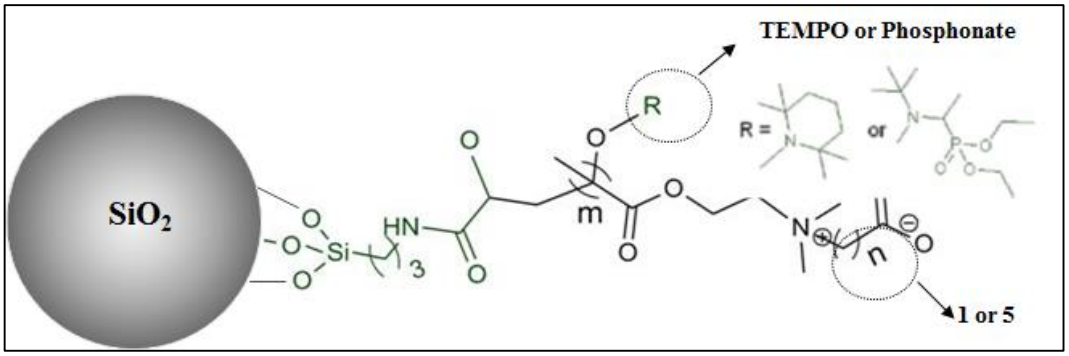

Figure 3-1. Chemical structure of PCBMA-modified nanoparticles; n represents the number of spacer groups and R represents the place where end-group is inserted. Note that R is bound to one oxygen molecule which is common between both TEMPO and Phosphonate chemistries. Hence, the TEMPO group is presented here in its reacted form rather than a radical.

Briefly, modification of silica NP with PCBMA chains included grafting of an alkoxyamine initiator containing triethoxysilyl functional group to silica

NPs in toluene solution. The initiator-grafted NPs were isolated from the non-reacted initiator using centrifuge. The carboxybetaine monomers were synthesized with various spacer groups between the carboxylic acid and quaternary amine so as to be able to control the surface charge and hydration state. Nitroxide mediated free radical polymerization (NMFRP) was applied to attach carboxybetaine monomers to initiator-grafted NPs, as explained previously [25].

The physicochemical properties of all modified NPs have been previously characterized and reported in another work [23]. Size of functionalized NPs was shown to be between 86-89 nm for Phospho end-group and 71-72 nm for TEMPO end-group. Furthermore, it was observed that the actual water content of C-5 NPs was higher than that for C-1 NPs (i.e. ~33-34% for C-5 NPs *vs*. ~29-31% for C-1 NPs). Also, at pH 7.0, which is the working pH of this study, all modified NPs had positive surface charge. The PCBMA-modified NPs were used for the protein adsorption experiments without further modification.

Human serum albumin (HSA) (lyophilized powder, protein ≥ 96%) was purchased from Sigma-Aldrich (St. Luis. MO) and used without further purification. All experiments were performed in phosphate buffer (10 mM, pH 7.4) prepared using disodium phosphate (J.T. Baker), potassium phosphate and sodium chloride (Sigma-Aldrich); components that were not further purified prior to use.

3.2.1. Characterization of Protein Secondary Structure

Far UV Circular Dichroism (CD) spectra were collected at 25 and 37^{o}C for HSA using a Jasco J-810 CD/ORD (Japan) at 100 mdeg sensitivity, bandwidth of 1 nm, and data pitch of 0.5 nm. The buffered protein solution was pipetted into a cuvette with a 2 mm path length for acquiring the spectra, and each reading was repeated 5 times (average data plotted). A blank buffer reference was subtracted from the data before calculating the molar ellipticity. Molar ellipticity was calculated using well established methods [26]. Buffered protein solution concentration was verified using an Agilent UV-Vis Spectrophotometer at the fixed wavelength of 280 nm and molar extinction coefficient of 36,600 $M^{-1}cm^{-1}$ for HSA. The results of these experiments are presented in Appendix B of this thesis.

3.2.2. ITC Characterization of Protein Adsorption

ITC was utilized to study the interaction of HSA with all modified and unmodified NPs in order to determine the strength of binding, binding stoichiometry, enthalpic-entropic nature of the binding, etc.

A set of survey titrations were conducted to obtain optimum solution concentrations for protein relative to NPs, as required for ITC characterization to be possible. In order to isolate the background heat associated with dilution of samples, stirring noise, etc. from the heat generated due to protein-NP interaction, blank experiments where protein (sample in the syringe) solutions were injected into an identical solution within the cell that contained buffer only were conducted. This step was performed also to ensure that no dissociation or

precipitation of the protein occurred upon injection. The background heat was then subtracted from the enthalpy profile as a function of protein:NP concentration ratio inside the ITC cell so as to determine the absolute enthalpy change upon binding [27]. HSA adsorption experiments involved injecting protein solution into the ITC cell containing a NP solution.

Experimental Procedure: All experiments were performed using a Nano-ITC (950 µl, TA Instruments, New Castle, DE). All solutions were prepared in phosphate buffer (10 mM, pH 7.4) and sodium chloride was used for varying ionic strength. The reference cell was filled with distilled water for all the experiments. Buffered solutions of NPs and protein were degassed under vacuum at room temperature, prior to each experiment for 10 minutes. A small amount of HSA solution (1 µl) was firstly injected into ITC cell and the heat signal was ignored in enthalpy calculations in order to compensate the error generated by insertion of the needle into the ITC cell and/or leakage of the solution inside the syringe. After a 300 s interval, the experiment was followed by 19 more injections (12.5 µl injection volume and 300 s injection interval). The stirring rate of the syringe inside the reaction cell was set at 270 rpm.

The binding stoichiometry (n), binding constant (K), and enthalpy change (ΔH) were determined using the NanoAnalyze software (TA Instruments). A model for single set of independent binding sites (SSIS) was applied to the ITC data. Subsequent Gibbs free energy changes (ΔG) and entropy changes (ΔS) were then calculated using standard thermodynamic equations:

$$\Delta G = RT\ln(K)$$ Equation (3-1)

$$\Delta G = \Delta H - T\Delta S$$ Equation (3-2)

where R is the gas constant and T is the absolute temperature.

The numbers of proteins on NP surface at 100% surface coverage was obtained by calculating the surface area of a sphere with a radius equal to that of NP plus the protein's stokes radius (3.51 nm) and dividing it into protein cross-sectional surface area. The experimental protein:NP ratio, obtained *via* ITC, was then divided into theoretical number for 100% coverage and the percentage of surface coverage was determined. More details on experimental procedure and data analysis are presented in Appendix A of this thesis.

3.3. Results and Discussion

3.3.1. Thermodynamics of Protein Adsorption

Due to the interplay of many different factors, it is often very hard to completely elucidate the mechanisms behind the formation of the protein corona on surfaces. However, through thermodynamic analysis of protein adsorption it was made possible to identify the contribution of different molecular phenomena occurring at the interface of protein and NP. Rotello *et. al.* were the first group who utilized thermodynamics of protein adsorption to gain insight toward the type of molecular forces involved [28]. The sign and magnitude of enthalpy and entropy changes upon protein adsorption are important factors which can

represent valuable information; removal of water molecules or counter-ions from interface are usually characterized by favorable entropy change (i.e. $\Delta S>0$), while formation of non-covalent bonds (hydrophobic, electrostatic, etc.) is often accompanied by negative enthalpy change ($\Delta H<0$). On the other hand, the kinetics of protein adsorption to NPs (binding constant, stoichiometry, etc.) is also another factor of crucial importance in determining the composition and conformation of the protein corona as well as NP's fate inside the body [29].

Utilizing ITC, enthalpy change upon protein adsorption to PCBMA modified NPs as well as protein binding constant and stoichiometry were obtained. Figure 3-2 (Top) shows a representative raw ITC heat flow profile, the control blank experiment, as well as the protein-NP interaction enthalpy curve. Figure 3-2 (Bottom) illustrates the calculated molar enthalpy curve for the interaction between HSA and C-1(Phospho) modified NP at 25^{o}C. The higher heat signals observed for the experiment in presence of NP inside ITC cell (Figure 3-2, Top-Black line) compared to the raw data peaks for blank experiment (Figure 3-2, Top-Grey line) proved there was an interaction occurring between NP surface and HSA molecule. The enthalpy change of interaction was found to be endothermic (i.e. $\Delta H>0$) with a final plateau phase (which confirmed saturation of NP surface) by the end of experiment (Figure 3-2, Bottom).

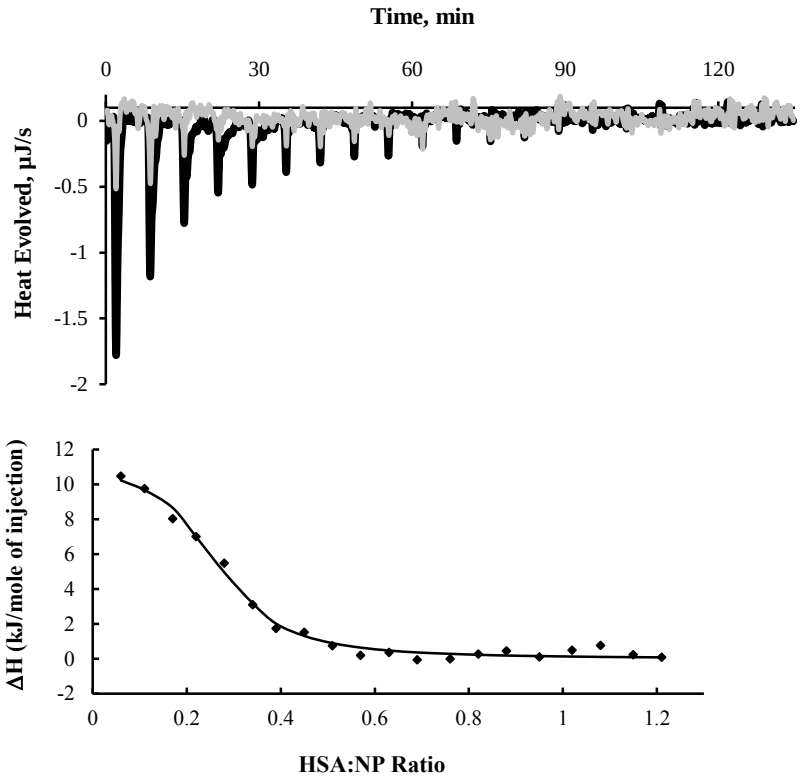

Figure 3-2. Representative plot illustrating the results obtained from an ITC experiment. Top: Raw data for HSA (0.6 mM) titration into C-1 (Phospho) solution (0.15 mM) at 25°C (black line) and HSA (0.6 mM) titration into buffer at 25°C (blank experiment - grey line). Each peak corresponds to an injection volume of 12.5 µL. Bottom: Molar enthalpy change for HSA titration into C-1(Phospho) solution at 25°C, obtained by integrating the area under each peak in the raw data after subtracting background, divided by the moles in each injected volume (solid line represents fitting *via* Eq. 2, SD=2.28).

The same type of experiments was performed on all other modified NPs as well as bare silica nanoparticles (SNP). HSA adsorption to all PCBMA-modified NPs, at 25°C, was found to be endothermic (Figure 3-3). However, there could be

no ITC signal recorded for the interaction of HSA and SNP at this temperature. Considering the isoelectric point for HSA protein (pI of ~4.7), this molecule is expected to be negatively charged at pH 7.4 (of this study) repelling the negatively charged SNP. Although the hypothesis regarding electrostatic repulsion between HSA and SNP seems plausible, lack of ITC signal does not imply a "zero" protein adsorption to this surface. This is due to a possibility for the adsorption to be merely entropically driven, generating weak or no sign of enthalpy change, causing the interaction to become undetectable *via* ITC.

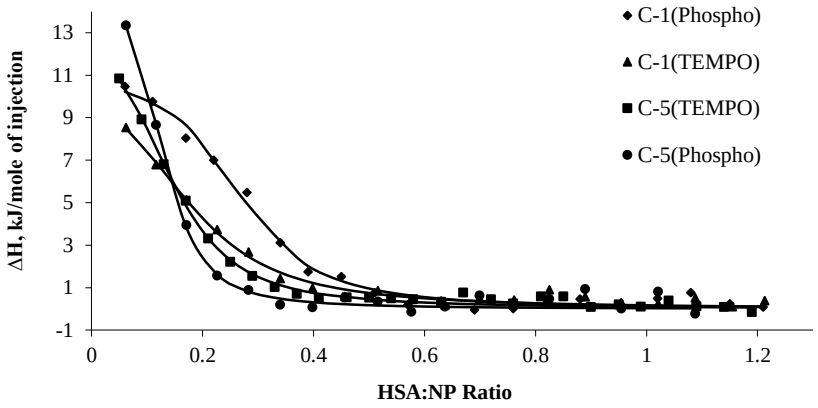

Figure 3-3. Molar enthalpy change upon titration of HSA (0.6 mM) into NP solutions (0.15 mM) at 25°C (solid lines represent fitting *via* SSIS model).

Although Figure 3-3 demonstrated positive enthalpy change for adsorption of HSA to all PCBMA-modified surfaces, the shape of ITC curves in this figure indicated various extent of interaction between HSA and different surfaces at 25^{o}C. This was confirmed by calculation of thermodynamic parameters obtained *via* fitting the enthalpy curves (Figure 3-3) to a model for single set of independent binding sites (SSIS); results of which is presented in Table 3-1.

Interestingly, C-5(Phospho) NPs formed the most stable complex with HSA (i.e. the largest binding constant ($K=5.03\times10^5\ M^{-1}$)) although the least amount of HSA was adsorbed to this surface (surface coverage of 0.01%, Table 3-1). Hence, it can be concluded that the amount of protein bound to a surface and the strength of binding are two independent factors simultaneously influencing the corona formation process. Overall, the protein binding constant to NPs studied herein were fairly small; as the K values ranged between 1×10^5 and $5\times10^5\ M^{-1}$. However among NPs modified with the same end-group chemistry, the ones with longer spacer group demonstrated larger binding constants (as for Phospho-NPs: 5.03×10^5 >3.23×105 and for TEMPO-NPs: 2.01×10^5 $>1.27\times10^5$, Table 3-1). It is known that as the inter-charge distance inside the zwitterion increases the overlap of coordination shells of the quaternary amine and carboxyl group decreases and this leads to increase of the dipole moment inside the zwitterion resulting in weaker adsorption-resistance properties [30]. On the other hand, A larger binding constant may speak to the level of protein's denaturation upon binding; since protein's structural perturbation can lead to an increase in strength of interaction (as more interactive regions of the protein structure get exposed to the surface). This hypothesis is in agreement with the results of our previous study on the same NPs, demonstrating larger adsorption-induced conformational change of HSA molecule upon interaction with C-5 NPs [23].

It seemed that zwitterion's spacer length contributed to the extent of NPs' surface covered by protein as well. The results in Table 3-1 showed that at 25^{o}C, NPs modified with 1 spacer group adsorbed larger amount of HSA (i.e. surface

coverage of 0.028 and 0.025 for C-1 (Phospho) and C-1 (TEMPO), respectively) compared to NPs modified with 5 spacer groups (i.e. surface coverage of 0.010 and 0.020 for C-5 (Phospho) and C-5 (TEMPO), respectively). The steric hindrance of the polymer with longer monomeric chains could be the factor responsible for lower number of adsorbed proteins on the surface of C-5 NPs. As for the effect of end-group chemistry, for NPs modified with the same length of spacer group, surfaces which contained TEMPO end-group demonstrated slightly higher degrees of surface coverage in Table 3-1.

Table 3-1. Thermodynamic parameters for the binding of HSA to various PCBMA-grafted silica NPs at 25°C, derived from the fitting of ITC curves using the independent binding sites model. The errors denote the standard deviation of non-linear least-squares analyses.

NP	[a]K x10^{-5} (M^{-1})	n	Coverage (%)	ΔH (kJ/mol)	TΔS (kJ/mol)	ΔG (kJ/mol)
SNP	N/A	N/A	N/A	N/A	N/A	N/A
C-1 (Phospho)	3.23±0.91	0.25±0.01	0.028±0.001	11.46±0.85	42.60±1.61	−31.14±0.76
C-1 (TEMPO)	1.27±0.37	0.16±0.02	0.025±0.003	12.45±1.74	41.57±2.37	−29.12±0.63
C-5 (Phospho)	5.03±1.69	0.10±0.01	0.010±0.001	16.80±1.56	49.33±2.28	−32.53±0.72
C-5 (TEMPO)	2.01±0.35	0.13±0.01	0.020±0.002	14.99±1.23	45.24±1.62	−30.25±0.39

[a]K:binding constant, n:binding stoichiometry (protein:NP ratio), ΔH:enthalpy change, ΔS:entropy change, ΔG: free energy change.

It is known that HSA molecule, as the most abundant protein in plasma, has a very high affinity for a wide range of materials such as metal ions, fatty acids, amino acids, and metabolites [31]. The results of our ITC analysis strongly confirmed the important role of hydrophobic interactions in adsorption of HSA to

PCBMA-modified NPs; as positive and unfavorable enthalpy changes (Table 3-1) is known to be a sign for disruption of highly organized hydration layers [21] thought to surround hydrophobic patches on the surface of solutes. In fact, large and positive entropy change along with a positive and unfavorable enthalpy change has been attributed to hydrophobic forces dominating the interaction [35]. The unfavorable enthalpy changes in Table 3-1 was compensated by favorable entropy change ($\Delta S>0$), caused by desolvation of the interface (due to hydrophobic interactions) and/or conformational changes of interacting systems. The question being raised here is why despite the protein adsorption being hydrophobically driven, NPs modified with hydrophilic Phospho end-group demonstrated the strongest interaction with HSA at 25°C (i.e. greater K values in Table 3-1). As demonstrated earlier [23], NPs modified with Phospho end-group contain larger amounts of water within their polymeric shell; therefore the entropic gain associated with removal/reorganization of the water layer at the interface of HSA and NP might be the driving force for stronger interaction between the protein and NPs modified with Phospho end-group. This hypothesis is evidenced by larger $T\Delta S$ values in Table 3-1 for interaction between HSA and NPs modified with Phospho end-group.

3.3.2. Effect of Temperature on Protein Adsorption

In order to ensure that temperature-associated conformational changes of the protein is not a factor influencing protein adsorption at two different temperatures of this study (25 and 37°C); CD spectra of HSA molecule at 25°C

and 37°C was acquired. The results confirmed that increasing the temperature from 25°C to 37°C caused no alteration in protein's secondary structure (data presented in Appendix B). Hence, it should be safe to exclude the impact of temperature on protein's secondary structure while discussing the effect of temperature on HSA adsorption to NPs presented herein.

As shown in Figure 3-4, increasing the temperature to 37^{o}C did not affect the sign of enthalpy change upon protein-NP interactions as endothermic ITC curves were generated upon adsorption of HSA onto different NPs at 37^{o}C (Figure 3-4). Although undetectable at 25^{o}C, HSA adsorption to SNP generated ITC signal at 37^{o}C demonstrating endothermic enthalpy change; however the signal for this interaction was much lower compared to PCBMA-modified NPs. It stands to reason to assume that increasing the temperature from 25^{o}C to 37^{o}C contributed to HSA-SNP interaction through increasing internal energy of the system to an extent allowing positive and favorable entropy change to exceed the unfavorable enthalpic cost associated with electrostatic repulsion effects present at the interface.

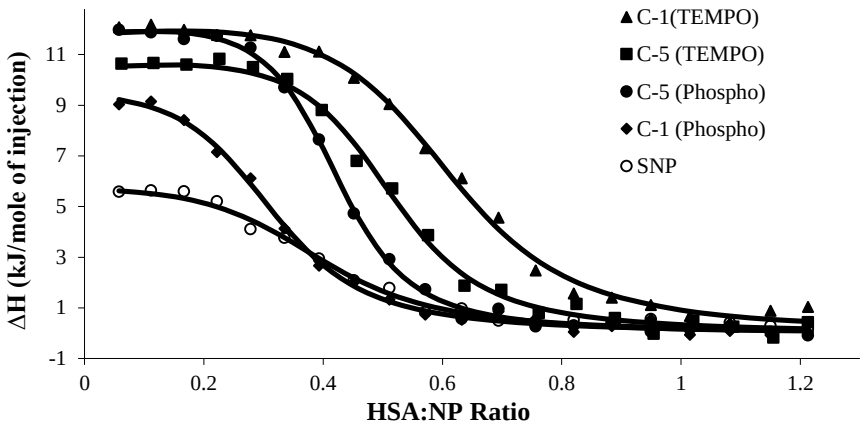

Figure 3-4. Molar enthalpy change upon titration of HSA (0.6 mM) into NP solutions (0.15 mM) at 37°C (solid lines represent fitting *via* SSIS model).

The results of ITC data analysis obtained using NanoAnalyze software is presented in Table 3-2. It should be noted that although SNP demonstrated the lowest binding constant as well as the lowest enthalpy change upon HSA adsorption, the protein's degree of coverage for this surface was much larger (~1.0%) compared to PCBMA-modified NPs (~0.03%-0.09%). This clearly implies that despite electrostatic repulsion present between HSA and SNP surface, greater amount of protein was loosely bound to SNP. However, in case of PCBMA-modified NPs although the protein was sparsely adsorbed, the interaction was stronger.

Comparing thermodynamic parameters for protein adsorption to NPs at 25^{o}C, binding constant values for HSA adsorption to all NPs was found to be slightly larger at 37^{o}C. This can be explained *via* van't Hoff relationship; where changes in binding constant (K) with respect to temperature are directly related to

enthalpy change (i.e. $\frac{d\ln(K)}{dT} = \frac{\Delta H}{RT^2}$). Since enthalpy change was shown to be endothermic for all interactions under study, it can be expected that increasing the temperature make the interaction more thermodynamically favorable resulting in larger binding constant values. Furthermore, comparing the numbers reported for surface coverage in Tables 3-1 and 3-2, it can be concluded that increased temperature has caused larger amounts of HSA to get adsorbed onto NPs. This might also be related to the increased rotational mobility of the system due to higher levels of internal energy at the higher temperature.

Table 3-2. Apparent thermodynamic parameters for the binding of HSA to various PCBMA-grafted silica NPs 37°C, derived from the fitting of ITC curves using the independent binding sites model. The errors denote the standard deviation of non-linear least-squares analyses.

NP	[a]K x10^{-5} (M^{-1})	n	Coverage (%)	ΔH (kJ/mol)	TΔS (kJ/mol)	ΔG (kJ/mol)
SNP	2.25±1.11	0.38±0.02	1.004±0.053	6.14±0.60	37.90±1.63	−31.76±1.03
C-1 (Phospho)	2.81±0.67	0.30±0.01	0.033±0.001	10.14±0.47	42.48±1.02	−32.34±0.55
C-1 (TEMPO)	3.53±1.07	0.59±0.02	0.093±0.003	12.27±0.56	45.19±1.24	−32.92±0.68
C-5 (Phospho)	6.80±1.18	0.40±0.01	0.041±0.001	12.23±0.29	46.84±0.70	−34.61±0.41
C-5 (TEMPO)	5.04±1.53	0.48±0.01	0.075±0.002	10.87±0.44	44.71±1.12	−33.84±0.68

[a]K:binding constant, n:binding stoichiometry (NP:protein ratio), ΔH:enthalpy change, ΔS:entropy change, ΔG: free energy change.

Changes in ΔH values *vs.* temperature normally produce a line, the slope of which returns the heat capacity change (ΔC_P) of interactions. Although precise determination of heat capacity change requires measuring the enthalpy change at

more than two different temperatures, but for the sake of identifying the sign of ΔC_P, the two data points can provide a rough estimate for this parameter. The sign of heat capacity change is of interest due to valuable information it presents regarding reorganization of water molecules associated with interacting surfaces [32,33]. Since heat capacity of water molecules associated with hydrophobic patches on a surface is higher than that of free bulk water, negative heat capacity changes have been attributed to hydrophobically-driven interactions [34]. Hence is the decrease in enthalpy change values at 37^{o}C (Table 3-2) compared to 25^{o}C (Table 3-1).

Although at 25^{o}C the effect of end-group chemistry was largely pronounced in the values reported for binding constant (K), it was found that length of spacer group inside the zwitterion was dominating the strength of binding at 37^{o}C; as interaction of HSA and NPs modified with 5 spacer groups demonstrated larger binding constant values ($K=6.8\times10^5$ and 5.0×10^5) compared to NPs modified with 1 spacer group ($K=2.8\times10^5$ and 3.5×10^5). Moreover, the results presented in Table 3-2 revealed that comparing PCBMA-modified surfaces -regardless of the length of spacer group- larger amounts of protein was adsorbed to surfaces containing hydrophobic TEMPO end-group (surface coverage of ~0.093 and ~0.075 for NPs modified with TEMPO end-group *vs.* ~0.033 and ~0.041 for NPs modified with Phospho end-goup). An effect that, although expected, was not observed at 25^{o}C (probably due to steric repulsions). However, it stands to reason to assume that slight increase in temperature (from 25^{o}C to

37^{o}C) led to expansion of polymeric chains and allowed for the end-groups to more readily get exposed and interact with the protein.

3.3.3. Role of Water Molecules and Counter-ions in Protein Adsorption

The role of surface chemistry in protein adsorption has been a source of controversy in this field of research; raising questions about whether it is the functional groups on the surface of adsorbent which should be taken into account or the molecular mediators (such as water molecules and counter-ions) at the interface. Vogler *et.al.* have suggested that rather than the chemistry, it is the energetics of dehydration taking place at protein-surface interface which is the main factor influencing non-specific protein adsorption [35].

In order to be able to monitor water molecules and counter-ions involved in interaction of HSA and NPs, the Preferential Interaction (PI) theory was utilized. This theory explains how salt molecules influence protein adsorption process through controlling the transfer of solvent molecules (ions and water molecules) from/into interface [36]. It is basically demonstrating that interaction of a surface with any solute depends on whether the surface prefers the solvent molecules (i.e. ions and waters) to remain associated with it or to get displaced with a more favorable molecule (such as protein). In other words, the solutes that prefer to remain associated to water molecules will facilitate processes which reduce the wetted surface area (such as protein adsorption). It is believed that a salt's rank in the Hofmiester series [37], determines the way it interacts with water molecules associated with surfaces. More specifically for hydrophobic

interactions, a kosmotropic salt which tends to bind strongly to water would induce larger desolvation effect on the surface; this would generate a cavity in the interface allowing the protein to crawl in and get adsorbed. Conversely, a chaotropic salt which associates weakly with water would impede displacement of surface-bound water molecules by protein. It is important to note that one major assumption in application of PI theory to protein adsorption is the fact that the solution under study is composed of two independent regions: (i) bulk region which remains un-affected by the presence of protein; and (ii) local region where preferential accumulation/exclusion of solutes takes place. Therefore, in cases where the composition of bulk and local regions are identical, the PI coefficient is known to be zero.

PI coefficient has been theoretically attributed to the mass distribution of different species in solution (i.e. water and salt molecules as well as protein). On the other hand, the variations in the equilibrium binding constant (K) of interactions with respect to the solution ionic strength has been shown to be correlated with PI coefficients. Hence, it is thought that PI analysis can be used for quantification of interfacial molecules involved in processes such as protein adsorption.

Based on PI theory, the equilibrium constant for interaction of a protein with a surface is related to the salt concentration *via* following equation [38]:

$$\ln(K) = C - \frac{n\Delta v_w}{m_w g} m_s + \frac{(\Delta v_+ + \Delta v_-)}{g} \ln(m_s) \qquad \text{Equation (3-3)}$$

where, n is the valence of salt ions, $\Delta\upsilon_w$ is the number of water molecules released upon binding, m_w is molal concentration of water= 55.51 m, m_s is molal concentration of salt, $\Delta\upsilon_+$ and $\Delta\upsilon_-$ are the number of cations and anions transferred upon binding, and g is the activity coefficient (obtained *via* Debye-Hückle equation) which is a constant for each salt (as for NaCl, g= 1.6). It is important to note that, since in our experiments the relationship between variations in equilibrium binding constants and m_s was not linear, the distribution of water molecules and counter-ions could be assumed to be a constant value that is independent of salt concentration and the PI equation in the form of equation (3-3) could be utilized.

Equation (3-3) can be further simplified to:

$$\ln(K) = C - Bm_s + A\ln(m_s) \qquad \text{Equation (3-4)}$$

Where B and A are the PI parameters and the total number of water molecules ($\Delta\upsilon_w$) and counter-ions ($\Delta\upsilon_+ + \Delta\upsilon_-$) can be calculated using the following relationships:

$$\Delta v_w = \frac{B.g.m_w}{n} \qquad \text{Equation (3-5)}$$

$$\Delta v_+ + \Delta v_- = A.g \qquad \text{Equation (3-6)}$$

The salt used in these studies was decided to be NaCl which is a neutral salt (based on Hofmeister series ranking) and interact moderately with water. A

set of ITC experiments at different NaCl concentrations were performed to look at the impact the presence of salt has on HSA adsorption to NPs. Equation (3-4) was fitted to ITC results through non-linear least square regression method and PI parameters for interaction of each NP with HSA at both temperatures of study were obtained (equations (3-5) and (3-6)). The result of this analysis is presented in Figure 3-5. PI parameters (B and A) are directly proportional to $\Delta\upsilon_w$ and $\Delta\upsilon_+ + \Delta\upsilon_-$, as presented in equations (3-5) and (3-6). Therefore changes in these two parameters can be attributed to changes in number of water molecules and counter-ions at the interface.

As it was expected from hydrophobic nature of HSA adsorption to NPs studied herein, PI analysis confirmed that protein adsorption was accompanied by removal of water molecules from all NP surfaces, although with varying degrees (Figure 3-5, Top). The unmodified SNP surface demonstrated the largest degree of water removal upon HSA adsorption. This clearly indicates the effective role of PCBMA modification in maintaining a hydrated layer on the surface. Among all PCBMA-modified NPs, our data proved lower number of water molecules was released upon adsorption of HSA onto surfaces modified with C-5 spacer group (an effect which is more largely pronounced at 37^{o}C, perhaps due to increased internal energy of molecules at higher temperature). This finding is in agreement with the results of thermodynamic analysis presented in Tables 3-1 and 3-2 where it was shown that at both temperatures of study, for PCBMA-NPs modified with the same end-group chemistry, the ones with longer spacer group demonstrated lower degrees of surface coverage. Previously reported Differential Scanning

Calorimetry measurements [23] demonstrated larger water content inside the matrix of PCBMA coatings with C-5 spacer group compared to the ones with C-1 spacer group; a property which might be responsible for observed differences in B parameter for these surfaces (Figure 3-5, Top). On the other hand, the end-group chemistry seemed to also contribute largely to the numbers reported for B parameter at both temperatures of study (Figure 3-5, Top). As it can be inferred from this graph, greater number of water molecules were removed upon adsorption of HSA to NPs modified with TEMPO end-group; this can be explained considering the hydrophobic nature of TEMPO end-group present on these surfaces.

Interestingly, regardless of end-group chemistry, the B parameter for (C-1) NPs and (C-5) NPs was affected oppositely by temperature (Figure 3-5, Top): The increase in temperature from 25^{o}C to 37^{o}C caused a drastic increase in the number of water molecules removed from interface of HSA and (C-1) NPs (B parameter for these surfaces equals to ~ -14 and ~ -25 at 25^{o}C *vs*. ~ -53 and ~ -54 at 37^{o}C). Conversely, for NPs modified with 5 spacer groups (C-5) a decrease in the number of removed water molecules was observed by increasing the temperature (B parameter for these surfaces equals to ~ -11 and ~ -33 at 25^{o}C *vs*. ~ -3 and ~ -12 at 37^{o}C). The results presented in Tables 3-1 and 3-2 further validates this finding as increasing the temperature caused the values for entropy change to increase upon adsorption of HSA to C-1 NPs while it resulted in lower entropy change at higher temperature for C-5 NPs. Therefore, we conclude that zwitterion's spacer length influences the behavior of molecular mediators (mainly

water molecules) involved in protein adsorption, ultimately controlling the energetic of protein-surface interactions.

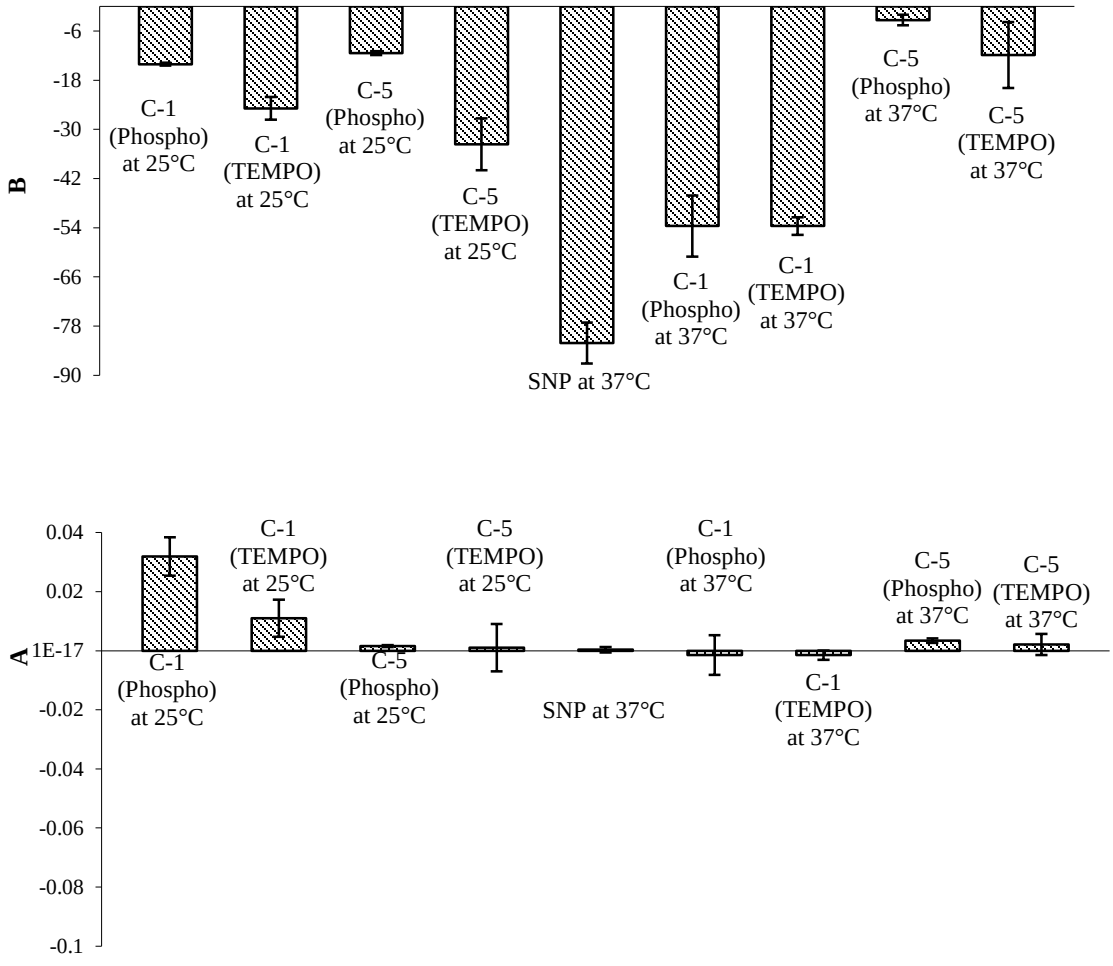

Figure 3-5. Preferential Interaction parameters B (top) and A (bottom) obtained through fitting of ITC results into equation 3-4. The error bars represent standard deviation of the obtained parameters calculated within the error margin of ITC results.

The calculated A parameter for different surfaces is presented in Figure 3-5, Bottom. Based on the reported values, changes in number of protein-associated counter-ions upon adsorption ($\Delta v_+ + \Delta v_-$) ranged between ~ -0.002 and ~ +0.05 (calculated *via* Equation (3-6)). Since these numbers are quite smaller than 1, we conclude that the role of counter-ion exchange in HSA adsorption to all surfaces studied herein was negligible. Although ITC analysis presented in preceding sections proved hydrophobic adsorption of HSA onto all surfaces under study; it is important to note that hydrophobic interactions dominating the adsorption process, does not necessarily imply zero ionic contribution to the adsorption. In fact, due to the complex nature of hydrophobicity, there have been two different types of hydrophobic adsorption mechanisms proposed by Estephan *et.al.* including ion-coupled and ion-decoupled categories [13]. Formation of ion pairs between a protein and a surface might be accompanied by release of water molecules giving rise to ion-coupled hydrophobic interactions. On the other hand, there are ion-decoupled hydrophobic phenomena where hydrophobic patches on the protein's surface would directly get exposed to hydrophobic groups on the surface, merely due to reorganization/release of water molecules [13].

Overall, PI analysis on adsorption of HSA to NPs revealed that ion-decoupled hydrophobic interactions are the main driving force for protein adsorption to surfaces studied herein. Moreover, the major role of zwitterionic coatings in maintaining a hydrated layer on the surface was quantitatively explained and it was shown that lower number of water molecules was removed from interface of HSA and PCBMA coatings with longer spacer group.

3.3.4. Enthalpy-Entropy Compensation

Although the values for enthalpy and entropy change varies for interaction of HSA with different NPs (Tables 3-1 & 3-2), the calculated ΔG for protein adsorption was almost in the same range for all surfaces under study. This is known as a hall mark for enthalpy-entropy compensation (EEC). Established originally on the basis of studies on host-guest complexations [39]; this empirical rule has been extended to carbohydrate-NP [40] and protein-NP [28] interactions as well. It stems from the hypothesis that enthalpy and entropy compensate for each other to keep the free energy change relatively constant. The relationship introduced for this compensatory effect between enthalpy and entropy is as follows [41]:

$$T\Delta S = \alpha\Delta H + T\Delta S_0 \qquad \text{Equation (3-7)}$$

The slope of the plot for TΔS *vs.* ΔH, symbolized by α in Equation (3-7), is known to represent the fraction of enthalpy change (generated due to structural reorganization of protein, polymer, and solvent molecules upon protein adsorption) which gets compensated by TΔS [41]. In other words, 1-α is the fraction of ΔH which directly contributes to the overall changes in ΔG. Hence, it has been suggested that α parameter can be a representative of conformational changes occurring in the system upon protein adsorption [28]. Alternatively, the positive intercept ($T\Delta S_0$) was related to the extent of entropically-favored events

(such as surface desolvation, counter-ion removal, etc.) that take place upon interactions.

The plots presented in Figure 3-6 demonstrated linear relationship between enthalpy and entropy for both PCBMA-modified NPs and SNP surfaces, indicating that enthalpy-entropy compensation exists for HSA-NP systems under study. This is consistent with previous reports by Rotello group, investigating protein adsorption to amino-acid functionalized gold NPs; where the slope and intercept for the enthalpy-entropy compensation plot was calculated to be 1.07 and 35.2 kJ mol^{-1}, respectively [28]. Interestingly, α parameter for interaction of HSA with PCBMA-functionalized NPs (~1.078, Figure 3-6, Top) appeared to be quite close to α for protein-NP systems studied by Rotello *et.al*. On the other hand, due to the rigid surface of SNP and in the absence of flexible PCBMA chains on the surface, a much smaller α for HSA-SNP systems was expected. It is striking that EEC plot for this surface demonstrated a larger α of ~1.097 (Figure 3-6, Bottom). This would partially explain non-fouling properties of PCBMA; as it can be concluded that modification of the SNP surface with zwitterionic polymer led to less structural perturbation in the protein and associated solvent molecules. Moreover, the larger intercept for SNP surface (~33 kJ mol^{-1}) compared to the intercept for PCBMA-modified surfaces (~31 kJ mol^{-1}) indicates larger desolvation effects accompanied the adsorption of protein onto SNP; a finding which is in agreement with the results of PI analysis presented earlier in this chapter.

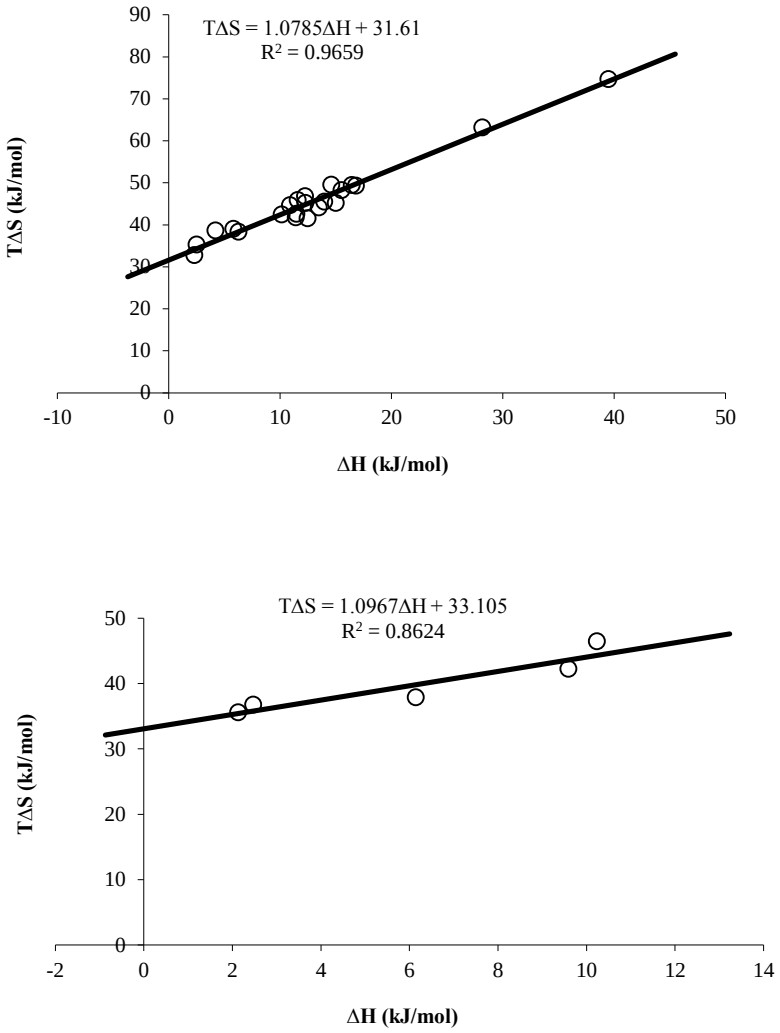

Figure 3-6. EEC plots for HSA adsorption onto PCBMA-modified NPs (Top) and SNP (Bottom). Data points represent enthalpy changes *vs.* entropy changes obtained from Tables 3-1 and 3-2, as well as ITC experiments at different ionic strengths. The solid lines were linearly fitted to the data points.

3.4. Conclusions

In this work, HSA molecule as a hydrophobic probe was utilized to investigate the thermodynamics of protein adsorption to zwitterionic PCBMA-modified NPs in order to gain a molecular-level understanding of their non-

fouling behavior. ITC study of the protein adsorption revealed that although a larger amount of HSA was loosely bound to unmodified SNP, surprisingly a sparsely adsorbed layer of this protein was more tightly bound to the surface of PCBMA-modified NPs. On the other hand, it was found that NPs modified with longer spacer group (C-5) interact more strongly with the protein (i.e. larger binding constants), while NPs which contain shorter spacer group or hydrophobic TEMPO end-group adsorb larger amounts of protein to their surface. Moreover, it was observed that increasing the temperature from 25^{o}C to 37^{o}C made the protein adsorption more thermodynamically favorable leading to larger binding constants for protein-NP interactions as well as higher degrees of surface coverage by protein. Our results proved that presence of PCBMA coatings on NP surface leads to lower number of water molecules removed from the interface as the hydrophobically interactive protein gets adsorbed; a finding which largely confirmed the hypothesis regarding strong electrostatic interaction of zwitterionic chains with water molecules. Collectively, ITC results, PI analysis, and EEC plots revealed that the main mechanism for adsorption of HSA to surface of NPs studied herein was ion-decoupled hydrophobic interactions. The major impact of PCBMA coatings on HSA adsorption was shown to be less interfacial dehydration and lower conformational changes of the interacting systems; factors directly linked to the superior anti-fouling characteristics of zwitterionic polymers.

3.5. References

[1] Jiang, S.; Cao, Z. *Adv Mater* **2010,** 22, 920-932.

[2] Chen, S.; Zheng, J.; Li, L.; Jiang, S. *J. Am. Chem. Soc.* **2005,** 127, 14473-14478.

[3] Chen, S. F.; Li, L. Y.; Zhao, C.; Zheng, J. *Polymer* **2010,** 51, 5283-5293.

[4] Zhang, Z.; Chen, S. F.; Chang, Y.; Jiang, S. Y. *J Phys Chem B* **2006,** 110, 10799-10804.

[5] Zhang, Z.; Vaisocherova, H.; Cheng, G.; Yang, W.; Xue, H.; Jiang, S. Y. *Biomacromolecules* **2008,** 9, 2686-2692.

[6] Yang, W.; Xue, H.; Li, W.; Zhang, J. L.; Jiang, S. Y. *Langmuir* **2009,** *25, 11911-*11916.

[7] Shih, Y. J.; Chang, Y. *Langmuir* **2010,** 26, 17286-17294.

[8] Chang, Y.; Higuchi, A.; Shih, Y. J.; Li, P. T.; Chen, W. Y.; Tsai, E. M.; Hsiue, G. H. *Langmuir* **2012,** 28, 4309-4317.

[9] Brault, N. D.; Sundaram, H. S.; Li, Y. T.; Huang, C. J.; Yu, Q. M.; Jiang, S. Y. *Biomacromolecules* **2012,** 13, 589-593.

[10] Lynch, I.; Dawson, K. A. *Nano Today* **2008**, 3, 40-47.

[11] Klein, J.; *Proc. Natl. Acad. Sci. U. S. A.*2007, 104, 2029-2030.

[12] Dong, Z.; Mao, J.; Yang, M.; Wang, D.; Bo, S.; Ji, X. *Langmuir* **2011**, 27, 15282–15291.

[13] Estephan, Z. G.; Schlenoff, P. S.; Schlenoff, J. B. *Langmuir* **2011**, 27, 6794–6800.

[14] Muro, E.; Pons, T.; Lequeux, N.; Fragola, A.; Sanson, N.; Lenkei, Z.; Dubertret, B. *J. Am. Chem. Soc.* **2010**, 132, 4556–4557.

[15] Liu, X.; Zhu, H.; Jin, Q.; Zhou, W.; Colvin, V. L.; Ji, J. *Adv. Healthcare Mater.* **2013**, 2, 352–360.

[16] Yang, W.; Zhang, L.; Wang, S.; White, A. D.; Jiang, S. *Biomaterials* **2009**, 30, 5617–5621.

[17] Noh, H.; Vogler, E. A. *Biomaterials* **2007,** 28, 405-422.

[18] Parhi, P.; Golas, A.; Vogler, E. A. *J Adhes. Sci. Technol.* **2010,** 24, 853-888.

[19] Shao, Q.; He, Y.; White, A. D.; Jiang, S. Y., *J. Phys. Chem. B* **2010,** 114, 16625-16631.

[20] Norde, W. *Adv. Colloid Interface Sci.* **1986**, 25, 267–340.

[21] Norde, W. *Pure Appl. Chem.* **1994**, 66, 491–496.

[22] Record, M. T.; Anderson, C. F.; Lohman, T. M. Q. *Rev. Biophys.* **1978**, 11, 103–178.

[23] Abraham, S.; So, A.; Unsworth, L. D. *Biomacromolecules* **2011,** 12, 3567–3580.

[24] Cedervall, T.; Lynch, I.; Lindman, S.; Berggård, T.; Thulin, E.; Nilsson, H.; Dawson, K. A.; Linse, S. *Proc. Natl. Acad. Sci. U. S. A.* **2007,** 104, 2050–2055.

[25] Abraham, S.; Unsworth, L.D. *J. Polym. Sci., Part A: Polym. Chem.* **2011,** 49, 1051-1060.

[26] Zhang, Y.; Li, J-H; Ge, Y-G; Liu, X-R; Jiang, F-L; Liu, Y. *J. Fluoresc***. 2011,** 21, 475-485.

[27] Velazquez-Campoy, A.; Leavitt, S.A.; Freire, E. *Methods Mol. Boil*. **2004,** 261, 35-54.

[28] De, M.; You, C.; Srivastava, S.; Rotello, V. M., *J. Am. Chem. Soc.* **2007**, 129, 10747-10753

[29] Mahmoudi, M.; Lynch, I.; Ejtehadi, M. R.; Monopoli, M. P.; Baldelli Bombelli, F.;, Lauren, S. *Chem. Rev*. **2011**, 111, 5610–5637.

[30] Shao, Q.; Jiang, S. *J. Phys. Chem. B* **2013**, 117, 1357−1366.

[31] Sugio, S.; Kashima, A.; Mochizuki, S.; Noda, M.; Kobayashi, K. *Protein Engineering* **1999**, 12, 439-446.

[32] Livingstone, J. R.; Spolar, R. S.; Record, M. T. *Biochemistry* **1991**, 30, 4237-4244.

[33] Spolar, R. S.; Livingstone, J. R.; Record, M. T. *Biochemistry* **1992**, 31, 3947-3955.

[34] Hildebrand, A.; Garidel, P.; Neubert, R.; Blume, A. *Langmuir* **2004**, 20, 320-328.

[35] Vogler, E. A. *Biomaterials* **2012**, 33, 1201-1237.

[36] Perkins, T.; Mak, D.; Root, T.; Lightfoot, E. *J. chromatogr., A* **1977**, 766, 1-14.

[37] Record, M.T.; Anderson, C.F.; Lohman, T.M. *Q. Rev. Biophy*. **1978**, 11, 103-178.

[38] Xia, F.; Nagrath, D.; Garde, S.; Cramer, S.M. *Biotechnol. Bioeng.* **2004,** 87, 354-63.

[39] Leffler, J. E. *J. Org. Chem*. **1955**, 20, 1202-1231.

[40] Zeng, Z.; Patel, J.; Lee, S-H.; McCallum, M.; Tyagi, A.; Yan, M.; Shea, K. J. J. *Am. Chem. Soc.* 2012, 134, 2681−2690.

[41] Rekharsky, M. V.; Inoue, Y. *Chem. Rev.* **1998**, 98, 1875-1917.

Chapter 4

Protein adsorption onto PCBMA-modified silica nanoparticles: insight into classically held electrostatically induced adsorption events

4.1. Introduction

Non-specific protein adsorption at the biomaterial-tissue interface has garnered significant attention due to the correlations made between this event and the initiation of multiple deleterious host effects (i.e. coagulation, immune response and inflammation) [1]. This issue becomes even more important when considering the design and implementation of cardiovascular biomaterials, where the surface is in permanent and direct contact with blood; a situation that directly affects the therapeutic efficacy of numerous applications of biomaterials, including drug delivery vehicles, stents, heart valves, etc. [2-4]. Surface modification is a well-known method for suppressing non-specific protein adsorption [5]. Several approaches involve the modification of biomaterial surfaces with various polymer structures, perhaps the most employed being poly (ethylene oxide) (PEO) [6-10]. Although widely studied, the use of PEO as a biomaterial coating has some major disadvantages, namely, loss of function due to oxidation *in vivo* [11,12]. As another class of non-fouling materials, poly (carboxybetaine methacrylamide) (PCBMA) belongs to a family of zwitterionic polymers that have been reported as being resistant to non-specific protein adsorption; a result that has been conjectured to be related to a highly hydrated outer surface [13,14]. That said, however, a detailed investigation on how PCBMA modification imbues the surface with non-fouling characteristics has not yet been executed. Also, a mechanistic understanding of how the polymer layer properties (internal film hydration and ion content, charge, end-group chemistry, etc.) affect protein-surface interactions is largely superficially defined. It is

thought that through obtaining a complete thermodynamic profile for non-specific protein adsorption, the underlying mechanisms responsible for inhibiting biofouling will be clarified. The application of this knowledge should directly affect the therapeutic efficacy of all biomaterials exposed to physiological environments.

Classically, the ITC technique has been employed for investigating protein-ligand interactions [15]. However, with the advent of medical applications of NPs, ITC has recently begun to be used to characterize protein-NP interactions. Recent work has shown that NP size and hydrophobicity play an important role in the adsorption of human serum albumin (HSA) onto N-isopropylacrylamide-co-N-tert-butylacrylamide (NIPAM/BAM) copolymer modified NPs; providing insight on the binding affinities, stoichiometries and entropy as a function of surface properties [16,17]. Other work has focused on investigating how electrostatic forces are involved in the adsorption of oppositely charged proteins to amino acid-modified Au NPs [18,20]. Adsorption of protein onto the surface of unmodified NPs (such as ZnO) has also been studied using ITC as a means of elucidating the fundamental mechanisms at work [21]. In fact, this methodology was employed to determine that the denaturing effect of ZnO NPs on the structure of adsorbed protein was due to strong electrostatic interactions that existed between this protein and NP [21]. That said, it is important to note that because of the various states in which a protein may reside at the interface, ITC results may only provide apparent thermodynamic properties for characterizing these adsorption events. However, whether the protein adsorption events inside the ITC

cell are reversible or not, does not affect the results obtained *via* ITC. According to Vogler *et.al.* thermodynamic equilibrium and reversibility are the two characteristics of ideal systems which are very hard to achieve through experimental methods used in the lab for protein adsorption studies, and lack of ideality in a system does not interfere with application of thermodynamics as a modeling tool [22].

Overall, hydration and charge are two surface properties that have recently been considered important when considering protein adsorption to any surface [23-26]. Herein, the role of hydration, ions, and charge in the protein-repellent behaviour of the zwitterionic surfaces will be discussed. It was suggested that protein adsorption onto PCBMA-modified surfaces is largely influenced by polymer chemistry [23]. The number of spacer groups (-CH_2-) present between the two poles of the zwitterion within the monomer being thought a key factor affecting hydration of the polymer chain that may, ultimately, affect conformation of adsorbed protein [23-27]. In order to obtain a quantitative understanding of the interfacial behaviour of proteins at these surfaces, the adsorption of model protein α-lactalbumin (Alpha-la) to various PCBMA-functionalized NPs was investigated using the ITC technique. Alpha-la is a small (14.2 kDa) protein with a pI of ~4.5 and a net surface charge of -11.2 (at pH 7.4) [28]. The fact that this protein has been studied extensively, and that it has a large surface charge at neutral pH were the primary reasons this protein was used, as it should represent most cases where charge effects are thought to dominant the adsorption process. For this study, silica NPs were functionalized with PCBMA differing in end-group chemistry

(either phosphonate (Phospho) or 2,2,6,6-tetramethylpiperidine-N-oxyl (TEMPO)) and the number of spacer groups (1 or 5 $–CH_2-$ group). The phosphonate end-group is a hydrophilic, negatively charged group and commercially available TEMPO end-group is a hydrophobic segment.

Other work from our group [23] illustrated that NPs bearing 5 spacer groups (C-5) are more hydrated than the ones containing one spacer group (C-1). In this work, other than looking into the effect of different surface chemistries on protein binding constants, the enthalpy and entropy changes at two different temperatures; the role of water molecules and counter-ions in protein adsorption onto these surfaces will be quantitavely discussed. This fundamental perspective should provide insight that can be used to further optimize the design of non-fouling surfaces.

4.2. Materials and Methods

Silica NPs (12 nm avg. diameter, Sigma-Aldrich) functionalized with PCBMA containing either one spacer group (C-1) or five of them (C-5), bearing different end-groups (Phospho/TEMPO) were prepared and characterized previously [14,23]. All aspects of polymerization and modification of the silica NPs used for this work including all polymer synthesis procedures with subsequent polymer and modified NP characterization, were previously reported [14]; the focus of this work being the interaction of these modified NPs systems with proteins and its thermodynamic characterization.

Briefly, NP modification involved an alkoxyamine initiator containing triethoxysilyl functional group being grafted to silica NPs in toluene solution. This NPs solution was centrifuged, so as to isolate the NPs from the initiator mixture. Synthesized carboxybetaine monomers, with various spacer groups between the carboxylic acid and quaternary amine, were employed as a method for controlling surface charge and hydration state. Nitroxide mediated free radical polymerization (NMFRP) was carried out to append carboxybetaine monomers to initiator grafted NPs, as detailed previously [14], and purified from solution free polymer and monomer mixture by centrifugation in distilled water prior to characterization.

Surface characteristics of all modified NPs have been previously reported in another work [23]. Size of functionalized NPs was 86-89 nm for Phospho end-group and 71-72 nm for TEMPO. Moreover, regardless of the end-group chemistry, the actual water content of C-5 NPs was higher than that for C-1 NPs (i.e. ~33-34% for C-5 NPs *vs*. ~29-31% for C-1 NPs). Also, at pH 7.0, which is the working pH of this study, all modified NPs had positive surface charge with NPs bearing Phospho end-group showing a more positive surface (ζ–potential value of ~24 mV) than NPs containing TEMPO end-group (ζ–potential value of ~10 mV), irrespective of the number of spacer groups. The PCBMA-grafted NPs were utilized for the protein adsorption experiments without further modification.

Bovine α-lactalbumin (calcium depleted, Type II, 14 kDa protein ≥ 85%), was purchased from Sigma-Aldrich (St. Luis. MO) and used without further

purification. All experiments were performed in phosphate buffer (10 mM, pH 7.4) prepared using disodium phosphate (J.T. Baker), potassium phosphate and sodium chloride (Sigma-Aldrich); components that were not further purified prior to use.

4.2.1. Characterization of Protein Secondary Structure

Far UV Circular Dichroism (CD) spectra were collected at 25 and 37^{o}C for α-lactalbumin using a Jasco J-810 CD/ORD (Japan) at 100 mdeg sensitivity, bandwidth of 1 nm, and data pitch of 0.5 nm. The buffered protein solution was pipetted into a cuvette with a 2 mm path length for acquiring the spectra, and each reading was repeated 5 times (average data plotted). A blank buffer reference was subtracted from the data before calculating the molar ellipticity. Molar ellipticity was calculated using well established methods [29]. Buffered protein solution concentration was verified using an Agilent UV-Vis Spectrophotometer at the fixed wavelength of 280 nm and molar extinction coefficient of 28,175 $M^{-1}cm^{-1}$ for α-lactalbumin. The results of these experiments are presented in Appendix B of this thesis.

4.2.2. ITC Characterization of Protein Adsorption

ITC was carried out for the express purpose of determining the nature of the binding event (enthalpic-entropic), strength of binding, binding stoichiometry, etc., upon interaction of Alpha-la and the various NPs. Survey titrations were conducted to obtain optimum solution concentrations for protein relative to NPs,

as required for ITC characterization to be possible. Blank experiments where titrant solutions were injected into an identical solution within the cell that contained buffer only were conducted so as to determine the background heat of dilution. Moreover, this was performed to ensure that no dissociation or precipitation of the titrant occurred upon injection. The dilution effect on enthalpy was then subtracted from the enthalpy profile as a function of titrant:titrand concentration ratio inside the ITC cell so as to determine the absolute enthalpy change upon binding [30].

α-lactalbumin adsorption experiments at 25^{o}C involved injecting protein solution into the ITC cell containing a NP solution, whereas experiments at 37^{o}C utilized inverse titrations (i.e. NP (titrant) and protein (titrand)). Inverse titrations are commonly used without affecting the analysis, and had to be performed due to very large background signals generated by injection of α-lactalbumin into buffer at this temperature [31-33]. The only effect inverse titrations have upon the data analysis is the inversion of the overall ratio of titrant to titrand (and hence the stoichiometry (n)) and has no other significant effect upon the analysis of the data obtained *via* mathematical modeling (described below), since the interfacial phenomena captured using ITC follows the rule of microscopic reversibility.

Experimental Procedure: All experiments were performed using a Nano-ITC (950 µl, TA Instruments, New Castle, DE). All solutions were prepared in phosphate buffer (10 mM, pH 7.4) and sodium chloride was used for varying ionic strength. The reference cell was filled with distilled water for all the

experiments. Prior to each experiment, buffered solutions of NPs and protein were degassed under vacuum, at room temperature, for 10 minutes. A small amount of titrant (1 µl) was firstly injected and the heat signal was ignored in enthalpy calculation to compensate the error generated by insertion of the needle into the ITC cell and/or leakage of the solution inside the syringe. After a 300 s interval, the experiment was followed by 19 more injections (12.5 µl injection volume and 300 s injection interval). The stirring rate of the syringe inside the reaction cell was set at 270 rpm.

The binding stoichiometry (n), binding constant (K), and enthalpy change (ΔH) were determined using the NanoAnalyze software (TA Instruments) utilizing the model for single set of independent binding sites [34]. Subsequent Gibbs free energy changes (ΔG) and entropy changes (ΔS) were then calculated using standard thermodynamic equations:

$$\Delta G = RT\ln(K) \qquad \text{Equation (4-1)}$$

$$\Delta G = \Delta H - T\Delta S \qquad \text{Equation (4-2)}$$

where R is the gas constant and T is the absolute temperature.

The numbers of proteins on NP surface at 100% surface coverage was obtained by calculating the surface area of a sphere with a radius equal to that of NP plus the protein's stokes radius (1.91 nm) and dividing it into protein cross-sectional surface area. The experimental protein:NP ratio, obtained *via* ITC, was then divided into theoretical number for 100% coverage and the percentage of

surface coverage was determined [17]. More details on experimental procedure and data analysis are presented in Appendix A of this thesis.

4.3. Results and Discussion

4.3.1. Thermodynamics of Protein Adsorption

Prior to all ITC experiments, CD experiments were conducted to ensure that the secondary structure of α-lactalbumin remained unaltered due to differences in solution temperature (i.e. 25 *vs.* 37°C). It was observed (results not shown) that the change in solution temperature did not alter the secondary structure of this protein and, therefore, it is probable that differences observed in adsorption properties are not related to temperature-associated secondary structure variations. Figure 4-1 (Top) illustrates a representative raw ITC heat flow profile, the control blank experiment, as well as the uncorrected protein-NP experimental curve. Figure 4-1 (Bottom) illustrates the calculated molar enthalpy curve for the interaction between Alpha-la and C-5(TEMPO) modified NP at 25°C. The area under each peak in raw data represents the enthalpy change.

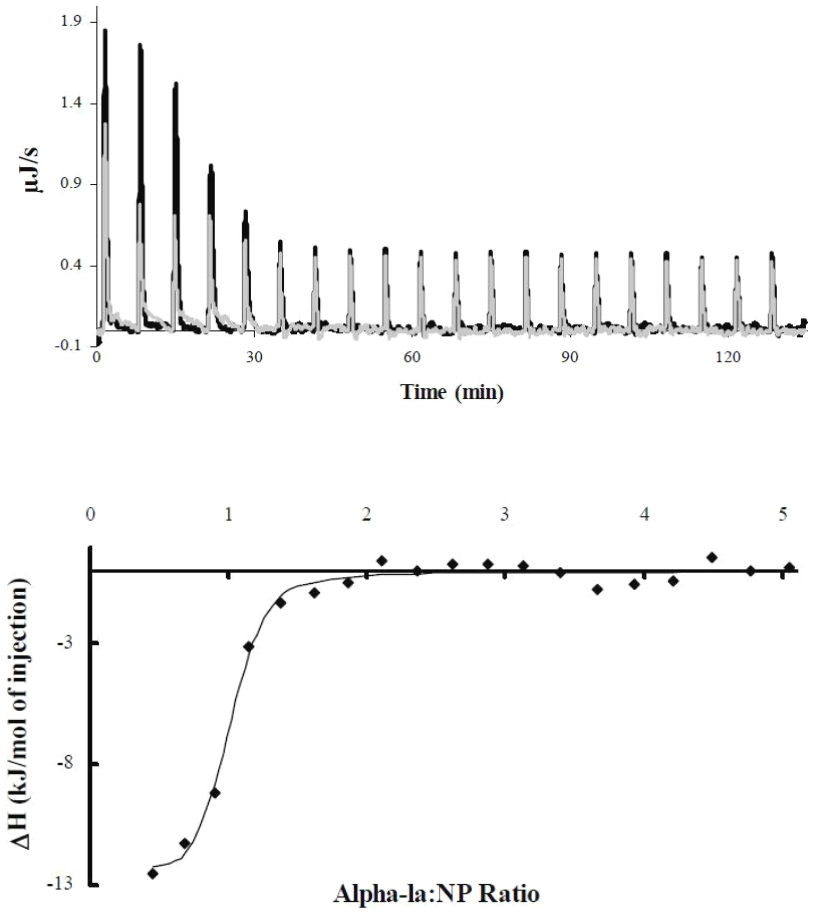

Figure 4-1. Representative plot illustrating the results obtained from an ITC experiment. Top: Raw data for Alpha-la (0.4 mM) titration into C-5 (Tempo) solution (0.025 mM) at 25°C (black line) and Alpha-la (0.4 mM) titration into buffer at 25°C (blank experiment - grey line). Each peak corresponds to an injection volume of 12.5 µL. Bottom: Molar enthalpy change for Alpha-la titration into C-5(TEMPO) solution at 25°C, obtained by integrating the area under each peak in the raw data after subtracting background, divided by the moles in each injected volume (solid line represents fitting of the data to the model for single set of independent binding sites, SD=1.8).

The background heat flow monitored *via* blank experiment was lower compared to heat signals generated upon NP-protein interaction (Figure 4-1, Top). In this specific case, the interaction between NP and protein was exothermic (i.e. $\Delta H<0$) and the NP-protein bonding approached saturation before the end of the experiment (Figure 4-1); the latter being crucial for modeling the obtained data.

As presented in Figure 4-2, at 25^{o}C the adsorption of Alpha-la onto all PCBMA modified NPs was found to be exothermic. However, the extent of changes in enthalpy was different for NPs modified with different polymer chemistries. Also, these curves clearly demonstrate that all NP surfaces were saturated by protein by the end of each experiment; hence the plateau phase at higher protein concentrations.

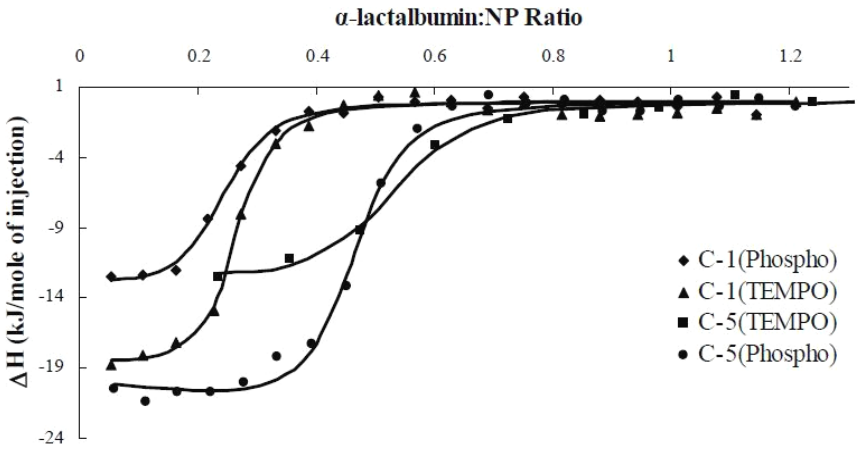

Figure 4-2. Molar enthalpy change upon titration of α-lactalbumin (0.2:0.4 mM, top) into NP solutions (0.025:0.05 mM) at 25°C (solid lines represent fitting *via* Eq. 4-2).

It has been shown that enthalpic and entropic contributions to the protein adsorption process may represent the nature of the driving force for the interaction [35]. While favorable enthalpic changes (i.e. $\Delta H<0$) are known to be a sign for formation of non-covalent bonds at the interface, favorable entropy changes (i.e. $\Delta S>0$) may largely represent desolvation of the interface that is primarily associated with hydrophobic interactions [35]. The importance of electrostatic contributions in Alpha-la adsorption onto different surfaces has been already demonstrated in previous studies [36,37]. Moreover, taking into account the positive charge on the surface of PCBMA-modified NPs and the negative charge of the protein at the experimental pH, the electrostatic interactions are expected to be present. This is opposed to the electrostatic repulsion that is probable between Alpha-la and negatively charged silica NPs (SNPs), which probably weakened the protein-SNP interaction to such an extent that it was undetectable at 25°C (Table 4-1). While it is plausible that the adsorption of Alpha-la onto SNP was so low that it did not generate any ITC signal, there is another possibility that this interaction was merely driven through entropic contributions resulting in enthalpy change to be minimal or zero and thus undetectable *via* ITC.

Adsorption of Alpha-la onto C-5(Phospho) NP exhibited the most negative enthalpy change compared to other surfaces, suggesting a stronger non-covalent contribution to protein bonding to these surfaces. In addition, regardless of end-group chemistry, the respective apparent binding constant for NPs modified with 5 spacer groups (6.28×10^6 M^{-1} and 5.94×10^6 M^{-1}) were larger compared to NPs

modified with 1 spacer group (3.61×10^6 M^{-1} and 4.11×106 M^{-1}) (Table 4-1). The protein-repellent behavior of PCBMA coatings is thought to be mainly due to the zwitterion segment of this polymer in which the positive quaternary ammonium salt and negative carboxylate of the monomers can interfere with the optimum exposure of surface charges on the interacting molecule [23]. Therefore, the results presented above can be explained knowing that a longer spacer group inside the pendant zwitterions would influence protein adsorption onto PCBMA coatings in such way that larger number of surface charges were allowed to get exposed and interact with oppositely charged groups on the surface of protein, resulting in a greater negative enthalpy change and larger binding constant.

Table 4-1. Apparent thermodynamic parameters for the binding of Alpha-la to various PCBMA-grafted silica NPs at 25°C, derived from the fitting of ITC curves using the independent binding sites model. The errors denote the standard deviation of non-linear least-squares analyses.

NP	[a]K x10^{-6} (M^{-1})	n	Coverage (%)	ΔH (kJ/mol)	TΔS (kJ/mol)	ΔG (kJ/mol)
SNP	N/A	N/A	N/A	N/A	N/A	N/A
C-1 (Phospho)	3.61±1.34	0.28±0.01	0.015±0.001	−13.03±0.67	24.38±1.45	−37.41±0.78
C-1 (TEMPO)	4.11±1.79	0.24±0.01	0.018±0.001	−18.92±0.87	18.81±1.77	−37.73±0.90
C-5 (Phospho)	6.28±1.82	0.44±0.01	0.022±0.001	−20.32±0.46	18.03±1.19	−38.35±0.73
C-5 (TEMPO)	5.94±1.73	0.94±0.21	0.071±0.015	−11.83±0.56	26.81±1.55	−38.64±0.99

[a]K:binding constant, n:binding stoichiometry (protein:NP ratio), ΔH:enthalpy change, ΔS:entropy change, ΔG: free energy change.

Table 4-1 also illustrates the effect of end-group chemistry on the adsorption of Alpha-la. As can be seen, for each group of NPs with equal number of spacer groups, systems modified with TEMPO end-group showed a larger apparent binding constant. The fact that Alpha-la adsorption onto PCBMA modified NPs was influenced by end-group chemistry coincides with our previous results investigating the conformational changes of the protein upon adsorption to these surfaces [23]. Although electrostatic forces are known as the main mechanism for Alpha-la adsorption, it should be noted that ~61% of this protein's surface area exhibits apolar nature [38] and this might be the reason for stronger interaction (reflected in binding constants) as well as greater adsorption-induced unfolding (shown in ref 23) of the protein upon adsorption onto surfaces containing hydrophobic TEMPO end-group.

The binding stoichiometries (n) reported in Table 4-1 illustrate protein:NP ratios at 25°C. However in order to be able to discuss the extent of protein adsorption more quantitatively, it is necessary to take the NP size into account and thus report the extent of its surface coverage instead. Hydrodynamic diameters of the NPs used in this study, measured *via* dynamic light scattering, were reported previously [23]. At 25°C the surface coverage of NPs was influenced by both length of spacer group and chemistry of end-group, as reflected in greater surface coverage for NPs modified with 5 spacer groups and/or TEMPO end-group (Table 4-1). Overall, the calculated numbers for surface coverage of modified NPs suggest that protein was sparsely adsorbed onto these surfaces.

As discussed earlier, for the interaction between Alpha-la and modified NPs, enthalpy and entropy were both favorable. However in cases where $|\Delta H|<|T\Delta S|$, it is thought that protein adsorption is entropically-driven [39]. Previous studies confirm loosening or unfolding of this protein upon adsorption onto NPs modified with PCBMA [23]. These types of conformational changes along with the induced reorganization of water molecules on the surface of newly-formed complexes might be a source for less favorable enthalpy change upon protein adsorption onto these surfaces. On the other hand, entropy is favorable and positive most likely due to the large disordering effects generated by water reorganization; a contribution which overshadowed the minimal unfavorable entropy changes caused by loss of molecular freedom upon protein binding. In the following section, the effect of temperature on Alpha-la adsorption onto these NPs is discussed.

4.3.2. Effect of Temperature on Protein Adsorption

A few previous reports discuss the effect of temperature on physicochemical properties of zwitterionic sulfobetaines [40,41]; even detailing an Upper Critical Solubility Temperature (UCST) of ~30°C for this polymer [42]. However, to best of our knowledge, there has been no such work conducted for carboxybetaines and the effect of temperature on either physicochemical properties of this polymer or its protein-repellent behaviour is currently unknown. Enthalpy curves (Figure 4-3) illustrate that protein adsorption (37°C) was exothermic and all interactions have reached saturation. Apparent thermodynamic

parameters (Table 4-2) demonstrated that increasing the temperature did not affect the sign of the enthalpy or entropy changes, only the values for enthalpy change were more negative compared to 25°C: suggesting a higher level of interaction between protein and surface.

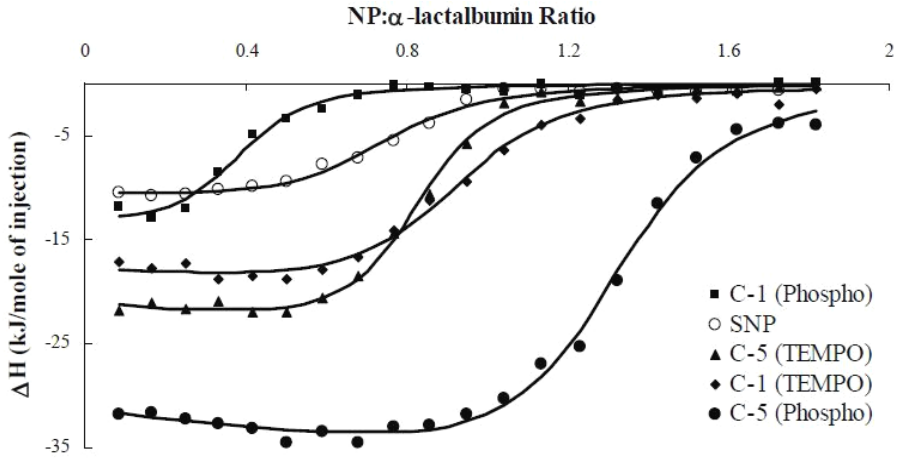

Figure 4-3. Molar enthalpy change upon titration of NP solutions (0.15 mM) into α-lactalbumin (0.025 mM) at 37°C (solid lines represent fitting *via* Eq. 4-2).

Interestingly, protein adsorption onto SNP surfaces generated a measureable response (Figure 4-3) upon increasing the temperature to 37°C. As can be seen in Table 4-2, adsorption of Alpha-la on SNP surface showed the largest entropy change compared to modified surfaces. Furthermore, the temperature increase also affected the extent to which the NP surface was covered by protein. Comparing the values presented in Tables 4-1 and 4-2, it can be concluded that larger amounts of protein were adsorbed at 37°C. This increased temperature also minimized the effect that the number of spacer groups in the zwitterion had on protein adsorption (which was observed at 25°C). However, the

greater surface coverage for TEMPO end-groups that existed at 25°C was still observed at 37°C (Table 4-2). Moreover, the degree of surface coverage for SNP (~2.39%) was shown to be drastically larger than that for modified surfaces (~0.04-0.1%). This clearly demonstrates the role of PCBMA grafting in inhibiting non-specific protein adsorption. Although it is important to note that the quantity of the adsorbed protein on one hand, and its affinity for the surface on the other, are both crucial factors in non-specific protein adsorption and neither should be overlooked. It has been established that a variety of serum-abundant proteins can bind to NP surfaces, and subsequently be replaced by proteins that may be at a lower concentration but have higher affinity for the surface [16,35,43,44]; an extension of the Vroman effect which has been widely recognized for flat surfaces [45]. Within the same context, while investigating adsorption of the same protein to different surfaces, it stands to reason to characterize the surface with lower binding affinity for that protein as a more efficient non-fouling surface. In the case of Alpha-la adsorption, it was surprisingly observed that although larger quantities of this protein were adsorbed to SNP surfaces, the protein was more tightly bound to some of the modified NPs: respective apparent binding constants for Alpha-la adsorption to modified and unmodified surfaces were $\sim 2\times 10^{6}$-4×10^{6} and $\sim 1.84\times 10^{6}$, respectively. Overall, while examining non-specific protein adsorption, protein affinity for the surface should be considered in parallel with its adsorbed amount.

Table 4-2. Apparent thermodynamic parameters for the binding of Alpha-la to various PCBMA-grafted silica NPs 37°C, derived from the fitting of ITC curves using the independent binding sites model. The errors denote the standard deviation of non-linear least-squares analyses.

NP	[a]K x10^{-6} (M^{-1})	n	Coverage (%)	ΔH (kJ/mol)	TΔS (kJ/mol)	ΔG (kJ/mol)
SNP	1.84±0.74	0.71±0.03	2.39±0.03	−10.80±0.60	26.32±1.49	−37.12±0.89
C-1 (Phospho)	0.90±0.30	0.50±0.02	0.11±0.00	−15.45±1.02	19.89±2.23	−35.33±1.08
C-1 (TEMPO)	2.10±0.31	0.89±0.03	0.09±0.00	−18.31±1.11	19.21±1.46	−37.52±0.35
C-5 (Phospho)	2.88±0.78	1.28±0.03	0.04±0.00	−32.08±1.79	6.25±2.41	−38.33±0.62
C-5 (TEMPO)	4.00±0.91	0.79±0.01	0.09±000	−21.56±0.63	17.62±1.16	−39.18±0.53

[a]K:binding constant, n:binding stoichiometry (NP:protein ratio), ΔH:enthalpy change, ΔS:entropy change, ΔG: free energy change.

4.3.3. Role of Water Molecules and Counter-ions in Protein Adsorption

In order to further define the role of electrostatic *vs.* hydrophobic interactions in Alpha-la adsorption to NPs, the role of water molecules and ions were investigated. The zwitterionic nature of PCBMA makes it sensitive to changes in solution ionic strength. For instance, poly-zwitterions have been identified with anti-polyelectrolyte activity which leads to an expansion of these polymeric chains in ion-containing solutions [46]. Moreover, it has been shown that increasing the ionic strength of the solution results in lower protein adsorption onto PCBMA-modified surfaces (due to screening effect, i.e. less exposed charge would result in this observation) [47]. On the other hand, ions and salt molecules are known to greatly influence proteins and the equilibrium conditions of their interactions through changing the water activity inside the

solution, or altering the existing electric field (Debye-Hückel screening effects) [48].

In order to examine the role of hydration and charge in non-fouling behavior of PCBMA coatings, ITC experiments at different salt concentrations were performed to be able to quantify the number of water molecules and counter-ions involved in the protein adsorption process. The salt used for varying the buffer ionic strength was NaCl (5-50 mM), a neutral salt (*vs.* kosmotropic and chaotropic salts) that binds moderately to water [49]. Calculations were performed using Preferential Interaction (PI) analysis proposed by Perkins *et.al*. [50]; a theory based on the interaction of salt and protein in aqueous solutions. PI analysis largely discusses the impact the presence of the protein has on the distribution of water and salt molecules. The binding affinity between the protein and the surface (K) has been related to the concentration of salt in solution (m_s) by [51]:

$$\ln(K) = C - \frac{n\Delta v_w}{m_w g} m_s + \frac{(\Delta v_+ + \Delta v_-)}{g} \ln(m_s) \qquad \text{Equation (4-3)}$$

where n is the valence of salt ions, $\Delta\upsilon_w$ is the number of water molecules released upon binding, m_w is molal concentration of water= 55.51 m, m_s is molal concentration of salt, $\Delta\upsilon_+$ and $\Delta\upsilon_-$ are the number of cations and anions released upon binding, and g is the activity coefficient which is a constant for each salt (as for NaCl, g= 1.6). Equation (4-3) can be further simplified to:

$$\ln(K) = C - Bm_s + A\ln(m_s) \qquad \text{Equation (4-4)}$$

where B and A are called preferential interaction parameters. Total number of water molecules and counter-ions transferred from or into a system consisted of bonded protein and surface can be calculated utilizing the following relationships:

$$\Delta v_w = \frac{B.g.m_w}{n} \qquad \text{Equation (4-5)}$$

$$\Delta v_+ + \Delta v_- = A.g \qquad \text{Equation 4-(6)}$$

Through non-linear regression fitting of Equation (4-4) to the results of ITC experiments at different salt concentrations (i.e. [NaCl] of 5-50 mM), preferential interaction parameters B and A for interaction of each NP with Alpha-la at both 25°C and 37°C were calculated (Figure 4-4). As shown in equations (4-5) and (4-6), B and A are directly related to Δv_w and $\Delta v_+ + \Delta v_-$ for the system, and can be attributed to changes in the number of water molecules or counter-ions transferred upon adsorption, respectively.

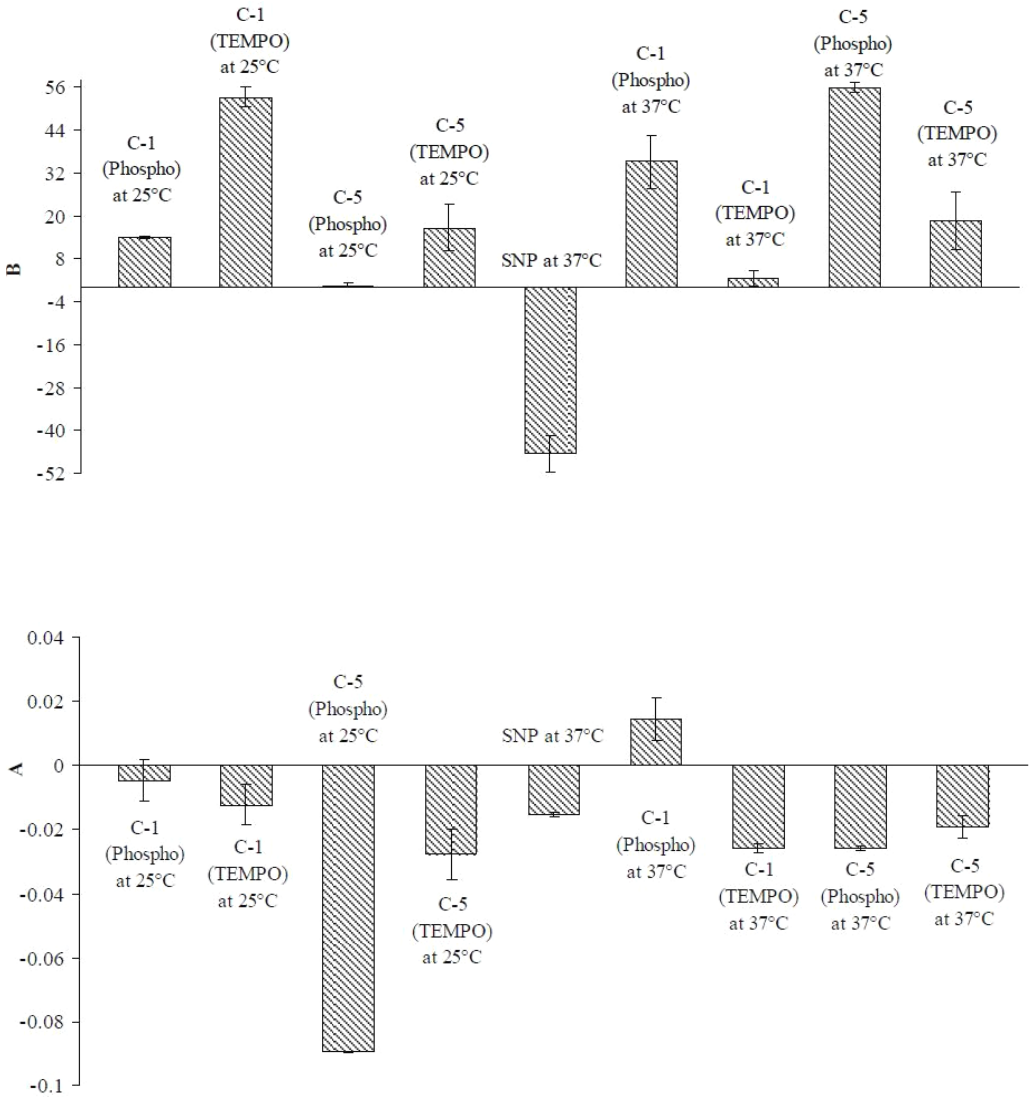

Figure 4-4. Preferential Interaction parameters B (top) and A (bottom) obtained through fitting of ITC results into equation 4-4. The error bars represent standard deviation of the obtained parameters calculated within the error margin of ITC results.

At 25°C, surfaces modified with shorter spacer group (C-1) showed the largest increase in the number of associated water molecules (i.e. ~1944 and ~509 mole water per mole of protein for C-1(TEMPO) and C-1(Phospho), respectively). While at 37°C, the effect of end-group chemistry was largely pronounced and the maximum increase in water density was observed for C-5(Phospho) NP (i.e. ~2063 mole water per mole of protein). Taking into account the numbers reported previously for the degree of surface coverage in Tables 4-1 and 4-2, it may be concluded that a larger increase in the local water density upon Alpha-la adsorption was observed for protein-NP systems with a lower degree of surface coverage. Therefore, surfaces that adsorbed less amount of protein allow for a larger number of water molecules to be associated with the formed complex. That said, however, a more robust speculation about the effect of polymer chemistry on the change in density of associated water molecules upon protein adsorption would require considering many different factors such as the initial hydration of the interacting surfaces, hydration states, and dynamic profile of the hydration layer.

The A parameter (related to changes in the number of protein-associated counter-ions: $\Delta v_{+}+\Delta v_{-}$) for adsorption of Alpha-la and various NPs is presented in Figure 4-4, Bottom. These results demonstrated that the amount of transferred counter-ions upon interaction of protein with all surfaces under study was quite negligible and very close to zero. The calculated number of exchanged counter-ions using Equation (4-6), ranged between ~0.03 to ~0.16 which is far from 1. In case of SNP, considering the fact that adsorption of this protein to SNP is driven

through hydrophobic interactions, zero counter-ion release was expected. However for PCBMA-modified NPs, negligible amount of counter-ions involved in protein adsorption led us to conclude that Alpha-la interaction with PCBMA-modified NPs was not an ion-coupled process.

Collectively, PI analysis revealed that the major impacts PCBMA modification had was the increase in number of associated water molecules as well as inhibition of counter-ion release upon protein adsorption. This was observed from the fact that protein adsorption to these surfaces led to an increase in the number of protein-associated water molecules for all modified samples, unlike the unmodified SNP surface that demonstrated a decrease in number of local water molecules upon protein adsorption (Figure 4-4, Top) indicating hydrophobic surface desolvation occurring. In conjunction with retention of the waters, the observed minimal counter-ion release from PCBMA-modified NPs would lead us to conclude that dipole-dipole or hydrogen bonding might be responsible for minimal adsorption of Alpha-la to PCBMA coated surfaces. Our result is in strong agreement with the widely-accepted hypothesis regarding protein-repellency mechanism of anti-fouling surfaces; as Estephan *et.al.* proposed that lack of counter-ion release from anti-fouling surfaces (such as Poly Ethylene Glycol and zwitterionic Poly Sulfobetaine) is the main reason behind their protein-repellent behavior [52].

4.3.4. Compensation Effects

The compensatory effect between enthalpy and entropy was introduced and empirically discussed by Leffler [53]. Performing comparative analyses on apparent thermodynamic parameters, reported for a wide range of molecular recognition systems, has led to finding a linear relationship between enthalpy and entropy *via* [54]:

$$T\Delta S = \alpha\Delta H + T\Delta S_0 \qquad \text{Equation (4-7)}$$

A positive intercept ($T\Delta S_0>0$), being the case where $\Delta H=0$, the complex would still be stable (i.e. $\Delta G<0$) [54]. Therefore, $T\Delta S_0$ is known as the intrinsic stability of any system and quantitatively defines the extent of induced dehydration that occurs upon interaction. The slope of the line (α) has also been experimentally attributed to conformational changes occurring in the entire system (protein, polymer, solvent molecules, etc.) upon interaction [54]. To ascertain the characteristics of the adsorbed state of the system more accurately, the apparent thermodynamic data obtained herein (Tables 4-1 and 4-2), as well as the data obtained from experiments at different ionic strengths, were used to generate a compensation plot: entropy changes ($T\Delta S$) plotted as a function of enthalpy changes (ΔH) (Figure 4-5). A linear relationship was observed between enthalpy and entropy for the adsorption of Alpha-la onto both modified and unmodified NPs; suggesting that enthalpy-entropy compensation (as previously observed for other systems) [18, 53, 54] exists for these systems as well.

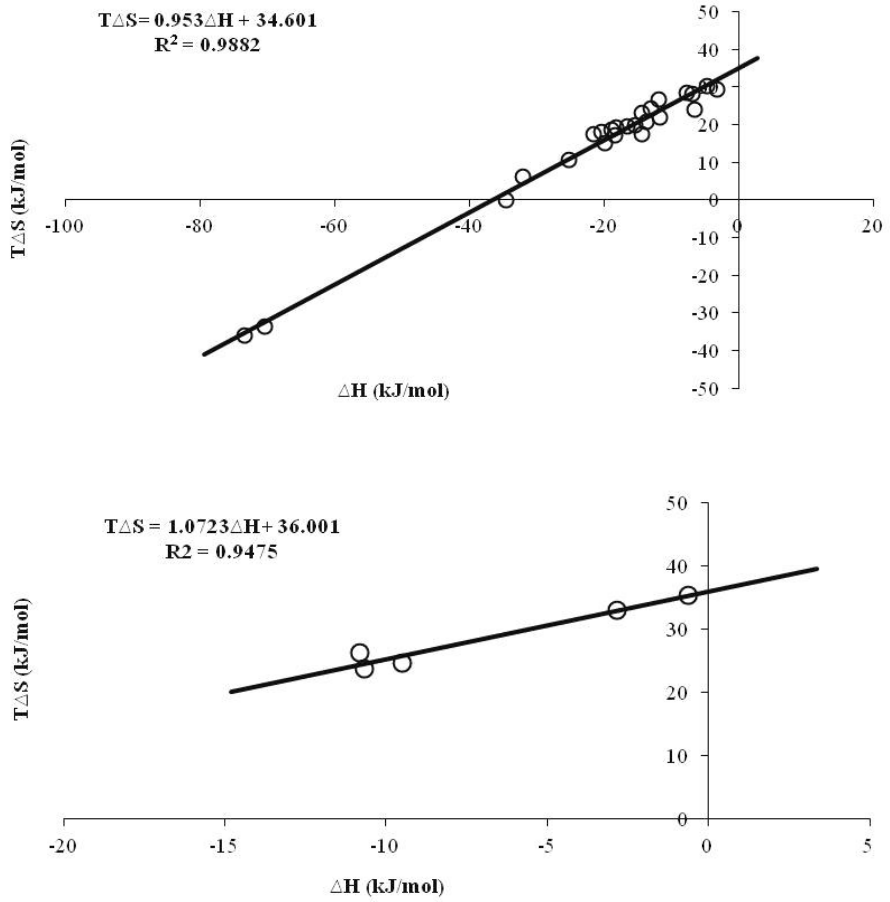

Figure 4-5. Compensation plots for Alpha-la adsorption onto PCBMA-modified NPs (Top) and SNP (Bottom). Data points represent enthalpy changes *vs.* entropy changes obtained from Tables 4-1 and 4-2, as well as ITC experiments at different ionic strengths. The solid lines were linearly fitted to the data points.

As depicted in Figure 4-5, α values are drastically different between PCBMA-modified surfaces (α = 0.95) and unmodified SNP (α = 1.07). Despite the presence of polymer chains on the surface of the PCBMA-modified NPs that may have a high potential for structural reorganization, systems consisting of these surfaces and Alpha-la underwent smaller conformational changes compared

to protein-SNP complexes. Suggesting the attributes of PCBMA coatings may lead to an overall lower reorganization upon protein-NP complex formation. This is in agreement with the results of our previous work investigating Alpha-la conformational changes upon interaction with PCBMA-modified NPs *via* CD [23]. Interestingly, α value for protein-PCBMA NP complexes were similar to protein-protein (α = 0.92) and protein-peptide (α = 0.96) systems studied previously [18]. Therefore, it can be concluded that interaction-induced conformational changes are very similar among PCBMA-modified NPs and physiologically relevant biomolecules. Conversely, Figure 4-5 illustrates that intercept ($T\Delta S_0$) points for protein-SNP complexes (~36 kJ/mol) are larger compared to that for PCBMA-modified NPs (~34 kJ/mol). A larger intercept would mean larger amount of water was removed from the surfaces upon interaction. This is consistent with hydrophobic interactions driving the adsorption of Alpha-la onto SNP and also the results of PI analysis presented formerly.

4.4. Conclusions

A fundamental, thermodynamic investigation of protein adsorption to PCBMA-functionalized NPs varying in surface charge and hydration was conducted. Based on our findings, longer spacer-group and/or hydrophobic end-group inside the polymer chain result in stronger interaction with Alpha-la as well as higher degrees of surface coverage. In general, even a mild increase in temperature from 25 to 37°C led to an increase in the degree of surface coverage

by protein. At 37°C, although surface coverage for unmodified SNP was significantly larger than that for PCBMA-modified NPs, the protein was more tightly bound to some of PCBMA-modified NPs. Therefore, we suggest that parallel consideration of the quantity of adsorbed protein on one hand, and its affinity for the surface on the other hand would result in a more efficient design of non-fouling materials.

The apparent thermodynamic profile for Alpha-la adsorption onto these systems demonstrated that while ion-decoupled non-hydrophobic processes (such as dipole-dipole and hydrogen bonding) was responsible for Alpha-la adsorption to PCBMA coated NPs, hydrophobic forces were dominant in adsorption of this protein onto SNP. This was further confirmed by the decrease in the local number of protein-associated water molecules upon adsorption onto SNP as well as larger desolvation-generated entropy monitored *via* compensation plots. It was also observed that zwitterionic polymers were able to maintain a tightly bound water layer on the surface, where PI analysis showed that for all modified surfaces the number of protein-associated water molecules increased upon protein adsorption. However, this analysis also proved zero counter-ion release upon adsorption of Alpha-la to all NPs; a result which might sound surprising due to the fact that electrostatic interaction of Alpha-la with various surfaces has been classically acknowledged.

In general, our findings indicated that presence of PCBMA film on the surface leads to: i) increase of water molecules at the interface, ii) prevention of

counter-ion release and iii) lower structural reorganization of the system upon protein-surface interaction. To summarize, this comprehensive thermodynamic analysis of protein adsorption to PCBMA modified substrates directly addressed the molecular mechanisms involved in non-fouling behaviour of zwitterionic coatings. The results of this study are thought to be crucial to the effective design of all blood contacting biosurfaces.

4.5. References

[1] Ratner, B.D.; Hanson, S.R.; Harker, L.A. In: Biomaterials Science: An Introduction to Materials in Medicine, 2nd ed.; Hoffman, A.; Lemons, J.; Schoen, F.; Academic Press: CA, USA, 1996; p 163.

[2] Arayne, M.S.; Sultana, N.; Qureshi, F. *Pak. J. Pharm. Sci.* **2007,** 20, 340-348.

[3] Kim, S.M.; Dean, L. S. *Cardiovasc. Ther.* **2011**, 29, 190-198.

[4] Shen, M.; Marie, P.; Farge, D.; Carpentier, S.; De Pollak, C.; Hott, M.; Chen, L.; Martinet, B.; Carpentier, A. *C.R. Acad. Sci. III,* **1997**, 320, 49-57.

[5] Kang, C.K.; Lee, Y.S. *J. Mater. Sci.: Mater. Med.* **2007**, 18, 1389-1398.

[6] Unsworth, L.D.; Sheardown, H.; Brash, J.L. *Biomaterials* **2005,** 26, 5927-5933.

[7] Unsworth, L.D.; Sheardown, H.; Brash, J.L. *Langmuir* **2005,** 21, 1036-1041.

[8] Unsworth, L.D.; Tun, Z.; Sheardown, H.; Brash, J.L. *J. Colloid Interface Sci.* **2005**, 281, 112-121.

[9] Unsworth, L.D.; Tun, Z.; Sheardown, H.; Brash, J.L. *J. Colloid Interface Sci.* **2006**, 296, 520-526.

[10] Unsworth, L.D.; Sheardown, H.; Brash, J.L. *Langmuir* **2008**, 24, 1924-1929.

[11] Shen, M.; Martinson, L.; Wagner, M.S.; Castner, D.G.; Ratner, B.D.; Horbett, T.A. *J. Biomater. Sci., Polym. Ed.* **2002**,13, 367–390.

[12] Li, L.; Chen, Sh.; Jiang, Sh. *J. Biomater. Sci., Polym. Ed*. **2007,** 18, 1415–1427.

[13] Jiang, Sh.; Cao, Zh.; *Adv. Mater.* **2010**, 22, 920-932.

[14] Abraham, S.; Unsworth, L.D. *J. Polym. Sci., Part A: Polym. Chem.* **2011,** 49, 1051-1060.

[15] Perozzo, R.; Folkers, G.; Scapozza, L. *J. Recept. Signal Transduction* **2004,** 24, 1-52.

[16] Cedervall, T.; Lynch, I.; Lindman, S.; Berggård, T.; Thulin, E.; Nilsson, H.; Dawson, K. A.; Linse, S. *Proc. Natl. Acad. Sci. U. S. A.* **2007,** 104, 2050–2055.

[17] Lindman, S.; Lynch, I.; Thulin, E.; Nilsson, H.; Dawson, K. A.; Linse, S. *Nano Lett.* **2007**, 7, 914-920.

[18] De, M.; You, C.; Srivastava, S.; Rotello, V. M., *J. Am. Chem. Soc.* **2007**, 129, 10747-10753.

[19] De, M.; Miranda, O.R.; Rana, S.; Rotello, V.M. *Chem. Commun.* **2009**, 16, 2157–2159.

[20] Chen, K.; Xu, Y.; Rana, S.; Miranda, O.R.; Dubin, P.L.; Rotello, V.M.; Sun, L.; Guo, X. *Biomacromolecules* **2011,** 12, 2552-2561.

[21] Chatterjee, T.; Chakraborti, S.; Joshi, P.; Singh, S.P.; Gupta, V.; Chakrabarti, P. *FEBS J.* **2010**, 277, 4184–4194.

[22] Vogler, E. A. *Biomaterials* 33 (2012) 1201-1237.

[23]Abraham, S.; So, A.; Unsworth, L. D. *Biomacromolecules* **2011,** 12, 3567–3580.

[24] Noh, H.; Vogler, E. A. *Biomaterials* **2007,** *28*, 405-422.

[25] Parhi, P.; Golas, A.; Vogler, E. A., *J Adhes Sci Technol* **2010,** *24*, 853-888.

[26] Holmlin, R. E.; Chen, X. X.; Chapman, R. G.; Takayama, S.;Whitesides, G. M. *Langmuir* **2001**, 17, 2841–2850.

[27] Zhang, Z.; Vaisocherová, H.; Cheng, G.; Yang, W.; Xue, H.; Jiang, S. *Biomacromolecules* **2008,** *9*, 2686–2692.

[28] Pasche, S.; Vörös, J.; Griesser, H. J.; Spencer, N. D.; Textor, M. *J. Phys. Chem. B* **2005,** *109*, 17545-17552.

[29] Zhang, Y.; Li, J-H; Ge, Y-G; Liu, X-R; Jiang, F-L; Liu, Y. *J. Fluoresc*. **2011,** 21, 475-485.

[30] Velazquez-Campoy, A.; Leavitt, S.A.; Freire, E. *Methods Mol. Boil*. **2004,** 261, 35-54.

[31] Chen, Z-X; Guo, G-M; Deng, S-P *J. Agric. Food Chem.* **2009**, 57, 2945-2954.

[32] Bonicna, M.; Lah, J.; Rescic, J.; Vlachy, V. *J. Phys. Chem. B* **2010,** 114, 4313-4319.

[33] Vorup-Jensen, T.; Waldron, T.; Astrop, N.; Shimaoka, M.; Springer, T. *Biochim. Biophys. Acta* **2007**, 1774, 1148-1155.

[34] Freire, E.; Mayorga, O.; Straume, M. *Anal.Chem*. **1990**, 62, 950-959.

[35] Goy-López, S.; Juárez, J.; Alatorre-Meda, M.; Casals, E.; Puntes, V. F.; Taboada, P.; Mosquera, V. *Langmuir* **2012**, 28, 9113−9126.

[36] Cosman, N. P.; Fatih, K.; Roscoe, S. G. *J. Electroanalytical Chemistry* **2005**, 574, 261-271.

[37] Gurgel, P. V.; Carbonell, R. G.; Swaisgood, H. E. *J. Agric. Food Chem.* **2001,** *49,* 5765-5770.

[38] Norde, W.; Haynes, C. A. In *Proteins at Interfaces II*; Horbett, T. A., Brash, J. L. Eds.; ACS Symposium Series 602; American Chemical Society: Washington, DC, 1995; pp 26-40.

[39] Bouchemal, K.; Couvreur, P.; Daoud-Mahammed, S.; Poupaert, J.; Gref, R. *J. Therm. Anal. Calorim.* **2009,** 98, 57–64.

[40] Schulz, D. N.; Peiffer, D. G.; Agarwal, P. K.; Larabee, J.; Kaladas, J. J.; Soni, L.; Garner, R. T. *Polymer* **1986**, 27, 1734-1742.

[41] Mary, P.; Bendejacq, D. D.; Labeau, M. P.; Dupuis, P. *J. Phys. Chem. B* **2007,** 111, 7767-7777.

[42] Azzaroni, O.; Brown, A. A.; Huck, W. T. *Angew. Chem. Int. Ed.* **2006**, 45, 1770 – 1774.

[43] Casals, E.; Pfaller, T.; Duschl, A.; Oostingh, G. J.; Puntes, V. *ACS Nano* **2010**, 4, 3623–3632.

[44] Monopoli, M. P.; Walczyk, D.; Campbell, A.; Elia, G.; Lynch, I.; Bombelli, F. B.; Dawson, K. *J. Am. Chem. Soc.* **2011**, 133, 2525–2534.

[45] Vroman, L.; Adams, A. L. *J. Biomed.Mater. Res.* **1969**, 3, 43–67.

[46] Lowe, A. B.; McCormick, C. L. *Chem. ReV.* **2002**, *102*, 4177–89.

[47] Ivanov, I. A.; Kamenova, I. P.; Georgieva, V. T.; Kamenska, E. B.; Georgiev, G. S. *Colloid Surf., A* **2006**, *282&283*, 129–33.

[48] Ha, J.H.; Capp, M. W.; Hohenwalter, M. D.; Baskerville, M.; Record, M. T.; *J. Mol. Biol.* **1992**, 228, 252-264.

[49] Record, M.T.; Anderson, C.F.; Lohman, T.M. *Quarterly Reviews of Biophysics* **1978**, 11, 103-178.

[50] Perkins, T.; Mak, D.; Root, T.; Lightfoot, E. *Journal of chromatography A* **1977**, 766, 1-14.

[51] Xia, F.; Nagrath, D.; Garde, S.; Cramer, S.M. *Biotechnol. Bioeng.* **2004,** 87, 354-63.

[52] Estephan, Z. G.; Schlenoff, P. S.; Schlenoff, J. B. *Langmuir* **2011**, 27, 6794–6800.

[53] Leffler, J. E. *J. Org. Chem*. **1955**, 20, 1202-1231.

[54] Rekharsky, M. V.; Inoue, Y. *Chem. Rev.* **1998**, 98, 1875-1917.

Chapter 5

Concluding Remarks and Future Outlook

5.1. Concluding Remarks

The main goal of this thesis was to shed light on molecular events and driving forces involved in macromlolecular self-assembly at nano-bio interface. The primary focus of this work revolves around two closely-related interactions with critical importance in biomedical applications *viz.* i) Nanofiber formation through peptide self-assembly, and ii) non-specific protein adsorption to nanoparticles. It is believed that a molecular-level understanding of protein and peptide self-assembly will not only lead us to elucidate the complicated nature of biomaterial-body interactions, but also it can profoundly influence our ability to design and engineer more optimal and advanced biomaterials in future.

Nanofiber-forming RADA4 is a well-known self-complementary peptide which has shown very promising in a vast array of biomedical applications [1-5]. There have been theories proposed regarding self-assembly mechanism of this peptide into nanofibers [6-8]; however a proof-of-concept study on this topic is largely missing in the literature. In **Chapter 2** self-assembly of RADA-based peptides was investigated at a molecular level utilizing Isothermal Titration Calorimetry (ITC) and Atomic Force Microscopy (AFM) techniques. In order to monitor the role of peptide chemistry, apart from $RADA_4$, two other chemistries namely $RADA_4$-S_5 and $RADA_4$-K_5 were investigated. Our results demonstrated that $RADA_4$ peptides with 5 serine residues were still able to form nanofibers in solution whereas appending 5 lysine residues to $RADA_4$ hampered the self-assembly process. This was perhaps due to electrostatic repulsion between

positive charges of lysine residues present on the peptide molecule, at the pH of our study (i.e. ~7.4).

The dissociation of self-assembled peptide structures (i.e. $RADA_4$ and $RADA_4$-S_5) generated endothermic heat signals upon injection into ITC cell, indicating exothermic nature of peptide self-assembly for both $RADA_4$ and $RADA_4$-S_5 chemistries. ITC thermo-grams also confirmed a critical assembly concentration (CAC) for these peptides (which was measured to be between ~0.1 and ~0.15 mM) and proved the self-assembly process to be driven by entropy. The fact that self-assembly was found to be entropically-driven called for considering temperature as a determining factor in self-assembly process. As expected, ITC experiments at different temperatures revealed that increasing temperature makes the self-assembly process more thermodynamically-favorable. Knowing the enthalpy change upon nanofiber dis-assembly at different temperatures, the heat capacity change was calculated accordingly. The values for heat capacity change revealed that $RADA_4$ self-assembly is driven by hydrophobic interactions (perhaps among alanine residues) whereas hydrogen bonding is the main driving force for $RADA_4$-S_5 self-assembly (probably due to interactions between hydroxyl groups on serine molecules). Since this finding was not in agreement with previous theories proposed for self-assembly mechanism of $RADA_4$, highlighting crucial role of electrostatic interactions in this process, further investigations were necessary to be conducted. Firstly, van't Hoff enthalpy was calculated; where its drastic variation from enthalpy values measured by ITC accounted for large contribution of water molecules and/or counter-ions in self-

assembly of $RADA_4$ and $RADA_4$-S_5. In order to further clarify the role of water molecules and counter-ions in peptide self-assembly, osmotic stress as well as ionic strength of the solution were utilized: Through modulating the osmotic stress of the solution (via variations in sucrose concentration), it was found that water molecules were removed from interface upon self-assembly of $RADA_4$ while association of $RADA_4$-S_5 molecules caused an increase in the number of water molecules associated with the peptide. On the other hand, ionic strength variation of the solution confirmed minimal contribution of counter-ions in self-assembly of either of these peptides. These findings further validated the conclusions drawn upon heat capacity measurement studies explained above.

In general, the results presented in **Chapter 2**, demonstrated that how small variations in peptide chemistry can drastically alter the molecular pathways and driving forces for peptide self-assembly. To best of our knowledge, this type of fundamental investigation on peptide self-assembly, utilizing thermodynamic parameters of the process, has never been reported in the literature. It is hoped that the results presented herein as well as the developed protocols can be used as a cornerstone for future studies in the field.

Conducting thermodynamic analysis on peptide self-assembly and identifying the molecular forces driving this process, led us to question whether we can obtain the same type of critical information (with comparable depth and accuracy) regarding non-specific protein adsorption to nanoparticles. Studies in this field mostly characterize non-fouling behaviour of surfaces based on the

amount of the adsorbed protein (mainly using spectroscopy methods or quartz crystal microbalance technique). ITC have been applied to describe the interaction of proteins with nanoparticles since 2007 [9]. However in **Chapters 3 and 4**, it was tried to focus on developing an in-depth understanding of the phenomena that a protein undergoes while interacting with non-fouling zwitterionic surfaces. Hence, two distinct and well-characterized proteins were chosen: HSA (a large and hydrophobically-interactive molecule), and Alpha-la (a low molecular weight and electrostatically-interactive protein). The surface of nanoparticles (NPs), on the other hand, was modified with four different groups of zwitterionic polymer chains differing in their end-group chemistry and length of zwitterion's spacer group.

In Chapter 3, it was shown that adsorption of Alpha-la (the electrostatically-interactive model protein) to PCBMA-modified NPs was exothermic and entropically-driven. The values for both binding constant and degree of surface coverage indicated that alpha-lactalbumin interacts more strongly with the surface of NPs bearing longer spacer-group and/or hydrophobic end-group. Monitoring the change in number of water molecules and counter-ions at the interface (*via* PI analysis) as well as enthalpy-entropy compensation plot demonstrated that alpha-lactalbumin adsorption to zwitterionic NPs mainly included dipole-dipole and hydrogen-bonding type of interactions. Whereas thermodynamic profile for protein adsorption indicated that, in the absence of zwitterionic coatings on NPs surface (i.e. in case of interaction with bare silica nanoparticle), the main driving force for protein adsorption was of hydrophobic

nature. These findings also validated the hypothesis regarding ability of zwitterionic polymers to create a tightly bound-water layer on the surface. Considering the electrostatically-active alpha-lactalbumin, the lack of counter-ion release from interface upon its interaction with polymer-grafted NPs was quite striking. However PI analysis revealed that the entropic drive for alpha-lactalbumin adsorption was provided through incorporation of bulk water molecules to the protein-NP interface.

The interaction of zwitterionic NPs with the hydrophobic model protein, HSA, was discussed in **Chapter 4**. ITC results revealed that HSA adsorption to the surface of all NPs under study was endothermic and entropically-driven. Interestingly, while modification of silica NP surface with zwitterionic polymer resulted in lower amount of adsorbed HSA on their surface; it also caused an increase in the binding constant between protein and NPs. In terms of the effect of polymer chemistry, it was found that NPs modified with longer spacer group demonstrated larger binding constants for HSA. On the other hand, larger amounts of protein got adsorbed to the surface of NPs with shorter spacer group or hydrophobic end-group.

As it was expected from hydrophobic nature of HSA, it was revealed that the main origin of the entropic drive for HSA adsorption was release of water molecules from interface. However, PI analysis proved that the number of water molecules released upon adsorption of HSA to zwitterionic NPs was much smaller than the amount of water displaced upon HSA interaction with

unmodified silica NP. Enthalpy-entropy compensation effect was also shown to exist for adsorption of HSA to all NP systems under study and it proved that modification of NPs with zwitterionic polymers resulted in smaller conformational change as well as lower desolvation of the system. Furthermore, the main mechanism for adsorption of HSA to NPs was concluded to be ion-decoupled hydrophobic interactions.

5.2. Future Outlook

Our findings indicated that appending 5 Lysine residues to C-terminus of $RADA_4$ peptide inhibits self-assembly. An avenue which can get further explored in future could be to study self-assembly of $RADA_4$-K_5 in solutions with different pH or ionic strength values in order to probe the contribution of lysine's charged groups in self-assembly process. Furthermore, the role of the length of the appended sequence could be investigated. It might lead to finding an optimum length for the appended residue where it allows for the self-assembly to take place or even the specific length at which self-assembly is driven by a desired type of interaction (i.e. enthalpically or entropically and hydrophobic or hydrogen-bonding). In future, it would also be valuable to utilize this method in studying the interaction of functionalized RADA peptide systems (e.g. RADA sequences containing enzymatic cleavable domains) with the molecule of interest (e.g. enzyme) in order to obtain kinetic and thermodynamic properties of the interaction and optimize the peptide structure accordingly.

As Alpha-la was picked as the electrostatically-interactive model protein in protein-nanoparticle studies presented herein, it would be interesting to perform follow-up studies utilizing a similar-sized protein with a different surface charge (e.g. Lysozyme) in order to see how the type of protein's surface charge impact its interaction with zwitterionic polymers. Utilizing the protocols developed in this thesis, it would be interesting to do comparison studies among different non-fouling coatings (e.g. zwitterions and PEG) in order to identify the major contributors to their protein-repellent behavior from a thermodynamic point of view. Protein adsorption is a very complicated phenomenon governed by protein and sorbent physicochemical characteristics as well as solvent properties. A new trend in protein-surface interaction studies is rapidly growing and it involves analyzing this process from a thermodynamic point of view. Studies similar to the work presented herein can be used as a building block for a future library of thermodynamic profiles for interaction of different proteins with biomaterial surfaces. Such library would be extremely beneficial to the design and engineering of more efficient non-fouling surfaces.

5.1. References

[1] Sieminski, A. L.; Semino, C. E.; Gong, H.; Kamm, R. D. *J. Biomed. Mater. Res., Part A* **2008**, *82*, 494–504.

[2] Wang, S.; Nagrath, D.; Chen, P.C.; Berthiaume, F.; Yarmush, M. L. *Tissue Eng., Part A* **2008**, *14*, 227-36.

[3] Kisiday, J.; Jin, M.; Kurz, B.; Hung, H.; Semino, C.; Zhang, S. *Proc. Natl. Acad. Sci. U. S. A.* **2002**, *99*, 9996–10001.

[4] Davis, M. E.; Motion, J.; Narmoneva, D. A.; Takahashi, T.; Hakuno, D.; Kamm, R. D. *Circulation* **2005**, *111*, 442–50.

[5] Schneider, A.; Garlick, J. A.; Egles, C. *PLoS ONE* **2008**, *3*, 1410.

[6] Amosi, N.; Zarzhitsky, S.; Gilsohn, E.; Salnikov, O.; Monsonego-Ornan, E.; Shahar, R.; Rapaport, H. *Acta Biomater.* **2012**, *8*, 2466–2475.

[7] Chow, D.; Nunalee, M. L.; Lim, D. W.; Simnick, A. J.; Chilkoti, A. *Mater. Sci. Eng., R* **2008**, *62*, 125-155.

[8] Yokoi, H.; Kinoshita, T.; Zhang, S. *Proc. Natl. Acad. Sci. U. S. A.* **2005**, *102*, 8414-8419.

[9] Lindman, S.; Lynch, I.; Thulin, E.; Nilsson, H.; Dawson, K. A.;Linse, S. *Nano Lett.* **2007**, 7, 914.

Appendix A

Experimental Procedure for Calorimetric Measurements

The purpose of this section is to provide details on sample preparation as well as the experimental procedure applied to measure different thermodynamic parameters discussed in this thesis.

Sample Preparation

The ability of ITC in measuring very small heat signals makes this devise very sensitive to environmental conditions. As even very small perturbations in physicochemical properties of the system can result in a noisy baseline or very large heat of dilution overtaking the heat directly related to macromolecular interaction. In order to minimize the heat associated with dilution of the sample in the syringe upon injection into ITC cell, it is necessary to make sure that the buffer conditions of the two solutions (one inside the syringe and the other one inside the ITC cell) are completely identical (in terms of pH, ionic strength, salt composition, osmotic stress agents, etc.).

Other than the solution conditions, determination of the accurate concentration of samples play an important role; as in the modelling stage even minimal deviations in concentration can result in distinctly different results. Furthermore, the concentrations which are picked should be in an optimal range in which the device is able to produce heat signals which can then be fit to a model. In order to be able to estimate the most optimal concentration range, there has been a dimensionless parameter (c) introduced as the following [1]:

$$c = nK[M_T] \qquad \text{Equation (A-1)}$$

where n is the stoichiometry of interaction, K is the binding constant and $[M_T]$ is the total concentration of the sample inside the ITC cell.

It has been proposed that in order to be able to precisely measure the binding affinity of the interaction it is necessary for c to be between 1 and 1000 [1]. However, in most cases the binding affinity of the interaction is not known prior to calorimetric measurements; therefore a set of "trial and error" experiments should be performed in order to find the optimal concentration range that returns the most accurate result.

In ITC studies on peptide samples, presented in this work, one potential concern was the difficulties in distinguishing between the heat produced due to dissociation of assembled naofibers and the heat produced because of the disruption of hydrogel structure. By choosing the concentration of peptide sample as low as possible and also, sonicating the samples right before performing the experiment it was made possible to avoid gel formation inside the syringe.

On the other hand, the optimal solution concentration for protein relative to modified NP is a requirement for ITC characterization of the adsorption event. In order to determine these optimal concentrations for the titrant (in syringe) and titrand (in cell) solutions, a set of survey titrations were performed over a range of different ratios of titrant to titrand concentrations. These allowed for an estimation of the binding constant (K), which could then be used to further resolve a titrant:titrand concentration ratio that yielded a sigmoidal relationship between molar enthalpy and molar ratio of titrant:titrand inside the cell. Blank experiments

where titrant solutions were injected into an identical solution within the cell that did not contain titrand were conducted so as to determine the background heat of dilution. This was performed to ensure that no dissociation or precipitation of the titrant occurred upon injection.

Data Analysis

For all experiments on peptide self-assembly the model for micelle formation has been applied (See chapter 2). In case of protein adsorption studies, however, the model for single set of independent binding sites has been utilized; the details of which are presented in the following.

Assuming n identical and independent binding sites on each nanoparticle and employing the equation derived by Freire *et. al.* (Equation A-2) [2], the amount of heat (Q) released or absorbed upon binding can be determined,

$$Q = \left(\frac{V\Delta H}{2K}\right)\left[\left(1+[np]nK+K[P]\right)-\sqrt{\left(1+[np]nK+K[P]\right)^2-4[np]nk^2[P]}\right]$$

Equation (A-2)

where V is the volume of ITC cell, [np] is the nanoparticle concentration, ΔH is the enthalpy change, K is the binding constant, and [P] is the protein concentration.

The change in the amount of heat released/absorbed between two successive injections can be determined from the following equation [3],

$$\Delta Q = Q_{i+1} - Q_i + \left(\frac{V_{i+1} - V_i}{V_i}\right)\left(\frac{Q_{i+1} + Q_i}{2}\right) \qquad \text{Equation (A-3)}$$

where Q_i and V_i are the heat content and the volume of the solution inside the cell after i^{th} injection, respectively. Using the experimental Q, [np], and [P] from equations (A-2) and (A-3), n, K, and ΔH were subsequently determined through non-linear least square regression method; as imbedded within the NanoAnalyze software (TA Instruments). Subsequent Gibbs free energy changes (ΔG) and entropy changes (ΔS) were then calculated by using the standard thermodynamic equations:

$$\Delta G = RT\ln(K) \qquad \text{Equation (A-4)}$$

$$\Delta G = \Delta H - T\Delta S \qquad \text{Equation (A-5)}$$

where R is the gas constant and T is the absolute temperature.

References

[1] Velázquez-Campoy, A.; Ohtaka, H.; Nezami, A.; Muzammil, S.; Freire, E. *Current Protocols in Cell Biology* **2004**, 17, 1-24.

[2] Freire, E.; Mayorga, O.; Straume, M. *Anal. Chem*. **1990**, 62, 950-959.

[3] Cedervall, T.; Lynch, I.; Lindman, S.; Berggard, T.; Thulin, E.; Nilsson, H.; Dawson, K.; Linse, S. *Proc. Natl. Acad. Sci. U. S. A.* **2007**, 104, 2050-2055.

Appendix B

Characterization of Protein Secondary Structure

Far UV Circular Dichroism (CD) spectra were collected at 25 and 37ºC for both HSA and α–lactalbumin proteins using a Jasco J-810 CD/ORD (Japan) at 100 mdeg sensitivity, bandwidth of 1 nm, and data pitch of 0.5 nm. The buffered protein solution was pipetted into a cuvette with a 2mm path length for acquiring the spectra, and each reading was repeated 5 times (average data plotted). A blank buffer reference was subtracted from the data before calculating the molar ellipticity. Molar ellipticity was calculated:

$$[\theta_\lambda] = \frac{\theta_{obs}}{10Lcn} \qquad \text{Equation (B-1)}$$

where $[\theta]_\lambda$ is the wavelength (λ) specific molar ellipticity (deg $cm^2/dmol$), θ_{obs} is the λ specific ellipticity (mdeg), L the path length (cm), c is protein concentration (M), and n is the number of amino acid residues [1]. The concentration of buffered protein solutions was verified using an Agilent UV-Vis Spectrophotometer at the fixed wavelength of 280 nm and molar extinction coefficient of 36,600 $M^{-1}cm^{-1}$ and 28,175 $M^{-1}cm^{-1}$ for HSA and α-lactalbumin, respectively.

The results of CD experiments on protein solutions at different temperatures and ionic strengths are presented below.

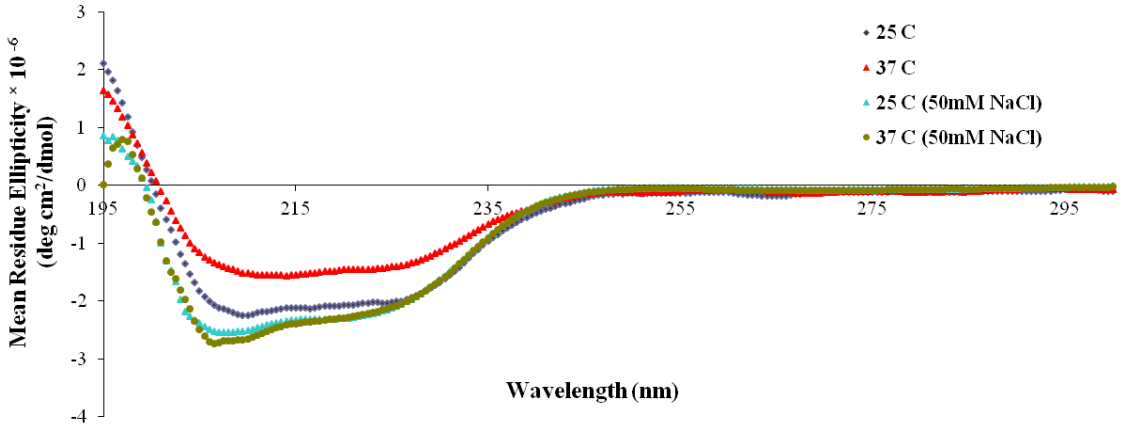

Figure B-1. CD spectra of Alpha-la solution in buffer at different temperatures and/or in presence of NaCl inside the solution. The results indicated that neither increasing the temperature nor the addition of salt has impacted the secondary structure of the protein.

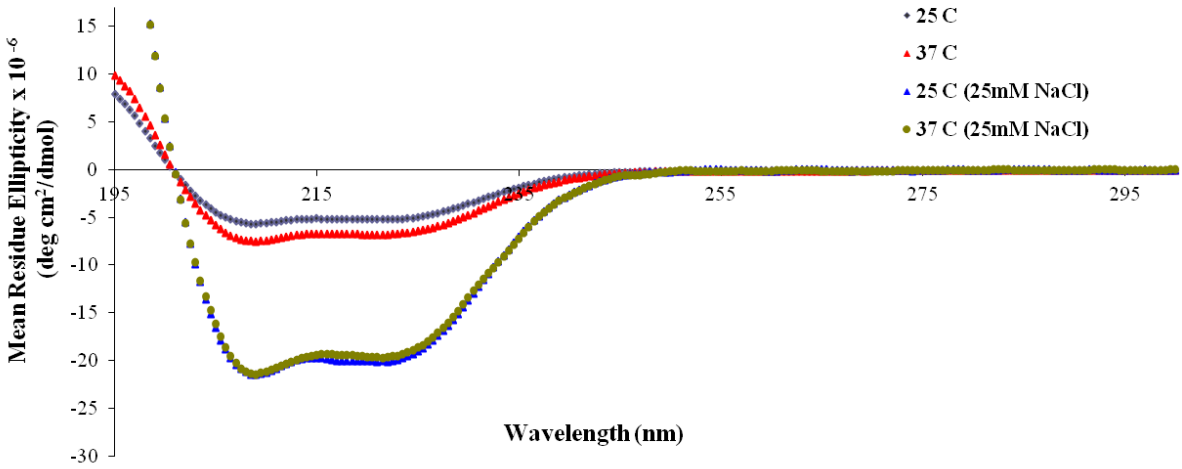

Figure B-2. CD spectra of HSA solution in buffer at different temperatures and/or in presence of NaCl inside the solution. The results indicated that neither

increasing the temperature nor the addition of salt has impacted the secondary structure of the protein.

References

[1] Zhang, Y.; Li, J-H; Ge, Y-G; Liu, X-R; Jiang, F-L; Liu, Y. *J. of Fluoresc*. **2011**, 21, 475-485.